PUNCHING SHEAR STRENGTH OF LIGHTLY REINFORCED ISOTROPIC BRIDGE DECKS

By

JOSE O. GUEVARA

A DISSERTATION PRESENTED TO THE GRADUATE SCHOOL
OF THE UNIVERSITY OF FLORIDA IN
PARTIAL FULFILLMENT OF THE REQUIREMENTS
FOR THE DEGREE OF DOCTOR OF PHILOSOPHY

UNIVERSITY OF FLORIDA

1990

ACKNOWLEDGMENTS

The author would like to express his gratitude to Dr. John M. Lybas, chairman of his supervisory committee, for his valuable guidance, long hours of discussion, critical review and correction of the manuscript and advice throughout the entire study. Special appreciation is extended to Dr. Clifford O. Hays, cochairman of his supervisory committee, for the advice, help and guidance through the various stages of this study. The author is very grateful to Dr. Fernando Fagundo for his valuable comments, suggestions, advice, help and encouragement throughout his graduate work and also for serving on his supervisory committee. Further gratitude is extended to Dr. Marc. I. Hoit for his advice during the analytical work. The help and advice by Dr. David Bloomquist during the experimental work is greatly appreciated. Special thanks is extended to Dr. James Keesling for serving on his supervisory committee.

The author wishes to express his appreciation to the Florida Department of Transportation (FDOT) for the financial support, materials and personnel that made this study possible, and in particular to Dr. Paul Csagoly for giving valuable suggestions.

Danny Richardson deserves special mention for the enormous help during the experimental work.

The advice and friendship from Fernando, Alfredo, Bouzid, Nour, Prasan, Joon, Lin, Mohan, Vinax, Shiv are also acknowledged.

Thanks are extended to Messrs. Bill Studstill, Kirk Waite, George, David, Alex, and all his friends and student colleagues for their help in the various stages of the experimental work.

Finally, the author would like to express his love and thanks to his family, especially his mother, for their continued encoragement and support.

TABLE OF CONTENTS

LIST OF TABLES

LIST OF FIGURES

Abstract of Dissertation Presented to the Graduate School of the Universtiy of Florida in Partial Fulfillment of the Requirements for the Degree of Doctor of Philosophy

PUNCHING SHEAR STRENGTH OF LIGHTLY REINFORCED ISOTROPIC BRIDGE DECKS

By

Jose O. Guevara

August 1990

Chairman: John M. Lybas
Cochairman: Clifford O. Hays
Major Department: Civil Engineering

A series of laboratory tests on approximately one-half scale models of concrete bridge decks were performed at the University of Florida laboratory using 0.3% isotropic reinforcement following the Ontario empirical design approach, except that transverse span to slab thickness ratios exceeded those permitted in the Ontario specification, and reflected the thinner slabs commonly used in the USA. Four specimens with slabs cast on steel girders were constructed, and three of them were tested statically to failure, while the fourth specimen was subjected to a large number of cyclic loads and then tested statically to failure. Additionally one specimen was cast on standard size bulb-tee girders, and was tested statically.

All of the above tests were performed at various locations on the bridge models, including interior spans and overhangs.

Observed punching loads were compared with standard AASHTO vehicle loading, and were also compared with computed results from the ACI punching model, the AASHTO formula, the Kinnunen and Nylander model, and the yield line theory. The Kinnunen and Nylander model was also used to estimate inplane boundary restraining forces consistent with observed punching loads. A finite element model was applied for the calculation of bracing forces.

CHAPTER 1
INTRODUCTION

1.1 General

Extensive experimental and some theoretical research [1] has demonstrated that the AASHTO [2] provisions for concrete bridge decks, based on two dimensional plate bending theory [3] are very conservative. Laterally restrained reinforced concrete bridge decks slabs usually carry higher compressive stresses and as a result higher load capacity than predicted by flexural response calculations. The flexural strength is enhanced to a level higher than that predicted by the flexural yield line theory mainly because a punching shear failure rather than flexural failure is usually observed. Apparently this is made possible by arching or compressive membrane action. The presence of Tensile membrane action has also been recognized in laboratory tests [4], the membrane action being sufficiently strong to allow deck models to endure large deflections before failure occurred with concrete crushing. Because of the above, there is reason to believe that a substantial reduction in the required steel reinforcement might be possible.

1.2 Previous Research and Implementation

The presence and beneficial effect of membrane forces were recognized as early as 1956 when Ockleston [5] tested a three-story reinforced concrete building in South Africa, and found that the collapse loads were three or four times the capacity predicted by yield line theory. In 1962 Guyon [6] suggested the consideration of arching action in designing slabs.

Since 1969, many bridges have been tested in the field by the Ontario Ministry of Transportation and Communications. From these tests it was observed that thin concrete deck slabs supported by beams or girders were capable of taking considerably more load than that predicted by flexural models.

A series of studies were conducted at Queen's University, Kingston, Ontario using one eighth scale models [7] which showed a large reserve of strength under static and fatigue loadings. On the basis of ultimate strength requirements along with shrinkage and thermal stress requirements, 0.2 percent isotropic reinforcement, top and bottom, was recommended.

This research work was supplemented by field tests of actual bridges [8]. It was concluded that there is a large increase in the capacity against failure because of the presence of boundary restraint.

Based on the punching shear research the Ontario Highway Bridge Design Code, (OHBDC) [9] adopted a simple

empirical design approach for bridge decks, allowing 0.3% isotropic reinforcement top and bottom in both directions. At first 0.2% was recommended, but for better crack control for live loads, shrinkage and temperature a ratio of 0.3% was adopted. To use this low steel ratio, certain requirements relative to slab thickness, transverse span to thickness ratio, transverse span, diaphragms, overhangs, and other parameters had to be met.

The convenience in construction of such decks, the savings in the amount of reinforcement required (from one fourth to one half the quantity of reinforcement in typical bridge decks) along with the improvement in the durability of exposed concrete decks associated with the better control of cracking using smaller bar sizes, have attracted the attention of researchers in the United States. However, there are several differences between Canadian and U.S. practice in bridge construction, which have motivated several states on the U.S. to do more research related to Punching Shear.

The need to determine the influence of heavily loaded, closely spaced wheels and axles on reinforced concrete bridge decks prompted the New York State Department of Transportation to initiate an analytical study of bridge deck behavior in 1977. During the course of the research, more evidence became available that the failure mode of reinforced concrete bridge decks was punching shear and not flexure[10]. Because of this evidence they decided to

investigate the ultimate capacity of bridge decks. Both the proposed Ontario reinforcing details and those consistent with the AASHTO code were tested, using reduced-scale bridge decks.

Tests on model bridge decks that have substantially less reinforcement than typical designs caused stresses no greater than 12 ksi at the design load. Test to failure resulted in capacities consistently larger than six times the design wheel load for slabs bounded by girders, regardless of the reinforcement pattern. The type of failure was always by punching shear.

In 1985 an extensive research program regarding the behavior of reinforced concrete bridge decks designed following the Ontario Code requirements was conducted at the University of Texas.

In the Texas investigation [11] a 20 by 50 ft. full scale model of a 7½" thick deck supported on three steel girders spaced at 7'-0" center to center was tested. Half of the bridge was cast in place and the other half was constructed using precast prestressed panels. The girders were 60 ft. long, with a span of 49 ft. between simple supports.

Fatigue and static loading were developed using AASHTO truck loadings, using a higher safety factor. Four wheel loads were applied simultaneously to represent a two-axle truck straddling the center girder. The wheel lines were thus located 3 ft. on either side of the center of the

steel girder, as this could produce the largest possible negative moment in the slab above the girders. The bridge was tested statically to a maximum load of 60 kips on each of the four wheels. This load represented approximately three times the service load including impact factors, and was chosen to produce cracking in the deck. Next, the deck was subjected to cyclic wheel loading between 5 and 26 kips for 5 million cycles of fatigue loading with an approximately frequency of 1 Hz. At intervals of about 1 million cycles the bridge was loaded statically to 30 kips to simulate an overload condition. After the cyclic loading, the wheel loads were again applied statically up to 40 kips. The bridge performed well in all areas.

The Texas researchers also studied the behavior of a continuous girder bridge in the negative moment region {12}. For this purpose they moved the supports inward, creating a span of 40ft, but used the same length specimen. Tiedown forces were applied at the resulting overhang at each end of the bridge creating negative moment in the deck. The bridge was loaded with four concentrated loads to represent a tandem axle formation, with two axles and four wheel loads. A series of static loads were applied, along with 5 million cycles of fatigue loading. Again the bridge behaved well under the static and cyclic loading. Then single point and double point concentrated load were applied to the specimen in both the cast in place and panel deck portions of the deck, with the specimen being loaded

to failure in each case. For the cast in place deck subjected to a single point load, the slab failed at 142 kips, and for the double point load the slab failed at 204 kips. For the panel deck the corresponding failure loads were even higher.

Finally, additional tests were made on a skewed slab specimen, which performed well under monotonic loading, to failure. The Texas researchers showed that the beneficial effect of lateral confinement exists even prior to cracking of the deck and the development of yield lines. This is important, because it shows that stresses in the steel, even at service load levels, may be substantially less than that given by AASHTO criteria.

The Texas test are very encouraging. However, they only involved one ratio of transverse span to thickness for the slab (11.2). The OHBDC allows the simplified isotropic design for transverse span to thickness ratios as high as 15. Also, the Texas research, like the Ontario research, did not involve tests in the overhanging areas of the slab.

In 1987 the Case Western University [13] performed a study involving a series of direct model tests (1/3 and 1/6.6 scale) under static, fixed pulsating and moving wheel-loads. The object was to study the effect of deck continuity and reinforcing pattern on the ultimate and fatigue strength of concrete bridge deck slabs supported on steel girders.

The results of direct model tests indicate that a wheel-load passage results in far more damage than a single-load cycle of a pulsating load applied at a fixed point, especially in the case of orthotropic reinforcement. One passage of the moving wheel-load on the isotropically reinforced specimens was equivalent in damage to about 34 cycles of the fixed pulsating load of equal maximum level. However one load passage on the orthotropically reinforced specimens was equivalent to more than 150 cycles.

The slabs tested under a fixed pulsating load failed in a punching shear mode with radial cracks that extended over a larger region for slabs with isotropic reinforcement than for slabs with orthotropic reinforcement. The specimens tested under the moving constant wheel-load failed in a punching shear mode of a different type, revealing more extensive and longitudinal flexure cracks that closely followed the location of the reinforcing bars.

In 1987 the school of Engineering at the University of Auckland, New Zealand [14], performed a study involving tests of three one-way strips supported on two opposite sides, representing support from girders. They were 4 inches deep and had a span to depth ratio of 12 with a length in the perpendicular (longitudinal) direction of twice the span.

Several boundary conditions on the supported edges were used. Membrane action was found to resist a significant portion of the load from the initial flexural

cracking condition through to the failure load. The membrane compressive forces under a central concentrated load were found to be concentrated within a slab width of 5/8 of the clear span, centered under the load. Failure of all specimens occurred with the load punching through the slab. The results showed that the punching shear strength increases and the ductility decreases as the inplane boundary restraint is increased, with resultant reduction in the tensile stresses in the flexural reinforcement.

1.3 Research Objectives and Scope

It would certainly be desirable to use the Ontario Code in the USA. There are, however, certain differences in construction practice between U.S. and Canada that make it necessary to perform some research studies beyond those described above, before this design approach can be applied with confidence. Furthermore, there are certain omissions in previous research that need to be addressed, providing additional impetus for further testing. The items that need to be considered include

1) The common practice in many states is to use typical thicknesses below the Ontario minimum of 8.85 inches.

2) Bulb-Tee girders are widely used with concrete bridge decks in Florida and other states of U.S. and the flanges of these girders are quite wide and tapered in thickness, so the definition of span to thickness ratio

needs to be clarified relative to bridge decks on steel girders.

3) Tests on the overhanging edges of slabs were not performed by the Ontario researchers, but a better understanding of these regions may also lead to cost savings, having in mind that while the capacity of confinement in overhangs and therefore arching would be slight, some tests are warranted, especially considering the edge stiffening effects of the parapets normally used at slab edges.

4) The use of larger spans with span to thicknesses ratios beyond the Ontario limit of 15 could imply savings in the use of longitudinal girders, but it might also cause more deterioration due to fatigue effects, and cracking may be aggravated.

A series of laboratory tests on approximately one-half scale models of concrete bridge decks were performed at the University of Florida laboratory using 0.3% isotropic reinforcement following the Ontario empirical design approach. Four specimens with slabs cast on steel girders were constructed, and three of them were tested statically, while the fourth specimen was subjected to a large number of cyclic loads and then subjected to static loading to failure. Additionally one specimen was cast on standard size bulb-tee girders, as recently adopted in Florida, and was tested statically. The purpose of these tests was to understand better the behavior of bridge decks on steel and

Bulb Tee girders under static and fatigue loading conditions, with span to thickness ratios beyond the Ontario Code limitations and following American standard practice with regard to bridge deck construction.

1.4 Summary of Current AASHTO Bridge Deck Design Provisions

According to the current AASHTO Code, the slab is considered as a 1-ft.-wide beam spanning in a transverse direction and continuous over several supporting beams or stringers. The slab is designed to resist both its own dead weight and wheel loads.

The live load bending moment in a simple span is given by

$M=\pm(S+2)P/32$ ...(1.1) (for spans between 2 and 24 ft.)

where S is the effective span length in feet and P is 12,000 lbs for the H15 and HS15 loading and 16,000 lbs for the H20 and HS20 loading.

In slabs continuous over three or more supports, the moment is calculated as above but is multiplied by 0.8 for both positive and negative values.

The effective length S is considered as clear span for slabs monolithic with concrete beams. For slabs supported by steel girders, S is considered as the center to center distance of beams minus one-half of the stringer flange width.

The above moment is modified by an impact factor, I, meant to represent dynamic effects. This impact factor expressed as a percentage is given by

$$I=[50/(L+125)](100)\leq 30 \text{....} \quad (1.2)$$

As the moment calculated in equation 1.1 is a transverse moment, transverse steel areas can be calculated directly from this result. In order to provide reinforcing steel in the longitudinal direction the AASHTO specification requires a ratio of positive moment steel in the longitudinal direction equal to $220/\sqrt{S}$ times the ratio of transverse steel with a maximum value of 0.67 times the transverse steel area, where S is the span in feet.

In addition, to control cracking due to temperature and shrinkage, reinforcing bars are required in the top of the slab, parallel to the traffic. The minimum specified is 1/8 in. of reinforcement per foot of slab with an 18-in. maximum spacing.

The minimum thickness is calculated as (S+10)/30 and is amplified by 10% for single spans.

Since spalling of concrete decks has become a serious maintenance problem, the minimum cover required is 2 in. to help prevent moisture from penetrating to the reinforcing steel.

1.5 Summary of Empirical Method of Current Ontario Highway Bridge Deck Design

The current Ontario Code contains provisions for design of composite slabs of multi-girder bridges, based mainly on the presumption of significant compressive membrane action in the deck slab. These provisions allow 0.3% isotropic reinforcement to be provided top and bottom in both directions and assure that the slab has both sufficient ultimate strength and that cracking at service loads is properly controlled. There are certain limitations, however, placed on the use of the 0.3% isotropic reinforcement.

1. The span length of a span panel perpendicular to the direction of traffic cannot exceed 12 ft. and the slab has to extend at least 3.25 ft. beyond the centerline of the external longitudinal supports of a panel, or have a monolithic curb or parapet with a combined cross-sectional area of slab and curb (beyond the centerline of the external girder) greater value than the cross-sectional area of 3.25 ft. of deck slab.

2. The ratio of span length to thickness cannot exceed 15.

3. The slab thickness can not be less than 8 inches and the spacing of reinforcing bars shall not exceed 12 inches.

4. Diaphragms shall be provided with a maximum spacing of 25 ft. for steel girders; both I-shape and box and must

also be used at girder supports. For concrete girders diaphragms are required only at supports.

When the empirical method is not applicable, ultimate resistance should be determined from yield line methods rather than elastic analyses. However, designs based on this method may lead to cracking which may be unacceptable at serviceability limit states, so in order to calculate the stress resultants in a slab, elastic methods of analysis, such as those due to Westergaard [15], may also be used. Refined elastic methods referred to in Section 3 of the Ontario Code are also permissible, especially if they take into consideration in-plane stresses in the system. Alternatively, empirical equations for the effective widths of slabs, as specified in the Canadian Standards Association and AASHTO Specifications, may be used. However, this approach is conservative and results in unnecessarily high reinforcement, especially in typical bridge deck slabs in which arching effects are pronounced. Thus, a method incorporating considerations of arching effects [16] is preferred where it can be used.

CHAPTER 2
TEST PROGRAM FOR SPECIMENS ON STEEL GIRDERS

2.1 Size and Scale Factors of Test Specimens

The general cross-section of the four specimens are shown in Figure 2.1.

Three W 21x44 Steel girders of 25'-8" length were used for all specimens. They were simply supported over two concrete piers spanning 24'-11" center to center as shown in Figure 2.2. Sacrificial steel plates were connected to the girder using pairs of 1/2" diameter A-325 bolts spaced at 12 inches to transfer the horizontal shear forces between the slab and the girders and to permit the easy removal of the decks after the testing was completed. The X-braces were welded to the top and bottom flanges of the girders at the three longitudinal positions shown in Figure 2.2. Two reinforcing steel bars of 7/8" of diameter were used for the X-braces in the first specimen and two single angles of 1½"x1½"x¼" were used for the remaining specimens.

A parapet was located on one side of the specimens while the other side had only a plain overhang. In order to simplify the construction of the parapet the standard FDOT parapet was modified slightly, while closely maintaining the flexural and torsional stiffness properties reduced to the appropriate scale.

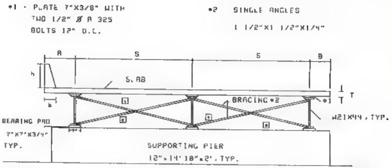

SPECIMEN	T	S	A	B	S/T	A/T	B/T	h	b	SCALE FACTOR
1	4 11/32	80	21.0	13.5	18.4	4.8	3.1	15.5	7.5	1.84
2	3 11/16	75 3/8	28.0	18.5	20.4	7.6	5.0	15.5	7.5	2.17
3	3 3/16	71 7/8	32.0	22.0	22.5	10.0	6.9	12.2	6.5	2.51

Figure 2.1 General Test Cross Section

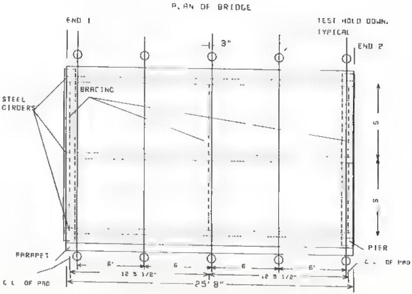

Figure 2.2 Plan View of Test Specimens

The three specimens were designed to have span to thickness ratios (S/T in Figure 2.1) of 18, 20 and 22 with the overhang to thickness ratios (A/T and B/T in Figure 2.1) increasing proportionally. The prototype deck thickness selected was an 8-inch deck. The table in Figure 2.1 shows the S/T, A/T and B/T ratios computed using the average thicknesses of the decks. These thicknesses were measured using a surveyor's level, and the results are shown in Appendix G. The effective scale factors for the specimens shown in the table of Figure 2.1 were computed such that the average measured deck thicknesses represented a prototype deck thickness of 8 inches.

The fourth specimen used for the dynamic testing was similar to the second specimen, such that the scale factors and detailing shown for specimen 2 in Figure 2.1 may be assumed to correspond to this specimen.

The first specimen was constructed entirely with University of Florida personnel and was satisfactory in all respects except for the finishing of the top of the concrete deck. For the remaining specimens, Durastress Concrete provided professional concrete finishers to assist in the placement and finishing of the concrete in the deck.

2.2 Material Properties of Specimens

For the scale factor of approximately two, a 3/8" maximum size of aggregate was considered to be appropriate, which corresponded approximately to a 3/4" size aggregate

in the prototype. Thus, the coarse aggregate used was FDOT designation #89. Because of the volume of concrete in the deck it was decided to use a ready-mix concrete. The concrete mix was a FDOT type II with a design strength of 3,400 psi at 28 days. Average compressive strengths at 28 days were 5590 psi, 5980 psi, 5720 psi and 6,800 psi for specimens 1,2,3 and 4, respectively.

Companion test cylinders and beams were cast at intervals during the casting period of the deck specimen, and were later tested to obtain the material properties.

The results of the cylinder compressive strength tests, splitting tensile strength tests and modulus of rupture tests are shown in Appendix F. Also, Appendix F contains an aggregate gradation curve and typical concrete mix proportions.

For the 0.3% isotropic reinforcement in an 8" deck a typical reinforcement pattern would be #4 @ 12" and for the corresponding scale factor of approximately 2.0 this implies #2 @6". It was difficult to obtain deformed reinforcement of #2 size, deformed reinforcement being deemed desirable for bond. Furthermore, it was difficult to obtain typical levels of yield strength and deformation capacities, as most deformed wire available is usually cold drawn and has higher strength and less ductility than conventional reinforcement. Ivey Steel in Jacksonville, Florida, cooperated with the University of Florida to

provide a steel wire with good ductility and a yield stress close to that for conventional reinforcement.

The stress-strain curve for the reinforcing wire, shown in Appendix F, indicates the well-defined yield plateau, implying good ductility. The wire used in the specimens was nominally a D5 (.05 in^2). However, the computed area based on weight was only about 0.0477 in^2. For the 0.0477 in^2 area the resulting yield stress was 76 ksi, and using the nominal area of 0.05 in^2 gives a yield stress of 72 ksi. These yield stresses were deemed to be reasonably close to that for prototype reinforcing steel.

The table in Figure 2.3 shows the primary reinforcement (D5 wires) for the specimens. Consistent with the Ontario method the steel provided 0.3% reinforcement top and bottom in both directions. As we stated before, the fourth specimen had the same characteristics as the second specimen. Extra transverse top bars were used on the side without the parapet, effectively doubling the reinforcement ratio in this region. In addition, the first specimen had extra transverse reinforcement on the side with the parapet, similar to that on the free edge. Extra transverse reinforcement, approximately quadrupling the reinforcing ratio, was used in the ends of the section in both the top and bottom layers to provide additional support at the discontinuous end of the slabs, as shown in Figure 2.3. The cover to the transverse top and bottom bars was 1 inch.

S	Sr
80" 75 3/8" 71 7/8"	6" 6 1/2" 7 1/2"

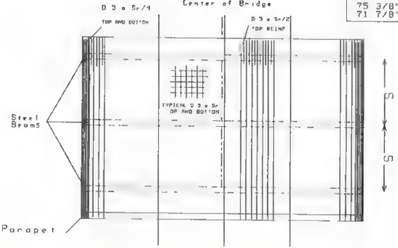

Figure 2.3 Reinforcement Spacing for Specimens

All reinforcing bars were tied appropriately with wires to secure the bars in each direction into a mat which was securely supported by chairs at the desired position in the slab to provide the required cover.

Strain gages installed on the reinforcing bars were waterproofed for protection prior to placing the bars. Wires leading to all instrumentation in the concrete were marked to identify gage locations, and were taken out through holes in the forms prior to placing the concrete.

Figure 2.4 is a photograph of specimen number three showing the general layout of the specimens.

2.3 Loading and Instrumentation of Static Tests

Previous research [17] had shown that the failure load was not significantly influenced by the position of the panel, by previous failures in adjacent panels, by the strength of the concrete, or by reasonable self-weight stresses. Because of this last point, it was deemed not necessary to provide additional weight of material to compensate for the loss of dead weight occurring due to scaling. Furthermore, relative insensitivity to previous failures in adjacent panels made it possible to load the slab in a variety of locations to study the relative effects of the parapets, the free overhang, and the confinement of the interior spans. The loading positions and patterns for the three specimens are shown in Figures 2.5, 2.6, and 2.7, respectively. Loads were applied to the

Figure 2.4 General Layout of Test Specimens

BRIDGE No 1

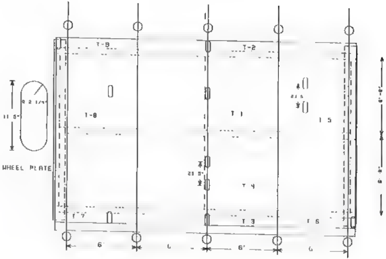

Figure 2.5 Loading Positions for Specimen One

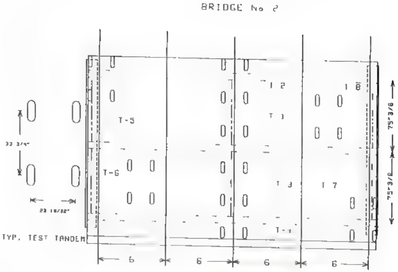

Figure 2.6 Loading Positions for Specimen Two

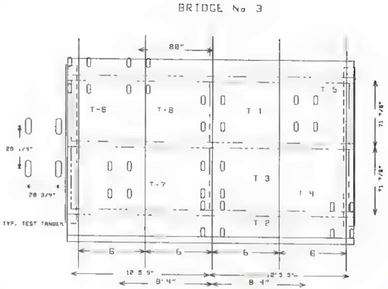

Figure 2.7 Loading Positions for Specimen Three

deck through heavy steel plates, shaped and sized to model the imprint of one dual wheel formation at approximately half scale.

The first specimen was loaded using either one set of dual tires or two sets of dual tires belonging to separate trucks passing close to one another. For the remaining bridges, considering the larger beam spacing and taking into account the realistic position of the critical loads [18], it was felt that the four-point loading, representing a complete tandem assembly, should be used. In all discussions of test loads, the entire load on the test is given, whether it is distributed to one-, two- or four-wheel plates. Dimensions of the prototype tandem were taken as 72 inches transversely and 51 inches longitudinally.

For the prototype the maximum tandem load that the slab could ever be subjected to was considered to be 153.3 kips. This considered the strongest commercially available axle unit with a maximum service load of 23 kips, and applying a factor of 2.5 to obtain a failure load. This assumes that the service load is at the typical endurance level of 40% of the strength. A factor of 0.75 was then applied to account for the combination of shear, flexure, and in-plane compression.

Figure 2.8 shows a view of the load assembly used to apply the tandem loads. Two W6x25 sections were supported on rollers placed on top of the wheel pads, except in the second specimen, where they were placed directly on the

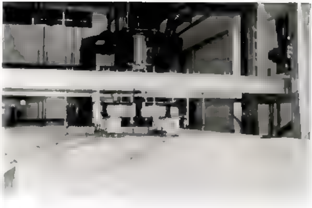

Figure 2.8 Load Assembly for Specimens

wheel pads. A W8x31 section spanned between the two lower steel sections and was loaded by the vertical hydraulic ram. Additional plates were welded on the beam to prevent local buckling of the test rig. The ram bore against a longitudinal beam that spanned between two lateral frames.

One hydraulic ram of 100 kips capacity was used to apply the load. A load cell connected to a voltmeter was used to measure the loads. Before the test, the load cell was calibrated using the laboratory's 400 kip Universal loading machine.

All specimens were instrumented with differential transformers (LVDTs) and electrical strain gages. The voltage readings of the LVDTs and strain gages were obtained using a HP 3497A data acquisition control unit and was then transferred to a HP 9825A computer using the HP-IB interface and finally transferred later to a PC computer for further evaluation.

A total of 15 LVDTs arranged on a pattern so as to define a deflection basin were used to measure vertical deflections. All LVDTs were supported on wooden support beams for the first specimen and on aluminum support beams for the remaining tests. Appendix A shows the location of the LVDTs for all tests, and Appendix B gives complete load-deflection plots for all tests. Appendix H gives the deflection basin corresponding to the maximum load applied.

Electrical resistance strain gages were used at various locations on the tests, including the top and

bottom surfaces of the deck, on the reinforcement, on the longitudinal girders and on the bracing. Two-inch gage lengths with high endurance leadwires were used on the concrete surfaces, 0.031-inch gage length general purpose miniature gages were used on the reinforcing steel, and 0.23-inch universal general-purpose weldable gages were used on the steel angle braces. Appendix C gives the locations of the strain gages for the various tests, and Appendix D contains all of the load-strain plots.

CHAPTER 3
BEHAVIOR OF TEST SPECIMENS ON STEEL GIRDERS SUBJECTED TO STATIC LOADING

3.1 General

The general load-deflection response and failure modes of the specimens are described in this chapter.

The general load-deflection response for all three specimens are shown in Figures 3.1, 3.2 and 3.3 as variations of total applied load with maximum deflection. Each specimen was tested at several locations; in essence, there were several tests for each specimen. A separate curve is provided for each test in Figures 3.1, 3.2, and 3.3. Each curve is labeled T-i where i represents the test number. The locations are shown in Figures 2.5, 2.6, and 2.7. Table 3.1 shows the maximum load attained during each test, the load at which a flexural yield pattern was well developed in the deck (yield load), and the maximum deflection during each test, along with the above results converted to full scale. Full-scale loads and deflections were obtained by multiplying the test values by the scale factor and the square of the scale factor for deflection and load values, respectively. The scale factors used were those shown in Figure 2.1. Appendix H shows the deflection basins corresponding to the maximum applied loads.

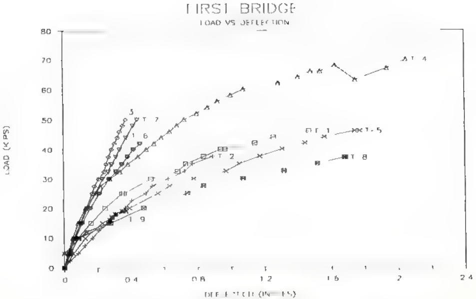

Figure 3.1 General Load-Deflection Curves for Specimen One

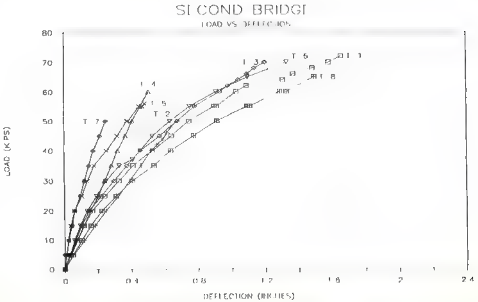

Figure 3.2 General Load-Deflection Curves for Specimen Two

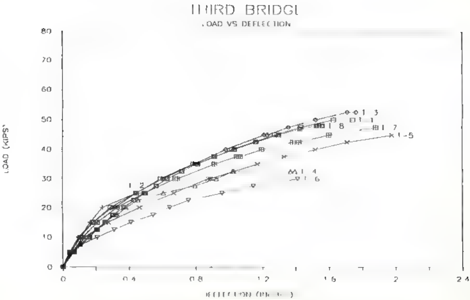

Figure 3.3 General Load-Deflection Curves for Specimen Three

Table 3.1 Summary of Maximum Loads and Deflections

	Load Pattern			Test Result				Test Result Converted to Full Scale	
Position	(Number of imprints)	Specimen	Test	Yield Load (Kips)	Maximum Load (Kips)	Failure?	Maximum Deflection in	Maximum Load (Kips)	Maximum Deflection (in.)
Interior (1/2 of total bridge length)	Single	1	1	30	46.0	Yes	1.47	155.0	2.70
	Double	1	4	32.5	73.0	Yes	2.05	244.0	5.77
	Quadruple	2	1	40	70.0	No	1.55	330.0	3.58
	Quadruple	2	3	40	70.0	No	1.20	330.0	2.60
	Quadruple	3	1	35	52.5	Yes	1.74	331.0	4.37
	Quadruple	3	3	35	54.5	Yes	1.78	343.0	4.42
Interior (1/8 of total bridge length)	Single	1	6	25	37.5	Yes	1.78	158.0	3.28
	Double	1	5	27.5	46.0	Yes	1.69	127.0	3.11
	Quadruple	2	6	35	70.0	Yes	1.33	330.0	2.88
	Quadruple	2	8	35	59.0	Yes	1.49	325.0	3.23
	Quadruple	3	5	30	45.0	Yes	1.98	283.0	4.87
	Quadruple	3	7	30	47.5	Yes	1.88	288.0	4.72
Free Edge	Single	1	2	25	37.5	Yes	0.69	127.0	1.84
	Quadruple	2	2	25	50.0	No	0.67	235.0	1.45
	Quadruple	3	6	32.5	48.0	Yes	1.56	309.0	3.92
Free Corner	Single	1	9	10	19.5	Yes	0.37	66.0	0.56
	Quadruple	2	5	25	38.0	Yes	0.48	273.0	1.04
	Quadruple	3	6	15	30.0	Yes	1.41	189.0	3.54
Parapet Edge	Single	1	3	48	50.0	No	0.38	189.0	0.70
	Single	1	7	25	50.0	No	0.44	188.0	0.81
	Quadruple	2	4	25	60.0	No	0.51	282.0	1.11
	Quadruple	3	2	20	25.0	No*	0.50	158.0	1.28
Parapet Corner	Single	1	5	32.5	44.0	Yes	0.46	149.0	0.85
	Quadruple	2	7	25	55.0	Yes	0.25	259.0	0.54
	Quadruple	3	4	27.5	35.0	Yes	1.40	220.0	3.51

* Test stopped due to development of yield line for full length of specimen

Most of the tests were continued to complete failure. However, seven of the tests, as shown in Table 3.1., were stopped prior to failure. All of these except one were stopped due to limitations of the test set-up. The one exception was test T-2 on specimen 3, which was stopped because of the development of a negative moment yield line over the full length of the specimen. It was felt that to continue this test would make further testing anywhere on that side of the specimen completely unrepresentative of an actual undamaged deck. Note, however, that for all of the above seven tests the maximum loads raised to full scale were well beyond any reasonable highway loading.

3.2 Interior tests

This section describes the behavior of the specimen during the interior tests. Comparison of the maximum loads and the loads at which a flexural yield pattern was well developed in the deck in Table 3.1 indicate the reserve strength of the deck relative to the load associated with the flexural yield mechanism. The reserve strength beyond yielding was certainly considerable, even though the transverse span to thickness ratio was as high as 22, as opposed to the maximum of 15 in the Ontario Code. In-plane forces were developed in the slab which certainly increased the punching shear capacity of the slab but did not seem to significantly affect the response of the beams and bracing, as was reflected in the stress calculations of in-plane

forces and bracing forces using the Finite Element Method, as will be discussed in Section 7.4. Observation of the deflection response of the slab in cases where the welds failed indicated a considerable increase in the deflection of the slab after the bracing failed without increasing the load, but it is difficult to say how much of the reduction of the strength was due to this effect. Although the presence of bracing seems to increase the strength of the slab, this increase seems to be considerably less for smaller transverse span to thickness ratios, such as those reported in the Texas report, which concluded that the bracing has little effect.

Observation of the deflection response of the girders provided some insight on the relative importance of the bracing for loading at various locations and for various ratios of transverse span to thickness. For load on the interior span adjacent to the free edge, the two adjacent girders indicated approximately equal load distribution until the welds in the bracing for the loaded span failed. After the welds in the bracing had failed, the deflection of the inner girder became greater than the deflection of the girder adjacent to the free edge, indicating a redistribution of load toward the interior of the slab. (Figures 3.4, 3.5). For loading on the interior span adjacent to the parapet, however, the relative deflection of the two girders adjacent to the load was not affected by the failure of the welds in the bracing (Figures 3.6, 3.7).

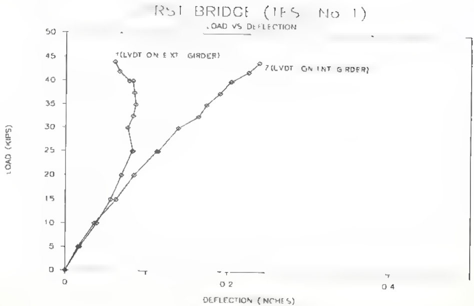

Figure 3.4 Load-Deflection Curves of Girders (First Bridge-Test No 1)

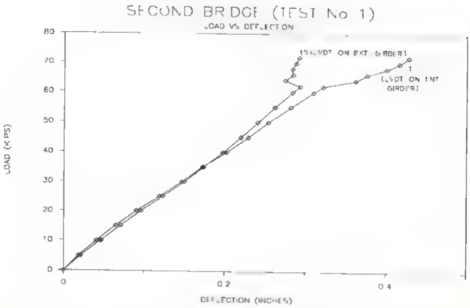

Figure 3.5 Load-Deflection Curves of Girders (Second Bridge-Test No 1)

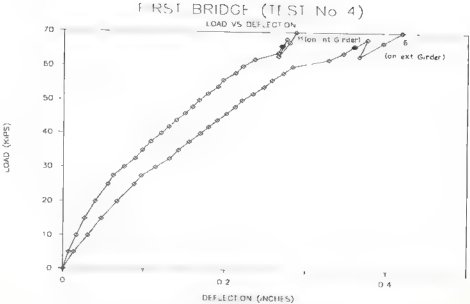

Figure 3.6 Load-Deflection Curves of Girders (First Bridge-Test No 4)

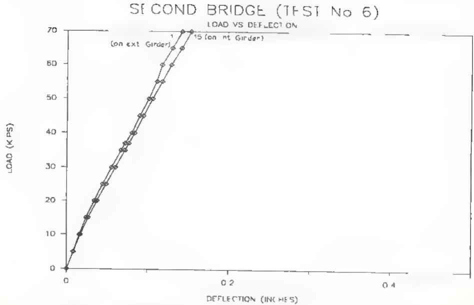

Figure 3.7 Load-Deflection Curves of Girders (Second Bridge-Test No 6)

However, the ratio of overhang to slab thickness was significant in this case, as specimen 1, with the lowest ratio of overhang to slab thickness indicated greater deflection for the girder adjacent to the parapet, indicating that the parapet drew some load from the adjacent slab. For specimens 2 and 3, with larger overhangs, the deflection of the two adjacent beams were approximately equal, indicating that this transfer of load to the parapet was no longer as significant.

The effect of the overhang to thickness ratios on the response of interior spans is further indicated in the punching shear strengths. As indicated in Table 3.1, for specimen 1, with the lowest overhang to thickness ratio, the punching load for the interior span adjacent to the parapet was approximately 40% higher than for the interior span adjacent to the free edge. For the other two specimens, with their larger overhang to thickness ratios, the parapet did not have such an effect upon the boundary conditions of the interior spans, as the punching loads for the interior span adjacent to the parapet was approximately equal to that for the interior span adjacent to the free edge.

Appendix E shows the observed crack patterns for the various tests. The crack was initiated at the bottom of the slab at approximately 25 to 30% to the ultimate load, while the crack at the top of the slab was initiated at approximately 50% of the ultimate load. When the load

reached 65 to 70% of the ultimate load the crack width on top of the bridge became significant (almost 0.01".). The mode of failure for all interior tests was clearly punching. For specimen 1, in places where a single wheel load was applied the punching area was considerable less than the entire width of the panel between girders, with a circular pattern of cracks on the top and a radial pattern on the bottom of the slab. For specimen 2, with four-point loading, there was some tendency for the pattern to not be as circular and to involve rather an elliptical pattern, perhaps reflecting the proximity of the load plates to the steel girders. For specimen 3, with its greater span between girders, the yield lines closely followed a circular pattern, and the cracks involved the entire width of the panel between girders and an approximately equal distance along the length of the slab. The number of cracks developed reflected the typical behavior of thin slabs, in that there was a broad band of relatively small cracks.

The basic ductility inherent in the failure mechanism for all interior tests was apparent in the nonlinearity of the load deflection relations and the large magnitude of the deflections, shown in Figures 3.1, 3.2 and 3.3.

The punching shear failure for thinner slabs, such as the specimens tested, tended to be more plastic rather than brittle, and this is evidenced by the fact that the

load deflection diagrams exhibited a longer plastic yield plateau.

From the strain gages, it was observed that the strains in the concrete went up to 0.0023 (first specimen) before failure with an average maximum strain of 0.0014 for all the interior tests in all the specimens tested. The measured strain indicated that both top and bottom, longitudinal steel did not yield, but that the transverse steel provided on the middle span had, in all cases, yielded when the load levels exceeded the yield loads listed in Table 3.1. The change in steel strain associated with the yield loads in Table 3.1 are indicated by the abrupt change in slope in Figures 3.8, 3.9 and 3.10.

From the load-deflection curves (Figure B.8 in Appendix B), it was observed that the deflections corresponding to the centerline of the girders have negative values for the final stages of loading, which is contrary to what can be expected. The apparent reason for this was that the real position of the LVDTs were not at the centerline of the girders, but were somewhat offset, such that rotation of the slab above the girder and twisting of the girder affected the LVDT reading.

In the interior tests in the span adjacent to the parapet, vertical and diagonal cracks were observed in the parapet just before the slab failed.

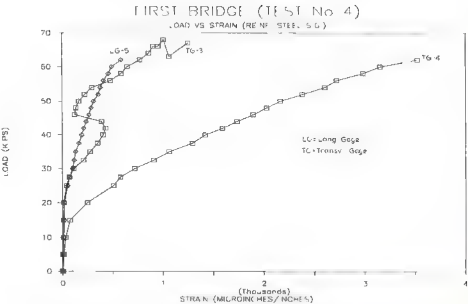

Figure 3.8 Load-Strain Curves (First Bridge, Test No 4, Reinforced Steel S.G.)

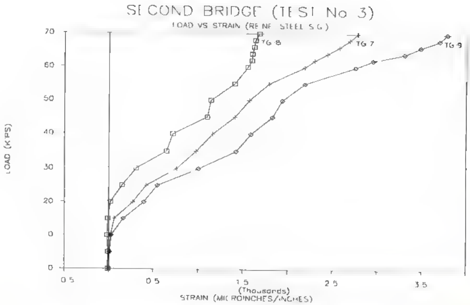

Figure 3.9 Load-Strain Curves (Second Bridge, Test No 3, Reinforced Steel S.G.)

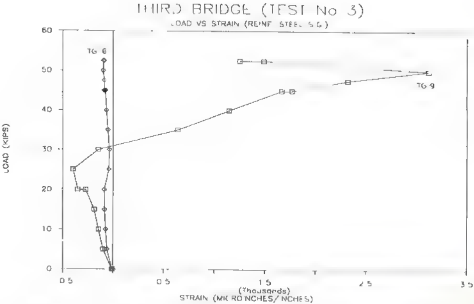

Figure 3.10 Load-Strain Curves (Third Bridge, Test No 3, Reinforced Steel S.G.)

3.3 Free Edge Within-Span and Corner Tests

This section discusses the behavior of the tests on the side of the bridge without the parapet, either within the span or at the corners. For all specimens, the yield lines on the overhang followed a half of an ellipse pattern, and as indicated in Table 3.1, implied considerable reserve capacity beyond the load at which the yield line pattern was well developed. This reserve capacity was evidently aided by the presence of the longitudinal steel, the additional transverse steel present at the edge and the ductility of the steel. For specimen 1 the failure load for the midspan edge was equal to the lowest failure load recorded for the interior tests. For specimen 2 the midspan edge had still not failed at 50 kips, and this increase in capacity was because of the location of the tandem load, as only two of the four wheels are located at the edge, with the other two wheels being located on the interior span, adjacent to the exterior girder. This manifested itself in an additional elliptical yield pattern in the interior span adjacent to the girder. In this manner the exterior girder participated directly in carrying the load, removing some load from the slab. For specimen 3 the test corresponding to the midspan edge was not possible because of previous damage related to the first test, so the location was shifted to approximately quarter span. In this location the failure was recorded at 49 kips, indicating higher strength as compared with tests

on interior spans at 1/6 of the total bridge length. Only one yield pattern was observed because the length of the overhang caused the two interior wheels of the tandem load to be extremely close to the flange of the exterior girder.

The yield lines on the corner, followed a quarter of an ellipse. For specimen 1, the failure load was only 19.5 kips, approximately half of the load attained in the midspan edge. For specimen 2, the corner had failed only after the load level was 58 kips, and this increase in capacity was because of the location of the tandem load, as only two of the four wheels were located at the corner, with the other two wheels being located on the interior span, adjacent to the exterior girder. This manifested itself in an additional semi-elliptical yield pattern in the interior span adjacent to the girder, which happened to be the region where the slab failed. For specimen 3, the corner had failed at 30 kips. Only one yield pattern was observed because the length of the overhang caused the two interior wheels of the tandem load to be extremely close to the flange of the exterior girder.

3.4 Parapet Within-Span and Corner Tests

This section discusses the behavior of the test on the side of the bridge with the parapet, either within the span or at the corners. Considering the behavior of the free edge, the reserve capacity of the parapet edge is not surprising. A major aspect of these results was the strong

interaction of the parapet with the slab. This was illustrated by load-deflection stiffnesses, which for both specimens were highest for the parapet edge tests, by the fact that for specimen 1 all three parapet edge tests involved the formation of wide inclined cracks over the entire height of the parapet, that failure was not attained for either specimen one or two at midspan, even though comparable interior tests failed at loads lower or not much higher than the maximum applied, and from the observation in specimen 2 that failure during the corner test occurred only when the deck vertically separated from the parapet. Furthermore the strength and stiffness of this region was illustrated by the fact that cracks over the entire height of the parapet, occurred after the load exceeded approximately 70% of the maximum load.

However, the development of a negative moment yield line over the full length of the specimen, for test T-2 on specimen 3, points out that some considerations of yield line theory should be given for the overhang condition.

From all tests it was clear that the yield line mechanism for parapet edge followed a line parallel to the parapet and directly above the center of the exterior beam. The fact that the first specimen perform relatively well in comparison with the second and third specimen was apparently related to the presence of additional transverse steel in the overhanging portion of the first specimen. For the second specimen, the test adjacent to the parapet

did not produce any new yield lines. Rather the yield lines caused by previous tests in the adjacent interior span were enhanced. This was apparently related to the reduced overhang relative to the first specimen, causing the location of the two interior wheels to be well into the interior span and the two exterior wheels to be on the overhang, but very close to the exterior girder.

3.5 Comparison to Highway Loads

The AASHTO axle load for a single axle with dual wheels is 32 kips, implying 16 kips on each dual tire pattern. Using an impact factor of 0.3, and a load factor of 2.2 implies a required ultimate wheel load of 59 kips. This is less than the maximum load (converted to full scale) for any of the single imprint tests, less than one half the load for any of the dual imprint tests, and less than one fourth the load for any of the four imprint (tandem) tests, with only four exceptions. All four of the exceptions occurred for the tandem loadings. And, as discussed subsequently, the assumption of two AASHTO axle loads in a single tandem is very conservative. Also, none of the exceptions occurred in the interior test; not even for the maximum S/T ratio of 22 (Figure 2.1).

One of the exceptions occurred in the free edge test for specimen 2, and for this test the maximum load recorded was not based on a slab failure. Also, it should be noted that the corresponding test for specimen 3, with a larger

B/T ratio carried a full scale tandem load of 306 kips implying a wheel load of 76 kips, well above 59 kips. The other three exceptions were in the overhangs for specimen #3 with the very high A/T and B/T ratios (Figure 2.1).

Evaluating the results in the above manner is very conservative, as it is unlikely for a tandem assembly to reach the individual design loads for a single axle. The results could be evaluated in a somewhat different manner based on the heaviest commercial axle, which is rated at 23 kips. Applying a safety factor of 2.5 results in an ultimate axle load of 57.5 kips, which translates into 28.75 kips on one dual tire formation, 57.5 kips on two dual tire formations, and 115 kips total on an entire tandem assembly. All of the full scale maximum applied loads in Table 3.1 exceed these levels by a considerable margin, even those for the overhangs of specimen number three. Clearly the isotropically reinforced slabs have a tremendous reserve load capacity compared to typical highway vehicle loads.

CHAPTER 4
BEHAVIOR OF TEST SPECIMENS ON STEEL GIRDERS SUBJECTED TO DYNAMIC LOADING

4.1 General

A specimen identical to the second specimen was tested under repeated loading, meant to asses the durability of the isotropically reinforced slabs under cyclic fatigue loading.

As for the previous specimens, the specimen was loaded at several locations, each constituting a test. For each test location a service-level static load was first applied to create a cracked condition in the specimen at that location, it being deemed not realistic to test an uncracked specimen for durability.

Five million cycles of fatigue loading, following a sinusoidal wave with a peak value of 16 kips and a frequency of 7 Hz. was applied. As for the static tests, the load applied was a four point loading representing a tandem assembly. At the completion of fatigue testing for all locations, each location was loaded statically to failure in succession.

4.2 Loading and Instrumentation

During the lifetime of the bridge, bridge decks will be subjected to a mix of traffic truck weights and the expected number of stress cycles in most bridges will be between 10 million and 150 million cycles. Therefore in testing, it could be impractical to apply a typical number of cycles to a bridge (100 million cycles) because of the amount of time required. Also it would be desirable to be able to apply one load instead of a mix or random loads.

The effective weight for a given traffic to represent a mix of traffic truck weights can be selected so that the fatigue damage caused by a given number of passages of a truck of this weight is the same as the fatigue damage caused by an equal number of passages of trucks of different weights in the actual traffic. Therefore an effective gross truck weight W, based on Miner's Law and developed from extensive fatigue tests can be expressed as:

$$W=(\Sigma f_i W_i^3)^{0.333} \text{ .... (1)}$$

where f_i is the fraction of gross weights within interval i and W_i is the weight corresponding to the midwidth of interval i. Using this procedure the basic weight of the fatigue truck was found for typical traffic patterns in ref.[19] to be 54 kips. This actual truck traffic spectrum was determined from recent weight-in-motion studies that

included 30 sites nationwide and over 27,000 observed trucks [19].

In order to transform this truck weight to the load on a tandem assembly it is necessary to multiply the total effective weight by the recommended AASHTO factor for weight distribution within the design truck. Consequently the load to use will be 21.6 Kips (54*0.4).

For typical vehicles with a speed of 60 mph going through a bridge of approximately 100 ft. the transit time (1 cycle) will be 0.01894 minutes, representing a frequency of almost 1 Hz. Furthermore it was found that a rate of testing between 1 and 7 Hz. has little or no effect on the fatigue strength of plain concrete [20]. Consequently the frequency of loading selected was approximately 7 Hz, considering that such a rate would enable a reasonable number of cycles to be applied in a reasonable time, yet still induce response similar to that occurring in the field. Applying 7 Hz. for 100 million cycles would require approximately 165 days of continuous testing, which is unreasonable. Therefore a reduction in the number of cycles was still needed.

Several studies have demonstrated that the variation of fatigue life (Y_f) in years (Power Law) with load can be expressed as:

$$Y_f = fKx10^6/(T_a C[R_s S_r]^3) \; ...... \; (4.2)$$

in which T_a is the estimated lifetime average daily truck

volume, C is the cycles per truck passage, a is the age of the bridge in years, S_r is the Stress and R_s is the factor on stress, and f and K are factors, based on allowable fatigue stresses proposed in studies at Lehigh University [21] and adopted by AASHTO[2].

Assuming that during its lifetime the bridge is subjected to 100 million cycles of the 21.6 kip tandem assembly load described previously, it is possible to use Equation 4.2 to compute the load which could be assumed to create the same level of damage in 5 million cycles.

It should be noted that even though some studies [13], have demonstrated that a given number of repetitions of moving wheel-loads could cause more damage to the slab than the same number of fixed pulsating repetitions, the maximum number of cycles selected was in accordance with AASHTO recommendations.

Assuming a particular cycling frequency, Y_f is directly proportional to the number of cycles applied. Therefore

$$\frac{N_{Test}}{N_{Field}} = \frac{fKx10^6/(T_aC[R_sS_{Test}]^3)}{fKx10^6/(T_aC[R_sS_{Field}]^3)} \quad \ldots.(4.3)$$

The objective is:

$$\frac{N_{Test}}{N_{Field}} = \frac{5}{100}$$

Hence, from Equation 4.3:

$$\frac{5}{100} = \frac{1/S^3{}_{Test}}{1/S^3{}_{Field}} = \frac{1/P^3{}_{Test}}{1/P^3{}_{Field}} \quad \ldots\ldots\ldots (4.4)$$

using P_{Yield}=21.6 Kips, the load P required for the test will be 58.6 Kips in full scale, which translated to the model, using a scale factor of 2.16 is equivalent to a load of approximately 13 Kips. Also considered were the results of the static tests, it being desired that the deck remain below its yield load during dynamic testing, as gross nonlinearity probably render Miner's Law and the Power Law not usable.

Before applying the dynamic load, a static load of approximately 20 kips was applied to assure that the bridge was in a cracked condition, representing previously applied loads, when dynamic testing was initiated, it being considered unrealistic to test an uncracked bridge.

The positions of the tandem load pattern for the preload and for the dynamic loading are shown in Figure 4.1. As for previous specimens, each loading position will be referred to as a test. A 50 kip capacity MTS actuator under load control was used for the loading.

Deflections from a total of 7 LVDTs and strains from four strain gages, together with the load were recorded. Complete deflection and strain response histories, are provided in Appendix I for all the test positions.

It was desired to monitor the variation of particular slab deflections or particular strains with the number of loading cycles, so as to identify any specimen deterioration with cycling. Because of the test durations it was both unnecessary and impractical to continually

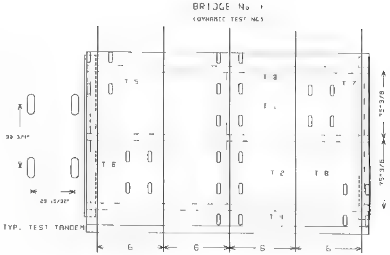

Figure 4.1 Loading Positions for Specimen Four (Dynamic Testing)

monitor deflections or strains. Rather deflections or strains were monitored for numerous intervals spaced throughout the duration of loading, with each interval representing approximately 7 cycles of loading.

The variation of deflections for a typical interval, i, is shown in Figure 4.2. A characteristic peak displacement for each interval was determined visually from plots such as those in Figure 4.2. These peak displacements were then plotted against the number of loading cycles before interval i, in plots such as Figure 4.3. Least squares curve fitting was then used to apply polynomial equations to the variation of peak deflection or strain with cycles, as in Figure 4.4. The results are shown for all the eight tests in Figure 4.5, where a separate curve is provided for each test. Each curve is labeled T-j, where j represents the test number whose locations are shown in Figure 4.1.

Deflections measured at 16 kips during the preload for each test, as well as deflections measured during the early stages of fatigue and deflections during the late stages of fatigue loading, are listed in Table 4.1.

For all test locations except one, after completion of the dynamic loading, static loading up to failure was applied to compare static test results after dynamic loading to that on an undamaged specimen. The single exception was the free corner test, which failed after applying 2,100,000 cycles.

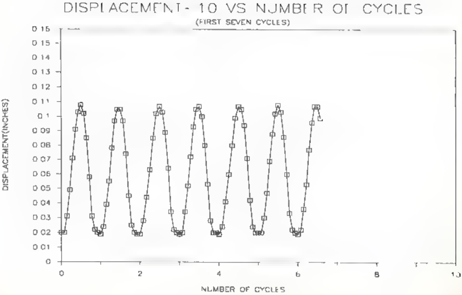

Figure 4.2 Typical Reading of Dynamic Testing

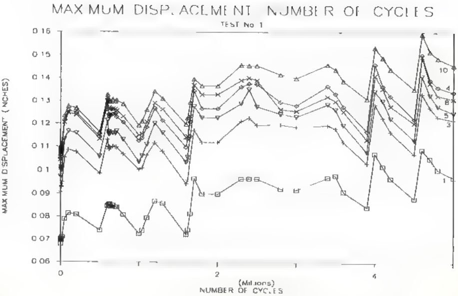

Figure 4.3 Maximum Displacement-Number of Cycles (Test No 1)

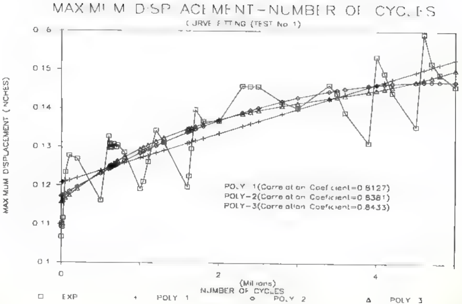

Figure 4.4 Curve Fitting (Test No 1)

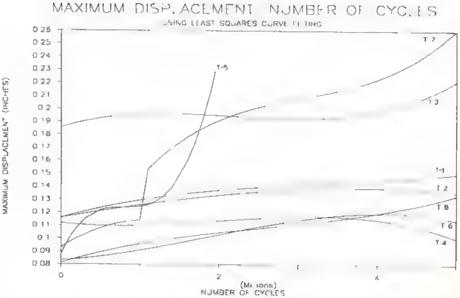

Figure 4.5 General Maximum Displacement-Number of Cycles Curves for Specimen 4

Table 4.1 Comparison of Deflections for Specimen 4 at Preload, Early and Late Stages

Position	Load Pattern (Number of imprints)	Stage	Test	Applied Load (Kips)	Test Result: Maximum Deflection (in.)	Test Result: Maximum Stiffness (K/in)	Test Result: % of Change of Deflection
Interior (1,2 of total bridge length)	Quadruple	Preload	1	16	0.115	139.13	
		Early	1	16	0.118	137.93	
		Late	1	16	0.145	110.34	28
	Quadruple	Before	2	16	0.115	139.13	
		Early	2	16	0.115	139.13	
		Late	2	16	0.135	118.52	17
Interior (1.5 of total bridge length)	Quadruple	Preload	6	16	0.085	188.23	
		Early	6	16	0.083	192.77	
		Late	6	16	0.117	136.75	40
	Quadruple	Preload	7	16	0.085	188.23	
		Early	7	16	0.088	181.82	
		Late	7	16	0.250	64.00	184
Free Edge	Quadruple	Preload	3	16	0.188	85.11	
		Early	3	16	0.185	86.49	
		Late	3	16	0.210	76.19	13
Free Corner	Quadruple	Preload	5	16	0.085	188.23	
		Early	5	16	0.085	188.05	
		Late	5	16	*		
Parapet Edge	Quadruple	Preload	4	16	0.11	145.45	
		Early	4	16	0.11	137.93	
		Late	4	16	0.111	144.14	1
Parapet Corner	Quadruple	Preload	8	16	0.060	266.67	
		Early	8	16	0.082	195.12	
		Late	8	16	0.131	118.52	60

4.3 Preload and Dynamic Loading

4.3.1 Interior Tests

This section describes the behavior of the specimen during the interior tests.

For all of these tests, when applying the preload, the cracks started to develop in the bottom of the slab at approximately 18 kips. The dynamic behavior for each test is discussed below:

4.3.1.1 First test

This test was located adjacent to the free edge, at midspan as shown in Figure 4.1. Table 4.1 lists a 25% increment in the maximum deflection between early and late stages of dynamic loading. This was a gradual increase as observed in Figure 4.5. New cracks started to form on the bottom of the slab at about 2,300,000 cycles, following a radial pattern, while the cracks on the top of the slab appeared only after 5 million cycles. The crack width under the load of 16 kips, reached a value of almost 0.01" on the bottom of the slab, as opposed to being barely noticeable under the 16 kip preload, while the width of the crack on top of the slab was considerable less than 0.01 during dynamic loading, and nonexistent during the preload.

4.3.1.2 Second test

This test was located adjacent to the parapet, at midspan, as shown in Figure 4.1. Referring to Table 4.1, there was a 17% increase in the maximum deflection during dynamic loading. Again the increase was gradual and tended

to stabilize, as shown in Figure 4.5. New cracks started to form on the bottom of the slab at about 1 million cycles following a radial pattern, while the cracks on the top of the slab appeared only after 5 million cycles. The crack width during dynamic testing, reached a value of 0.01" on the bottom of the slab while the crack on top of the slab was considerable less. Again these widths represented considerable increase relative to cracking under the static preload.

4.3.1.3 Sixth test

This test was located adjacent to the parapet at 1/6 of the total bridge length, as shown in Figure 4.1. There was a 40% increase in the maximum deflection of the slab during the dynamic loading, which again was gradual and tended to stabilize, as shown in Figure 4.5. New cracks started to form on the bottom of the slab after 70,000 cycles oriented in both longitudinal and transverse directions. The crack width during later stages of dynamic loading was less than 0.016" on the bottom of the slab, while the crack on top of the slab was less than 0.01". Again, these represented increased widths relative to preload, where only hairline cracks were observed.

4.3.1.4 Seventh test

This test was located at 1/6 of the total bridge length, closer to the free overhang as shown in Figure 4.1. As observed in Table 4.1, the total increase in maximum deflection during dynamic loading was as much as as 184%.

Before one million cycles had been applied, the welds in the bracing failed, causing a sudden increase in the maximum deflection of about 54% as shown in Figure 4.6, after which there was the more typical gradual increase in the maximum deflection. The deterioration in the slab seemed to be severe, and was reflected by the increase in crack widths after the welds in the bracing failed. After these weld failures had occurred, crack widths of more than 0.032" at the bottom of the slab were observed. The cracks on the top of the slab appeared at 3 million cycles and the crack width was less than 0.01" after 5 million cycles.

4.3.2 Free Edge Within-Span and Corner Tests

This section describes the behavior of the tests on the side of the bridge without the parapet, either within the span or at the corners.

For the test on the free edge within- span, when applying the preload, no cracks were observed. In the case of the corner test the cracks started to develop on the top of the slab at approximately 8 kips. The yield lines followed a quarter ellipse pattern after completion of the preload. Again dynamic tests produced significant additional cracks and deflections, and the behavior is discussed below:

4.3.2.1 Free Edge Within-Span Test

As observed in Table 4.1, the increase in deflection was moderate, being on the order of only 13%. Cracks were developed on the top of the slab only after 5 million

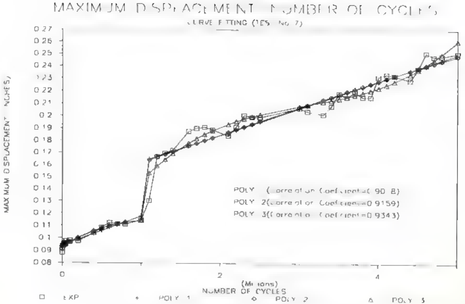

Figure 4.6 Maximum Displacement-Number of Cycles Curves (Test No 7)

cycles and had semi-elliptical yield pattern. The crack width was considerably less than 0.01". No cracks were developed on the bottom.

4.3.2.2 Corner Test

After 70,000 cycles, a shear crack, with a width of approximately 0.01" was observed to extend over the thickness of the slab, at the end of the span and at the edge. These were connected by a crack along the top of the slab. After 1,300,000 cycles, the crack width, both on the top and at the edges, was rapidly enhanced, and after 1,900,000 cycles the crack width became almost 0.125". The slab failed after 2,100,000 cycles.

4.3.3 Parapet Within-Span and Corner Tests

This section discusses the behavior of the tests on the overhang of the bridge adjacent to the parapet, either within the span or at the corners.

For the test within the span, when applying the preload, no cracks were developed. In the case of the corner test the formation of cracks started at 10 kips. The cracks followed a longitudinal direction above the center of the steel beam and on top of the slab, extending through the thickness at the end of the slab.

4.3.3.1 Parapet Within-Span Test

There was no observed deterioration of the slab at all during this dynamic test, the increase in the maximum deflection being less than 1%, and no cracks being developed.

4.3.3.2 Corner Test

As shown in Table 4.1 the increase in the maximum deflection during the dynamic loading was significant (60%). After 3 million cycles, new cracks were developed on top of the slab above the flange of the steel beam. Also one longitudinal crack, as well as one crack oriented approximately at 45° between longitudinal and transverse direction were developed on the bottom of the slab in the adjacent interior span, and close to the flange tip of the steel beam. After 5 million cycles, two new cracks had developed on top of the slab, one at the end of the slab and close to the parapet and another in the adjacent interior span, following a semicircular crack pattern. The crack width during the dynamic testing, was maintained below 0.01" on the top of the slab as well as on the bottom.

4.4 Static Loading

This section describes the behavior of the specimen during the static tests to failure that were performed after the dynamic loading was completed. These test results are compared with those on an undamaged specimen. The general load-deflection response is shown in Figure 4.7 as variation of total applied load with maximum deflection. The specimen was tested at several locations, in essence there were several tests for the specimen. A separate curve is provided for each test location in Figure 4.8.

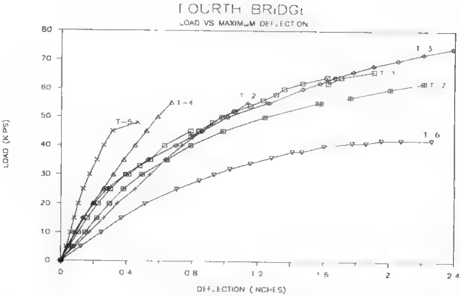

Figure 4.7 General Load-Deflection Curves for Specimen 4

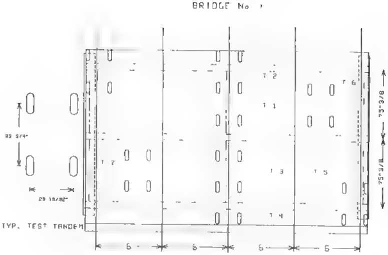

Figure 4.8 Loading Positions for Specimen Four (Static Testing)

Each curve is labeled T-i where i represents the test number. Note in Figure 4.8 that the specimen was tested statically in the same locations as for the dynamic tests, and further that these locations corresponded to the static test locations for the identical specimen 2. Note however that the sequence in which the locations were tested varied somewhat because of the failures during dynamic testing, and the tests are numbered differently. Table 4.2, shows the maximum load attained during each test, the load at which a flexural yield pattern was well developed in the deck (yield load), and the maximum deflection during each test, along with the above results converted to full scale. It lists the above for both the undamaged specimen (specimen 2) and the damaged specimen (specimen 4). Full scale loads and deflections were obtained by multiplying the test values by the scale factor and the square of the scale factor for deflection and load values, respectively. The scale factor used was 2. Appendix H shows the deflection basins corresponding to the maximum applied loads.

Most of the tests were continued to complete failure. However, two of the tests as shown in Table 4.2 were stopped prior to failure due to limitations of the test set-up.

4.4.1 Interior tests

This section describes the behavior of the specimen during the interior tests. Comparison of the maximum loads

Table 4.2 Summary of Maximum Loads and Deflections (Static Tests on both undamaged and damaged specimens)

Position	Load Pattern (Number of imprints)	Specimen	Test	Test Result: Yield Load (Kips)	Test Result: Maximum Load (Kips)	Test Result: Failure?	Test Result: Maximum Deflection (in.)	Test Result Converted to Full Scale: Maximum Load (Kips)	Test Result Converted to Full Scale: Maximum Deflection (in.)
Interior (1/2 of total bridge length)	Quadruple	Undamag	1	40	70.0	No	1.65	330.0	3.58
	Quadruple	Damaged	1	35	86.0	Yes	1.81	331.0	4.44
	Quadruple	Undamag	3	40	70.0	No	1.20	330.0	2.60
	Quadruple	Damaged	3	35	74.0	Yes	2.38	344.0	5.19
Interior (1/8 of total bridge length)	Quadruple	Undamag	8	35	70.0	Yes	1.33	330.0	2.88
	Quadruple	Damaged	7	30	82.0	Yes	2.21	292.0	4.80
	Quadruple	Undamag	8	35	69.0	Yes	1.49	325.0	3.23
	Quadruple	Damaged	6	25	42.0	Yes	2.26	198.0	4.90
Free Edge	Quadruple	Undamag	2	25	50.0	No	0.57	235.0	1.45
	Quadruple	Damaged	2	25	55.0	No	1.15	259.0	2.48
Free Corner	Quadruple	Undamag	5	25	58.0	Yes	0.48	273.0	1.04
	Quadruple	Damaged	-	·		Yes		-	
Parapet Edge	Quadruple	Undamag	4	25	60.0	No	0.31	282.0	1.44
	Quadruple	Damaged	4	25	55.0	No	0.67	259.0	1.45
Parapet Corner	Quadruple	Undamag	7	25	55.0	Yes	0.25	258.0	0.56
	Quadruple	Damaged	5	20	45.0	Yes	0.47	228.0	1.02

and the loads at which a flexural yield pattern was well developed in the deck in Table 4.2 indicate the reserve strength of the deck relative to the load associated with the flexural yield mechanism. Also comparison of the maximum loads attained on the damaged specimen with those attained on the undamaged specimen (Table 4.2) shows a reduction in the load capacity of no more than 10%, except for one test (T-6) in which the deterioration of the slab after the dynamic test was severe and the reduction in the load capacity was more than 40%.

The presence of the parapet seemed to be relevant. Comparison of maximum loads attained in Table 4.2 showed higher capacities (more than 10%) in test locations adjacent to the parapet relative to the test location adjacent to the free overhang.

Appendix E, shows the observed crack patterns for the various tests, and they are described below:

4.4.1.1 First Test

This test was located adjacent to the free edge, at midspan of the bridge as indicated in Figure 4.8. After applying 20 kips, the crack width in the bottom of the slab was almost 0.016" and also new cracks started to appear. The crack width increased to 0.02" at 30 kips, the point at which the transverse steel in the middle of the slab yielded. At 35 kips the crack width at the bottom of the slab reached a value of 0.031" and cracks following a circular pattern appeared on the top of the slab with a

crack width less than 0.01". The welds in the bracing started to fail at 45 kips, causing a drop in the load of about 2 kips. At this stage the crack width in the top of the slab was almost 0.016". The final failure of the welds in the bracing happened only after the load applied was 66 kips, causing a redistribution of the forces in the beams and a drop in the load of about 5 kips.

The slab failed at 63 kips after reloading. At this stage, strain gages indicated a strain of 0.0005 in the concrete directly beneath the load.

4.4.1.2 Third Test

This test was located adjacent to the parapet, at midspan of the bridge as indicated in Figure 4.8. After applying 20 kips the crack width in the bottom of the slab was almost 0.016" and new cracks started to develop on the bottom of the slab. New cracks on the top of the slab appear at 25 kips. The crack width increased to 0.02" at 30 kips, the point at which the transverse steel in the middle of the slab yielded. At 35 kips the crack width at the bottom of the slab reached a value of 0.031" and cracks following a circular pattern appeared on the top of the slab with a crack width less than 0.01". At 40 kips one side of the welds in the bracing failed and it was observed that the crack patterns were fully developed (circular on the top and a fan pattern on the bottom). The final punching failure happened explosively at 72 kips, with complete failure of the bracing welds. At this stage

strains of 0.0006 were observed in the concrete directly beneath the load.

4.4.1.3 Sixth Test

This test was located adjacent to the free edge, at 1/6 of the bridge length. After applying 16 kips the crack width on the bottom of the slab was almost 0.125", and increased to 0.1875" at 20 kips, reaching a value of 0.25" at 30 kips, while the crack width on top of the slab was almost 0.0625". These later cracks on top of the slab however, were related to a previous adjacent test carried up to failure.

The failure occurred at 42 kips, with the deflection and cracking pattern indicating flexure, much like a one-way slab.

4.4.1.4 Seventh Test

This test was located adjacent to the parapet, at 1/6 of the bridge length. After applying 16 kips the cracks extended to the end of the slab and included the entire thickness. The crack width on the bottom of the slab reached a value of 0.063" at 35 kips and 0.125" at 40 kips, while the crack width on the top of the slab was 0.0625" at 50 kips and 0.125" at 55 kips.

The slab failed at 62 kips and strains of 0.001 were observed in the concrete directly beneath the load.

4.4.2 Free Edge Within-Span and Corner Tests

This section discusses the behavior of the test on the side of the bridge without the parapet, either within the

span or at the corners. The yield lines on the overhang followed a half of an ellipse pattern, and as indicated in Table 4.2, implied considerable reserve capacity beyond the load at which the yield line pattern was well developed. This reserve capacity was evidently aided by the presence of the longitudinal steel, the additional transverse steel present at the edge and the ductility of the steel. From Table 4.2 it is observed that the specimen had still not failed at 55 kips. This increase in capacity was due to the location of the tandem load, only two of the four wheels being located on the overhang, with the other two wheels being located on the interior span, adjacent to the exterior girder. In this manner the exterior girder participated directly in carrying the load, removing some load from the slab. The corner test, was not performed because of the complete failure that occurred during dynamic testing.

For the one free edge test performed, after 25 kips, the cracks started to follow a semi-elliptical pattern. The crack width increased to 0.001" only after the applied load was 50 kips, and increased to 0.016" when the load was 55 kips. No failure of the slab was observed and the test was stopped.

4.4.3 Parapet Within-Span and Corner Tests

This section discusses the behavior of the test on the side of the bridge with the parapet, either within the span

or at the corner. Considering the behavior of the free edge, the reserve capacity of the parapet edge is not surprising. A major aspect of these results was the strong interaction of the parapet with the slab. This was illustrated by load-deflection stiffnesses, which were highest for the parapet edge test and by the fact that the parapet edge test involved the formation of wide inclined cracks over the entire height of the parapet.

Additional description is provided below.

4.4.3.1 Parapet Within-Span Test

After 20 kips, new cracks were observed on the top of the slab along the exterior girder and previous longitudinal cracks on the bottom of the interior span of the slab were enhanced. Cracks on the parapet appeared at 35 kips. The specimen had still not failed at 55 kips.

4.4.3.2 Corner Test

At 15 kips new cracks were developed on the bottom part of the slab at midspan of the adjacent interior span. These cracks were oriented longitudinally and extended to the end of the slab, indicating a flexural response. At 30 kips the width of these cracks increased to 0.001".

For loads above 35 kips, an additional semi-elliptical yield pattern in the interior span adjacent to the girder developed around the wheel load immediately adjacent to the end of the span. At 45 kips the crack width in the semi-elliptical pattern on the top of the slab was almost 0.031", and the shear cracks extended through the

thickness. The slab failed at 48 kips with an isolated punching failure in this region.

4.5 Comparison to Highway Loads

The AASHTO ultimate wheel load of 59 kips (discussed in section 3.5) is less than one third the maximum load (converted to full scale) for any of the tests.

Evaluating the results using the heaviest commercial axle, which is rated at 23 kips, and using the factors mentioned in section 2.4 gives a 115 kips total on an entire tandem assembly. All of the full scale maximum applied loads in Table 4.2 exceed these levels by a considerable margin.

Comparison of the maximum loads attained for specimens subject only to static loading and specimens subjected first to dynamic loading and then static loading up to failure in Table 4.1, shows a slight reduction in the capacity (no more than 10%), except for one interior test carried out at 1/6 of the total length of the bridge, which had suffered considerable damage during dynamic loading, the bracing having failed, causing the specimen to respond inelastically during the process of dynamic loading. But, despite this situation, the isotropically reinforced slabs have performed well after cyclic loading and the durability as well as the strength had not been diminished severely.

CHAPTER 5
TEST PROGRAM OF SPECIMEN ON BULB-TEE GIRDERS AND PROCEDURES

5.1 Size and Scale Factors of Test Specimen

The cross-section of this specimen is shown in Figure 5.1.

Two Bulb-Tee girders with the size and dimensions shown in Figure 5.2 representing a modified half scale standard model of Florida Bulb-T Prestressed beam type FBT72 standard were used. As the goal of the test was to study the behavior of the concrete deck, and only the shape of the top flange of the bulb-tee girder, along with the girder's general level of flexural stiffness, would be expected to affect this behavior, only the top flange of the bulb tee girders was modeled precisely. This facilitated construction of the model. The web and lower part of the section was modified to provide proper levels of flexural and torsional stiffness, while facilitating ease in casting. Since prestressing the modeled beams could had been costly and difficult, nonprestressed reinforced concrete was used with the span of the model being adjusted to account for the fact that the model girder will respond as a cracked section over much of the range of loading. This cracking made it possible to model the overall stiffness of an 83 ft. span prototype with a 25

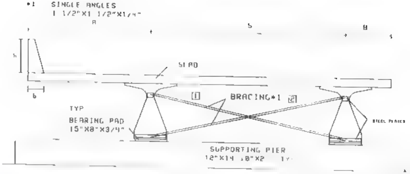

SPECIMEN	T	S	A	B	S/T	A/T	B/T	h	b	SCALE FACTOR
5	3 3/4"	90"	[illegible]	33	24	12	8.8	15.5	7.5	2

Figure 5.1 General Test Cross-Section

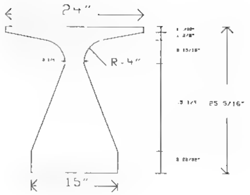

Figure 5.2 Cross-Section of Modified Bulb-Tee Girder

ft. span in the laboratory rather than the 42 ft. implied by a 1/2 scale model (Figure 5.3).

As the prototype is braced at the ends of the span, X braces were used to brace the model in the same manner. The X-braces were welded to small steel plates which were also welded to the rebars inside of the concrete beams at the two ends as shown in Figure 5.1. Two single angles 1¼"x1¼x¼" were used for the X-braces.

A parapet was located on one side of the specimen while the other side had only a plain overhang. In order to simplify the construction of the parapet the standard FDOT parapet was modified slightly, while closely maintaining the flexural and torsional stiffness properties, reduced to the appropriate scale.

The specimen was initially considered as having a span to thickness ratio (S/T) of 24, taking the effective span as center to center distance between beams, as in the case of steel beams. The prototype deck thickness selected was 7 1/2 inches which is a typical thickness in Florida. The table in Figure 5.1, shows the S/T, A/T and B/T ratios computed using the average thickness of the deck. The thicknesses were measured using a surveyors level and the results are shown in Appendix G.

The specimen was constructed with University of Florida personnel, expect for the finishing of the top of the concrete deck. Durastress Concrete provided

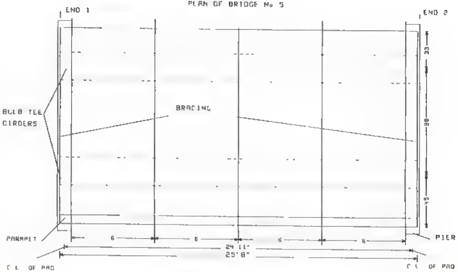

Figure 5.3 Plan View of Test Specimen

professional concrete finishers to assist in the placement and finishing of the concrete deck.

5.2 Material Properties of Specimens

For the scale factor of two, a 3/8" maximum size of aggregate was considered to be appropriate, which corresponded approximately to a 3/4" size aggregate in the prototype. Thus, the coarse aggregate used was FDOT designation #89. Because of the volume of concrete in the deck it was decided to use a ready mix concrete. The concrete mix was FDOT type II with a design strength of 3400 psi at 28 days. Average compressive strength at 28 days was 6020 psi.

Companion test cylinders and beams were cast at intervals during the casting period of the deck specimen, and were later tested to obtain the material properties.

The results of the cylinder compressive strength test, splitting tensile strength and modulus of rupture tests are shown in Appendix F. Also, Appendix F contains an aggregate gradation curve and typical concrete mix proportions.

For 0.3% isotropic reinforcement in a 7½" deck a typical reinforcement pattern would be #4 @ 13 1/3" and for the corresponding scale factor of approximately 2.0 this implies #2 @ 6 2/3". It was difficult to obtain deformed reinforcement of #2 size, deformed reinforcement being deemed desirable for bond. Furthermore it was difficult

to obtain typical levels of yield strength and deformation capacities, as most deformed wire available is usually cold drawn and has higher strength and less ductility than conventional reinforcement. Ivey Steel in Jacksonville Florida cooperated with the University of Florida to provide a steel wire with good ductility and a yield stress close to that for conventional reinforcement.

The stress-strain curve for the reinforcing wire, shown in Appendix F, indicates the well defined yield plateau, implying good ductility. The wire used in the specimens was nominally a D5 (A_b=.05in^2). However, the computed area based on weight was only about 0.0477 in^2. For the 0.0477 in^2 area the resulting yield stress was 72 ksi, which was deemed to be reasonable.

The Figure 5.4 shows the primary reinforcement (D5 wires) for the specimen. As for previous specimens, consistent with the Ontario method, the steel provided 0.3% reinforcement top and bottom in both directions. Extra transverse top bars were used on the side without the parapet, effectively doubling the reinforcement ratio in this region. Extra transverse reinforcement, approximately quadrupling the reinforcing ratio, was used in the ends of the section in both the top and bottom layers, to provide additional support at the discontinuous end of the slabs, as shown in Figure 5.4. The cover to the transverse top and bottom bars was 1 inch.

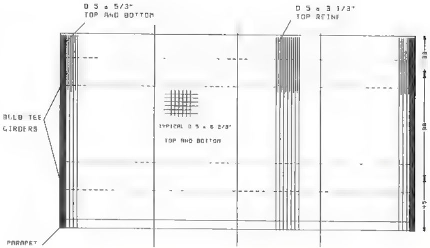

Figure 5.4 Reinforcement Spacing for Specimen

All reinforcing bars were tied appropriately with wires to secure the bars in each direction into a mat which was securely supported by chairs at the desired position in the slab to provide the required cover.

Strain gages installed on the reinforcing bars were waterproofed for protection prior to placing the bars. Wires leading to all instrumentation in concrete were marked to identify gage locations, and were taken out through holes in the forms prior to placing the concrete.

Figure 5.5 is a photograph of this specimen showing the general layout of the specimen.

5.3 Loading and Instrumentation

The deck was loaded in seven locations as shown in Figure 5.6. Each location constituted a test, and loading was applied to failure at each location similar to previous specimens. Loads were applied to the deck trough heavy steel plates, shaped and sized to model the imprint of one dual wheel formation at approximately half scale.

This specimen was loaded using a four-point loading, representing a complete tandem assembly. Dimensions of the prototype tandem were taken as 72 inches transversely and 51 inches longitudinally.

For the prototype, the maximum tandem load that the slab could reasonably need to carry was considered to be 153.3 kips (strongest commercially available unit with a

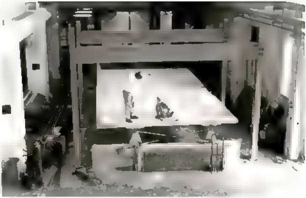

Figure 5.5 General Layout of Test Specimen

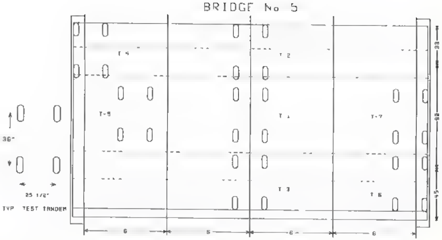

Figure 5.6 Loading Positions for Specimen Five

maximum service load of 23 kips and applying several factors) as discussed in Section 2.3.

As for previous specimens, Figure 2.8, shows a view of the load assembly used to apply the tandem loads. Two W6x25 sections were supported on rollers placed on top of the wheel pads. A W8x31 section spanned between the two lower steel sections and was loaded by the vertical hydraulic ram. Additional plates were welded on the beam to assure against local buckling of the test rig. The ram bore against a longitudinal beam that spanned between two lateral frames.

One hydraulic ram with 100 kips of capacity was used to apply the load. A load cell connected to a voltmeter was used to measure the loads. Before the test, the load cell was calibrated using the laboratory's 400 kip capacity Universal loading machine.

All specimens were instrumented with differential transformers (LVDTs) and electrical strain gages. The voltage readings of the LVDTs and strain gages were obtained using a HP 3497A Data acquisition control unit and were then transferred directly to a PC computer for further evaluation.

A total of 15 LVDTs arranged in a pattern such that they could define a deflection basin were used to measure vertical deflections. All LVDTs were supported on aluminum support beams. Appendix A shows the locations of the LVDTs for all tests and Appendix B gives complete

load-deflection plots for all tests. Appendix H, gives the deflection basins corresponding to the maximum load applied.

Electrical resistance strain gages were used at various locations on the specimen, including the top and bottom surfaces of the deck, on the reinforcement, on the longitudinal girders and on the bracing. Gages with two inch gage lengths and high endurance leadwires were used on the concrete surfaces, 0.031 inch gage length general purpose miniature gages were used on the reinforcing steel and 0.23 inch universal general purpose weldable gages were used on the steel angle braces. Appendix C gives the locations of the strain gages for the various tests and Appendix D contains all of the load-strain plots.

CHAPTER 6
BEHAVIOR OF TEST SPECIMENS ON BULB-TEE GIRDERS

6.1 General

The general load-deflection response and failure modes of the specimen are described in this chapter.

The general load-deflection response is shown in Figure 6.1 as variation of total applied load with maximum deflection. A separate curve is provided for each test in Figure 6.1. Each curve is labeled T-i where i represents the test number. The locations of the tests are shown in Figure 5.5. Table 6.1, shows the maximum load attained during each test, the load at which a flexural yield pattern was well developed in the deck (yield load), and the maximum deflection during each test, along with the above results converted to full scale. Full scale loads and deflections were obtained by multiplying the test values by the scale factor and the square of the scale factor for deflection and load values, respectively. The scale factor used was 2.

Appendix H shows the deflection basin corresponding to the maximum loads applied.

Most of the tests were continued to complete failure. However, two of the tests, as shown in Table 6.1, were stopped prior to failure. One of these two tests was test

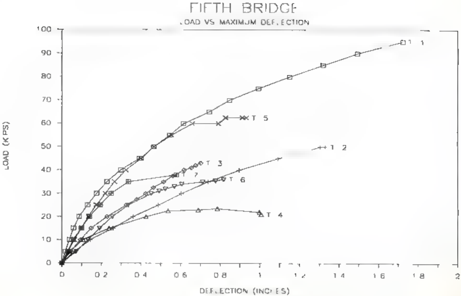

Figure 6.1 General Load-Deflection Curves for Specimen Five

Table 6.1 Summary of Maximum Loads and Deflections

Position	Load Pattern (Number of imprints)	Specimen	Test	Test Result: Yield Load (Kips)	Test Result: Maximum Load (Kips)	Test Result: Failure?	Test Result: Maximum Deflection (in.)	Test Result Converted to Full Scale: Maximum Load (Kips)	Test Result Converted to Full Scale: Maximum Deflection (in.)
Interior (1/2 of total bridge length)	Quadruple	5	1	45	95.0	Yes	1.72	380.0	3.44
Interior (1/8 of total bridge length)	Quadruple	5	5	45	65.0	No**	0.93	260.0	1.86
Interior (End)	Quadruple	5	7	35	38.0	Yes	0.58	152.0	1.16
Free Edge	Quadruple	5	2	25	55.0	Yes	1.34	220.0	2.68
Free Corner	Quadruple	5	4	20	23.5	Yes	1.00	94.0	2.00
Parapet Edge	Quadruple	5	3	25	43.0	No*	0.71	176.0	1.42
Parapet Corner	Quadruple	5	5	30	36.0	No*	0.82	144.0	1.64

* Test stopped due to development of yield line for full length of specimen

** Test stopped due to deterioration of the End-beam caused by bracing failure

No 5, which was located at approximately 1/6 of the length of the bridge, and was stopped when complete failure of the joint between the adjacent X-brace and the girder occurred. The other test for which the specimen was not failed was test No 3, which was located on the parapet edge within the span, and was stopped when a flexural crack developed along the entire length of the specimen.

6.2 Interior tests

This section describes the behavior of the interior tests. Comparison of the maximum loads and the loads at which a flexural yield pattern was well developed in the deck in Table 6.1 indicate the reserve strength of the deck relative to the load associated with the flexural yield mechanism. Only one test, Test No 7, adjacent to the end of the specimen, did not indicate large increase in load beyond that associated with yield. This failure was by punching, but it is reasonable to think that confinement could be much less significant at this discontinuous end.

Observing the measured deflection basin, it is apparent that little deflection occurred in the girder flanges. Apparently the increased thickness and strength in the flange region caused the cracking patterns to confined to the slab between flange tips.

The yield lines closely followed a circular pattern of cracks on the top and a radial pattern on the bottom of the slab, with the exception of the test No 7, which was

located at the end of the bridge, and exhibited a pattern of semi-circular cracks on the top. Details of each test are described below:

6.2.1 First Test

This test was located at midspan of the bridge. Relative to this test, some comments about the flexural response of the girders is appropriate. The variation of girder midspan deflection with load applied to the specimen in test No 1, is shown in Figure 6.2. After applying 20 kips the concrete girders started to crack at the bottom. This correlated well with the change in the slope of the deflection curve. Note that after this well-defined cracking point the stiffness of the girder remains constant for the rest of the test, maintaining a fully-cracked section.

The slab itself began to show some hairline cracks on the bottom surface at 20 kips. These became well defined at 30 kips. The crack width on the bottom of the slab increased to 0.01" at 40 kips and these cracks extended towards the ends of the slab. At 45 kips strain gages on the transverse reinforcement (Gage No GT-2) located in the middle of the slab, as shown in Figure 6.3, indicated yielding, (Figure 6.4) and cracks following a circular pattern appeared on the top of the slab with major cracks along the edges of the flanges of the concrete girders. The crack width in this region was 0.01" when the load applied was 60 kips. Vertical cracks developed on the

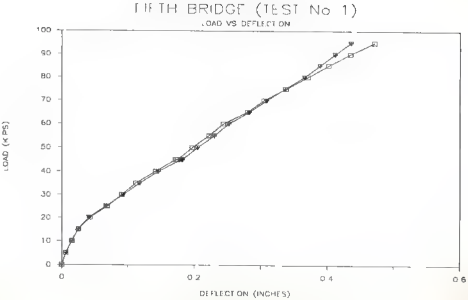

Figure 6.2 Load-Deflection Curves of Girders

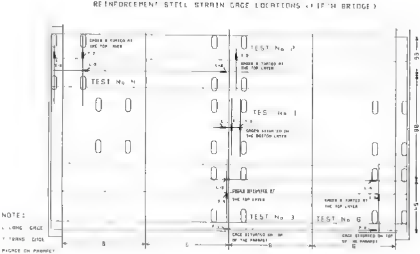

Figure 6.3 Reinforcement Steel Strain Gage Locations

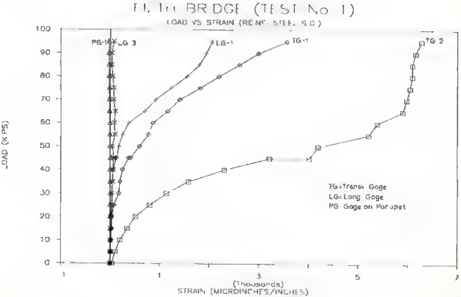

Figure 6.4 Load-Strain Curves (Fifth Bridge, Test No 1, Reinforced Steel S.G.)

exterior face of the parapet when the load level was 65 kips, these cracks appeared on the interior face of the parapet when the load level was 75 kips. At this stage the crack width on the top of the slab was almost 0.031".

The slab failed in an explosive manner at a load of 95 kips. At this point the longitudinal steel in the middle of the slab along with most of the transverse steel had not yielded. This was indicated by strain measurements of gages GL-1 and GT-1 (Figure 6.3), as shown in Figure 6.4.

6.2.2 Fifth Test

This test was located at 1/6 of the total length of the bridge. After applying 20 kips, cracks on the bottom of the slab first appeared and the crack width increased to 0.01" after 40 kips of load was applied. At 45 kips cracks started to appear on the top of the slab following a circular pattern with a major crack along the tip of the flange of the concrete girders. At 50 kips the crack width on the bottom of the slab was more then 0.016". At 55 kips, cracks on the top of the slab, produced by a previous adjacent test were significantly enhanced, and had a width of 0.031", accompanied by vertical faulting of the slab. After applying 65 kips the concrete surrounding the connection of the X-bracing to both adjacent girders started to spall, causing a drop in the load of about 5 kips. After reloading to 65 kips a new drop of more than 2 kips was registered caused by complete failure of the X-brace to girder connection. At this stage the test was stopped.

6.2.3 Seventh Test

This test was located at the end of the bridge. After applying 15 kips cracks appeared on the top and bottom part of the slab. These cracks were completely developed when the load applied was 35 kips, forming a semi-elliptical pattern on the top of the slab and encompassing both exterior load plates. The slab failed at 38 kips. This test was unusual in that there was damage to the flange of one girder. Toward the end of the test a horizontal crack occurred between the flange and the slab above it, indicating some loss of composite action. Shortly thereafter a vertical crack occurred over the entire thickness of the girder flange at the point where the steel terminated.

6.3 Free Edge Within-Span and Corner Tests

This section describes the behavior of the tests on the side of the bridge without the parapet, either within the span or at the corners.

For the test carried out on the free edge within the span, as shown in Table 6.1, there was considerable reserve load capacity beyond the load at which the yield line pattern was well developed. This reserve capacity was not observed for the corner test.

6.3.1 Free Edge Within-Span Test

After applying 15 kips cracks appeared on the top of the slab, following a semi-elliptical pattern. At 30 kips,

the transverse steel yielded (Figure 6.5) and the crack width increased to 0.01". This crack width increased to 0.047" when the applied load was 45 kips and reached a value of 0.063" when the load level was 50 kips. At this point there was visible vertical faulting of the slab at the widest cracks in the crack pattern. The slab failed at a load level of 55 kips.

6.3.2 Corner Test

After applying 15 kips, cracks appeared on the top of the slab following a quarter of an elliptical pattern. These cracks extended through the thickness of the slab. The transverse steel yielded completely when the load was 20 kips. At 22 kips shear cracks were formed on the slab edges, over the entire thickness of the slab, cracks widths increased tremendously at 23 kips, and the slab failed at 23.5 kips. After failure, it was apparent the crack was inclined for the entire length of the quarter ellipse pattern, extending from one slab edge to the other.

6.4 Parapet Within-Span and Corner Tests

This section discusses the behavior of the test on the side of the bridge with the parapet, either within the span or at the corners. Considering the behavior of the free edge, the reserve capacity of the parapet edge is not surprising. A major aspect of these results was the strong interaction of the parapet with the slab which was reflected by the presence of inclined cracks over the

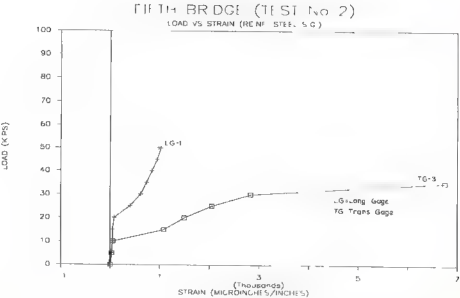

Figure 6.5 Load-Strain Curves (Fifth Bridge, Test No 2, Reinforced Steel S.G.)

entire height of the parapet. From these tests it was clear that the failure yield line mechanism constituted longitudinal flexural cracks in the slab along the tip of the flange of the concrete girder.

6.4.1 Parapet Within-Span Test

After applying 20 kips cracks started to develop along the tip of the flange of the concrete girder, starting at the ends of the bridge and extending more than 1/4 of the total bridge length in both sides. No cracks were observed on the bottom part of the slab. The transverse steel yielded at 30 kips (Figure 6.6). At 42 kips there was a visible vertical faulting of the slab, which became more serious at 43 kips and the test was stopped.

6.4.2 Corner Test

After applying 10 kips cracks associated with a previous adjacent test were enhanced. When the load level was 20 kips a vertical faulting of the slab became apparent. The vertical separation attained a magnitude of almost 0.047" at a load level of 30 kips, and had increased to 0.063" when the load level was 32 kips. The faulting continued to become more serious, and the test was stopped at 36 kips.

6.5 Comparison to Highway Loads

The AASHTO ultimate wheel load of 59 kips (discussed in Section 3.5) is less than the maximum load (converted to full scale) for the test carried out on the free corner,

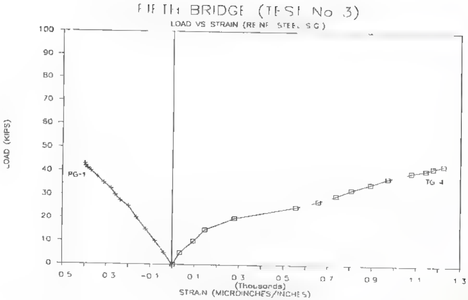

Figure 6.6 Load-Strain Curves (Fifth Bridge, Test No 3, Reinforced Steel S.G.)

less than one half for the test on the parapet corner, less than one third for the test on the free edge and parapet edge and less than one fourth for all the interior tests, except for the one test that was carried out at the end of the slab, which behaved almost as a free edge test.

Evaluating the results using the heaviest commercial axle and using the factor mentioned in Section 2.3 gives a 115 kips total load on an entire tandem assembly. All of the full scale maximum applied loads in Table 6.1 exceed these levels by a considerable margin, except the test carried out at the free corner, indicating that care should be taken in designing any sizeable overhangs.

CHAPTER 7
COMPARISON OF TEST RESULTS WITH ANALYTICAL MODELS

7.1 Theoretical Punching Shear Capacity

7.1.1 ACI Punching Shear Formula

Research studied by ACI-ASCE Committee 426 [20] indicated that the critical section for shear in slabs subjected to bending in two directions follows the perimeter at the edge of the loaded area.

A general punching shear model for a load applied on a rectangular footprint is shown in Figure 7.1. This model was used for the derivation of the ACI formula and assumed a failure surface which is propagated downward to the average effective depth of the section under consideration (d), following the same angle of inclination in all the four sides. From equilibrium:

$$V_c = (2d/\tan\theta)(b_1+b_2+2d/\tan\theta)\sqrt{f_c'}(2+4/\beta_c) \quad \ldots.(7.1)$$

where:

V_c= nominal shear strength from concrete

b_1, b_2= short and long sides of the footprint

β_c=Ratio of long side to short side of concentrated load, (β_c=b_2/b_1, and $\beta_c \le 2.0$)

$\sqrt{f_c'}$=Square root of specified compressive strength of concrete in psi.

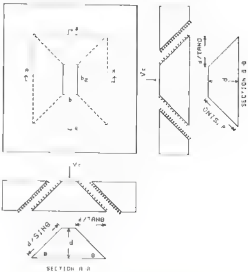

Figure 7.1 Plan and Sectional Views of Failure Surface (ACI Punching Shear Model)

Because of the difficulty in estimating the angle θ a value of 45 degrees was used in the ACI-ASCE formula:

$V_c = 2d(b_1+b_2+2d)\sqrt{fc'}(2+4/\beta_c)$ ....(7.2)

Some judgement was necessary in defining b_1 and b_2 for the single, double and four-point load patterns. These definitions are illustrated in Figure 7.2. Note that for four-point loading there are two alternate definitions. One is for the case in which crack patterns suggest that the four loads acted together, the other is for cases in which two distinctly separate crack patterns formed.

In cases where the tandem assembly straddled the girders, only the portion bearing on the overhang was considered, since this represented the critical condition.

7.1.2 AASHTO Punching Shear Formula

The AASHTO formula can be expressed as:

$V_c = 2(0.8+2/\beta_c)(b_1+b_2+2d)d\sqrt{fc'}$ ....(7.3)

but less than

$V_c = 2(1.8)(b_1+b_2+2d)d$

where all variables are defined as for Equation 7.1 and $\beta_c \leq 2.0$

The AASHTO formula is very similar to the ACI formula, but the AASHTO formula is more conservative.

7.2 Yield-Line Theory

Yield-line theory is an accepted method for computing an upper bound to the ultimate load capacity in flexure for a slab. In this theory the strength of a slab is assumed to be governed by flexure alone; other effects, such as

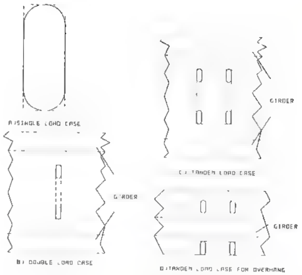

Figure 7.2 Idealized Loading Length

shear and deflection are to be separately considered. The steel reinforcement is assumed to be fully yielded along the yield lines at collapse and the bending and twisting moments are assumed to be uniformly distributed along the yield lines. Complete failure theoretically cannot occur until yielding has occurred at several locations so that a mechanism forms giving a condition of unstable equilibrium. Typical yield patterns, for calculation, taken to be consistent with test results, are shown in Figures 7.3 through 7.12, and the equations used for each case, along with one example calculation are presented in Appendix J.

7.3 Kinnunen and Nylander Model

7.3.1 Characteristics of Model

This model is the one extended by Hewitt [24], permitting the introduction of boundary restraints. These restraints include a boundary restraining moment, M_b, and a boundary restraining force, F_b, both per unit length of slab and acting at the level of the compression reinforcement at the boundary. Figure 7.13 shows the idealized model proposed for a restrained slab at punching failure, and indicates all forces acting, along with the symbols used in the development. The free body of Figure 7.13(b) represents a portion of the slab, including a sector of a circle between two radial cracks, as shown by a top view Figure 7.14. It is bounded on the outside by intact slab, which exerts boundary forces F_b and M_b, and

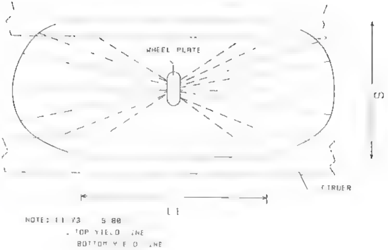

Figure 7.3 Assumed Yield-Line Pattern for Single Imprint Interior Test (Specimen 1)

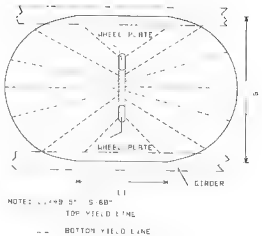

Figure 7.4 Assumed Yield-Line Pattern for Dual Imprint Interior Test (Specimen 1)

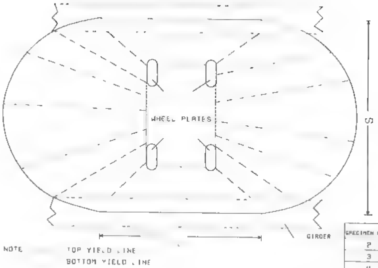

SPECIMEN No.	S	L
2	75.38	58.63
3	71.88	58.03
4	75.38	58.63

Figure 7.5 Assumed Yield-Line Pattern for Interior Tests (Specimens 2, 3, 4)

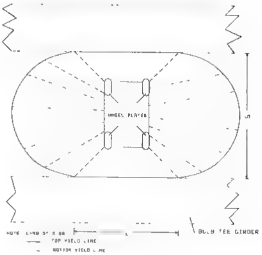

Figure 7.6 Assumed Yield-Line Pattern for Interior Tests (Specimen 5)

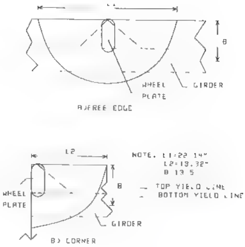

Figure 7.7 Assumed Yield-Line Pattern for Free Edge and Corner Tests (Specimen 1)

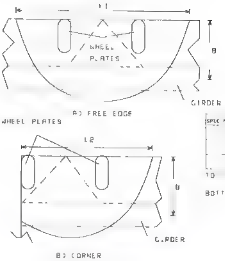

SPECIMEN No.	B	L1	L2
2	18 50	48 10	38.30
3	22 00	57 20	40 90
4	18 50	48.10	38 30

TO YIELD LINE

BOTTOM YIELD LINE

Figure 7.8 Assumed Yield-Line Pattern for F.E. and C.T. (Specimens 2, 3, 4)

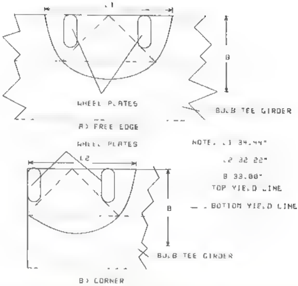

Figure 7.9 Assumed Yield-Line Pattern for Free Edge and Corner Tests (Specimen 5)

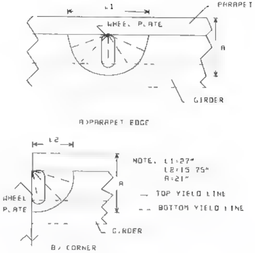

Figure 7.10 Assumed Yield-Line Pattern for Parapet Edge and Corner Tests(Specimen 1)

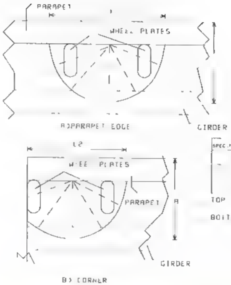

SPECIMEN No.	A	L1	L2
2	28.00	41.00	35.00
3	32.00	52.00	38.63
4	28.00	41.00	35.00

TOP YIELD LINE

BOTTOM YIELD LINE

Figure 7.11 Assumed Yield-Line Pattern for P.E. and C.T. (Specimens 2, 3, 4)

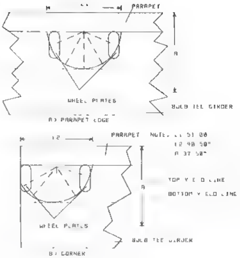

Figure 7.12 Assumed Yield-Line Pattern for Parapet Edge and C.T. (Specimen 5)

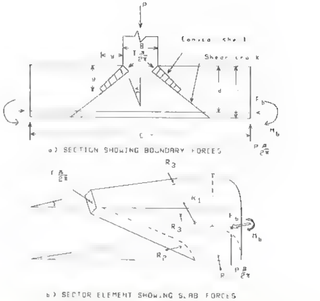

Figure 7.13 Mechanical Model of Slab at Punching Shear Failure

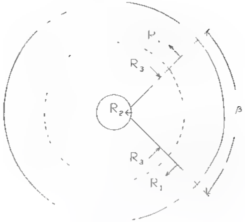

Figure 7.14 Plan View of Mechanical Model of Slab at Punching Shear Failure

bounded on the inclined face by the diagonal shear crack and the compression zone. It is loaded through the compressed conical shell that develops from the loaded area to the upper end of the shear crack. This shell can be thought of as the perimeter of the column base in Figure 7.13(a) and its thickness is assumed to vary in such a manner that the compressive stresses are uniformly distributed between the load area and the root of the shear crack.

The element [Figure. 7.13(b)] is acted on by the external load $P\beta/2\pi$ (β is the angle of sector element, in radians, shown in Figure 7.14), and by the following forces: (1) The oblique compression force, $T\beta/2\pi$, in the compressed conical shell; (2) horizontal forces in the circumferential reinforcement at right angles to the radial cracks, with resultant R_1; (3) horizontal forces in the radial reinforcement crossing the shear crack, with resultant R_2;(4) horizontal tangential compressive forces in the concrete, with resultant R_3 and (5) Boundary restraints M_b and F_b. Several important aspects of the Kinnunen and Nylander model are

1) It recognizes the existence of a three-dimensional state of compressive stress in the conical shell with the consequent increase in the strength and effective modulus of elasticity.

2) The tangential strain at the top surface of the slab at a distance, $(B/2)+y$, from the center of the loaded area is

taken as a measure of the supporting strength of the conical shell.

3) The failure takes place when the tangential strain mentioned above, reaches such a high value that the strength of the conical shell is impaired. Thus, in the Kinnunen and Nylander's model, failure takes place when the tangential strain reaches a characteristic value and the conical shell fails in compression.

7.3.2 Method of calculation for Slabs with Known Restraints

In this case the boundary restraints M_b and F_b are assumed as a property of the slab system, related to how the slab is supported and bounded.

The Punching load calculation involves two iterative processes, one being inside of the other. The theoretical load at punching, P, is calculated during the inner iterative process, assuming a depth y, of the compression zone in Figure 7.13 and a value for a parameter X, where $X = 4\pi(M_b/P)$. Note that X itself is a function of the load, P. Hence the calculation method is inevitably iterative. The calculation procedure as given by Hewitt an Bachelor [24] includes the following steps (notation refers to Figures 7.13 and 7.14):

1. Select a value for X.
2. Select a value for y/d.
3. Calculate:

   (a) The stress f_t, in the imaginary conical shell.

For B/d <2, use

$$f_t=825[0.35+(\frac{fc'}{375+0.0125})][1-0.22(\frac{B}{d})] \quad \ldots\ldots (7.4)$$

For B/d>2 use

$$f_t=460[0.35+(\frac{fc'}{375+0.0125})] \quad \ldots\ldots\ldots\ldots (7.5)$$

b) Calculate the parameter, α, from the expression

$$\frac{(K_z\tan\alpha-1)(1-\tan\alpha)}{1+\tan^2\alpha} = \frac{(1+y)\ln(C)}{4.7B(B+2y)} \quad \ldots\ldots (7.6)$$

where $K_z=K_y-\frac{3XC}{4(3d-y)}$ .... (7.7)

and $K_y=\frac{3(C-B)}{2(3d-y)}$

c) Calculate P from

$$P=T\sin\alpha=\pi(\frac{B}{d})\ (\frac{y}{d})\ \frac{B+2y}{B+y}\ f_t f(\alpha)d^2 \ldots\ldots\ldots\ldots (7.8)$$

Where $f(\alpha)=\tan\alpha(1-\tan\alpha)/(1+\tan^2\alpha)$

4. Calculate:

a) The parameter, ϕ (Angle of rotation of the slab beyond the shear crack)

For B/d≤2, use

$$\phi=0.0035[1-0.22(\frac{B}{d})]\ (\frac{1+B}{2y})$$

For B/d≥2 use

$$\phi=0.0019(1+\frac{B}{2y}) \quad \ldots\ldots\ldots\ldots\ldots\ldots (7.9)$$

Note that knowing ϕ, it is possible to calculate the slab deflection:

$$W_o=\phi(C-B)/2 \quad \ldots\ldots\ldots\ldots\ldots\ldots (7.10)$$

b) Kinnunen and Nylander have shown that the tension reinforcement within a zone of radius r_s has yielded at punching failure, in which r_s is

$$r_s = \frac{E_s \phi (d-y)}{f_y} \quad \text{.......................} (7.11)$$

They also stated that outside this zone the reinforcement is still in the elastic range.

c) C_o (radius of the shear crack) from

$$C_o = (c/2 + 1.8d) \quad \text{.......................} (7.12)$$

d) The forces R_1 and R_2

For $r_s \geq C_o$ use

$$R_1 = \rho f_y d [(r_s - C_o) + r_s \ln \frac{(C)}{2r_s}$$

$$R_2 = \rho f_y d C_o \beta \quad \text{.......................} (7.13)$$

for $r_s \leq C_o$ use

$$R_1 = \rho f_y d r_s \ln \frac{(C)}{2C_o} \quad \text{.......................} (7.14)$$

$$R_2 = \rho f_y d r_s \beta \quad \text{.......................} (7.15)$$

where ρ is the reinforcement ratio.

5. A new value of P is calculated using

$$P = \frac{2\pi}{X_z} [R_1 + (\frac{R_2}{\beta}) + F_b(\frac{C}{2})] \quad \text{.........} (7.16)$$

6. If the values of P from steps 3 and 5 differ significantly, select a new value for y/d and repeat the calculations starting at step 3. If the values of P from steps 3 and 5 are sufficiently similar proceed to step 7.

7. Calculate X from

$X=4\pi(M_b/P)$ .... (7.17)

8. If the selected and calculated values of X differ significantly, select a new value for X and restart the calculations at step 2. If the selected and calculated values of X are sufficiently close the theoretical punching load has been determined.

A computer program has been developed [24] that calculates P in the steps outlined above. The program uses starting values of 1.0 for X and 0.5 for y/d, and solves for P in usually less than 10 iterations in X and 20 in y/d. The calculated values of P (from steps 3 and 4) are considered sufficiently similar when they differ by less than 0.1%. The selected and calculated values of X (from step 7) are considered sufficiently similar when they differ by less than 1%. The calculated value of P is corrected for the dowel effect assuming that this effect remains unchanged by the boundary restraint and is taken as 20% of the uncorrected punching load for the corresponding simply supported slab. Consequently the following equation is used:

$V=1.2P$.................................... (7.18)

where V is the corrected punching load of the restrained slab.

7.3.3 Method of Calculation for slabs with Unknown Restraints

Because in practical situations it is difficult to know in advance, or even measure under laboratory conditions, the boundary restraining forces on a slab loaded to punching failure, it was proposed that a single factor termed as "restraint factor" be used to estimate the influence of practical boundary conditions.

Using the idealized geometry of displacement of a slab at failure as proposed by Brotchie and Holley [25], the maximum boundary stresses and forces, shown in Figure 7.15. are developed. The inclined line in the top portion of Figure 7.15 indicates the failure plane of Figure 7.13.

The geometry of the restraint is further indicated in Figure 7.16(a), with Figure 7.16(b) showing a free body of one half of the slab enlarged.

To estimate the magnitude of the boundary restraints it will be necessary to approximate the depth of compression zone associated with the free bodies of Figure 7.16. This is the distance denoted s in the Figure. The following steps are directed toward this:

At the central deflection W_o, the rotation and middle surface extension at the support are $\theta_a=-2W_o/C$ and δ_a (large displacement effect). At midspan, the corresponding values are $\theta_b=2W_o/C$ and δ_b (large displacement effect). The geometrical relation

$$(C/2-\delta_a-\delta_b)^2+W_o^2=(C/2)^2 \;\ldots\ldots\ldots\ldots\; (7.19)$$

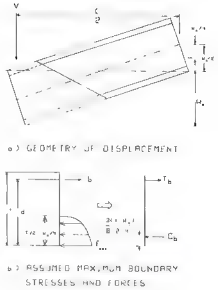

Figure 7.15 Idealized Displacement and Macimum Boundary Forces in Restrained Slab

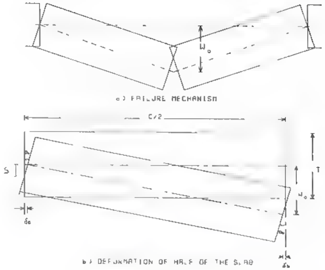

Figure 7.16 Failure of Slab Strip

reduces to

$$\delta_a+\delta_b=W_o^2/C \quad (7.20)$$

where higher order terms are neglected. Now it is possible to calculate the shift in the neutral axis, s. From Equation 7.20:

$$s|\theta_a|+s\ \theta_b|=W_o^2/C \quad (7.21)$$

Substituting $\theta_a=-2W_o/C$ and $\theta_b=2W_o/C$ into Equation 7.20, the shift in the neutral axis is

$$s=W_o/4 \quad (7.22)$$

From Figure 7.13, The maximum force, T_b, in the tensile reinforcement is

$$T_b=d\rho f_y \quad (7.23)$$

where the member width is assumed to be unity.

The maximum compressive force, C_b, in the concrete, is

$$C_b=\gamma f_{max}(h/2-W_o/4) \quad (7.24)$$

in which γ, the ratio of the average stress to the maximum stress f_{max}, depends on the stress distribution. A parabolic distribution of stress is assumed, giving a value of 2/3 for γ; and f_{max} is assumed to be 0.85 fc'. The idealized maximum boundary restraints, can now be determined.

The boundary moment, M_b, is referenced to the level of the compression reinforcement, as indicated in Figure 7.13. The maximum possible magnitudes of the boundary forces M_b and F_b may now be expressed as

$$M_{b(max)}=T_b(2d-t)-C_b(d-\frac{13}{16}t-\frac{3W_o}{32}) \quad (7.25)$$

$$F_{b(max)}=C_b-T_b \quad (7.26)$$

The restraint factor, η, is introduced due to the fact that the maximum boundary restraints of Equation 7.25 and 7.26 would rarely, if ever, be fully developed at punching failure. Therefore the following boundary restraints are obtained at failure:

$M_b = \eta M_{b(max)}$ .... (7.26)

$F_b = \eta F_{b(max)}$ .... (7.27)

When the magnitudes of F_b and M_b have been determined, the punching failure load may be computed as described in Section 7.3.2.

Practical values of η will lie between zero for simply supported slabs to unity for slabs with the idealized restraint and this value will depend on the properties of the slab, as well as on the slab geometry and properties of the boundaries, and can be determined empirically. A value of 0.5 for η was recommended for rectangular slabs of composite steel concrete bridges reinforced with relatively low quantities of reinforcement.

The punching loads for the test specimens were, of course, determined experimentally. It was desired to estimate the boundary restraints consistent with these observed failure loads. To accomplish this, numerous values of F_b and M_b were assumed and the punching loads were computed as described in Section 7.3.2. The results are summarized in Figures 7.17 through 7.22. The possible combinations of M_b and F_b for the test specimens were then

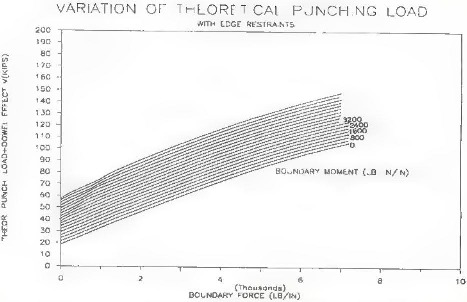

Figure 7.17 Theoretical Punching Load-Boundary Restraints for Single Imprint Tests

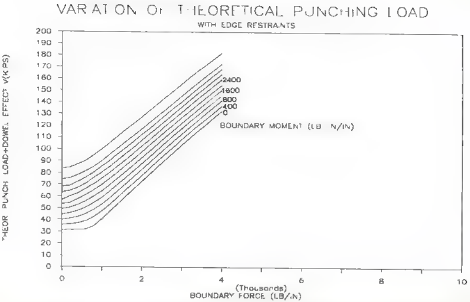

Figure 7.18 Theoretical Punching Load-Boundary Restraints for Dual Imprint Tests

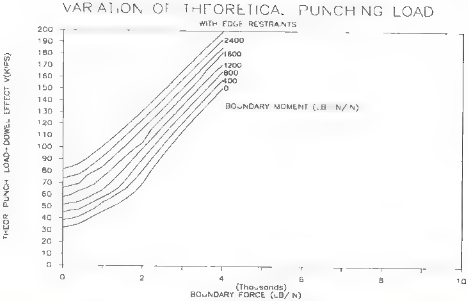

Figure 7.19 Theoretical Punching Load-Boundary Restraints (Specimen 2)

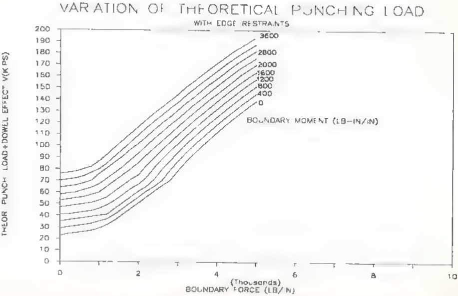

Figure 7.20 Theoretical Punching Load-Boundary Restraints (Specimen 3)

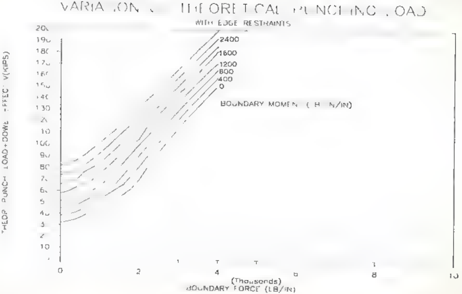

Figure 7.21 Theoretical Punching Load-Boundary Restraints (Specimen 4)

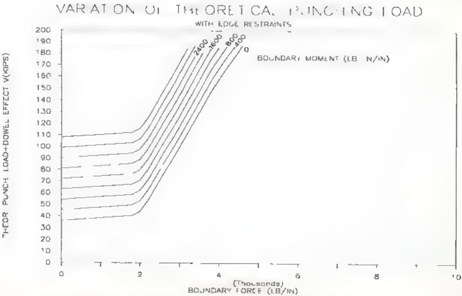

Figure 7.22 Theoretical Punching Load-Boundary Restraints (Specimen 5)

estimated by entering Figures 7.17 through 7.22 with the observed punching loads.

When using the figures of course, numerous combinations of M_b and F_b can be found for a given punching load. Not all combinations are reasonable, however, as $M_b = F_b(jd)$, where (jd) is a moment arm consistent with slab geometry. By estimating jd, as the ratio $M_{b(max)}/F_{b(max)}$, unique values of M_b and F_b were identified. These boundary forces would be, of course, be smaller than the maximum boundary forces consistent with the specimen geometry. These maxima $M_{b(max)}$ and $F_{b(max)}$, may be found from Equations 7.25 and 7.26. By comparing the actual boundary restraining forces from Figures 7.17 through 7.22 with the maxima, the restraint factor n could be estimated.

7.3.4 Limits of Application

Hewitt and Bachelor [24] state that the procedure is applicable to slabs whose parameters lie within the following limits: $4<C/d<17$, $0.05<w<0.45$, $4<\mu<20$; and $27x10^6$psi$<E_s<33x10^6$ psi, in which C= the slab diameter (or equivalent diameter for a non-circular slab); d=the slab effective depth; $w=pf_y/fc'$ (reinforcement index); E_s=the modulus of elasticity of the reinforcement; and $\mu=(V_{flex}/bd/fc')$ is the flexural factor used by Moe, where b is the perimeter of the loaded area.

7.4 Finite Element Model

Since the primary objective of this analysis was to evaluate the stresses in the bracing as well as to determine the effects of the boundary restraining forces in this elements, it was necessary to model properly the X-braces. Although a linear elastic analysis is insufficient for close comparison with experimental results, because it cannot predict the effect of cracking on the specimen's behavior, it was felt that such an analysis could be sufficient to analyze the effects in the beams and bracing, as they will be in the elastic range. As is explained shortly, the bridge was analyzed using a computer program called SIMPAL, developed in the University of California at Berkeley [25].

7.4.1 Modeling of the Deck slab

Shell elements were used to model the bridge deck. The thickness was assumed to be constant throughout the deck except over the girders where an altered slab thickness was used to account for the top flange of the girder.

Two cases were studied, one neglected the boundary restraining forces and another included them.

a) Case I (Neglecting the Boundary Restraining Forces)

Figure 7.23, shows a typical cross section and plan view of the bridge deck. For this model, the loads were applied on the same positions as in the tests, but the

Figure 7.23 Typical Cross Section and Plan View of Bridge Deck

imprint areas were not considered, each dual tire formation being treated as a concentrated load.

b) Case II (Including the Boundary Restraining Forces)

For this case, the boundary restraints obtained for the observed failure loads from Figure 7.17 through 7.22 in Section 7.3 were applied as loading to the slab system. The plan view of the model is shown in Figure 7.24, where the large ten-sided open area represents the region of the punching failure. The estimated boundary forces F_b and M_b were applied to the slab uniformly distributed around the perimeter of the opening. The vertical failure load was similarly distributed around the perimeter.

7.4.2 Modeling of the Girders

Shell elements were used to model the web and the bottom flange as shown in Figure 7.25.

7.4.3 Modeling of the Bracings

Beam elements were used to model the X-braces and they were connected to the two adjacent webs of the girders at the two ends as shown in Figure 7.26. The cross section is indicated in Figure 7.27. For the case of bridge decks supported by steel girders additional bracing was modeled at midspan consistent with test specimens, as indicated in Figure 7.28. The cross section is indicated in Figure 7.29.

7.4.4 Modeling of the Parapet

The parapet was modeled using shell elements and approximating the parapet shape as a series of steps, as shown in Figure 7.23.

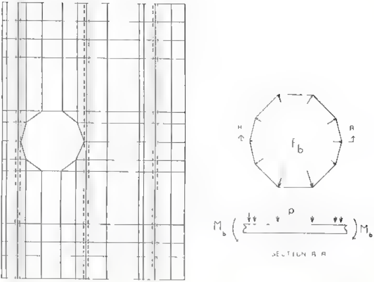

Figure 7.24 Typical Plan View of Bridge Deck Showing Boundary Forces

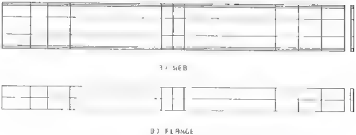

Figure 7.25 Typical Shell Elements

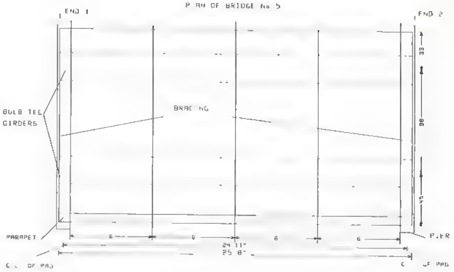

Figure 7.26 Plan View of Specimen on Bulb-Tee Girders

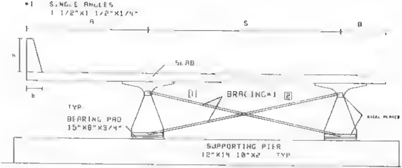

SPECIMEN	T	S	A	B	S/T	A/T	B/T	h	b	SCALE FACTOR
5	3 3/4"	90"	45"	33	24	.2	8 8	[illegible]	7 5	2

Figure 7.27 Cross Section of Specimen on Bulb-Tee Girders

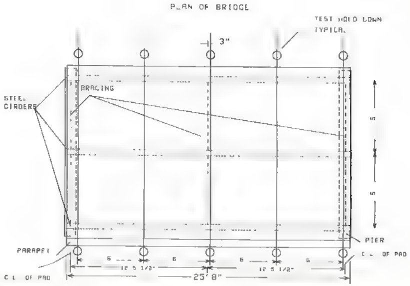

Figure 7.28 Plan View of Specimens on Steel Girders

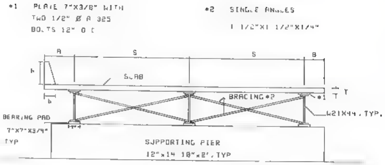

SPECIMEN	T	S	A	B	S/T	A/T	B/T	h	b	SCALE FACTOR
1	4 11/32	80	21.0	13.5	18.4	4.8	3.1	15.5	7.5	[illegible].84
2	3 11/16	75 3/8	28.0	18.5	20.4	7.6	5.0	15.5	7.5	2.17
3	3 3/16	7[illegible] 7/8	32.0	22.0	22.5	10.0	6.9	12.2	6.5	2.51

Figure 7.29 Cross Section of Specimen on Steel Girders

7.4.5 Modeling of the Bearing Pads

The bearing pads were modeled as three truss elements connected to the bottom flange of the girders at the two respective ends as shown in Figure 7.23, and the stiffness was taken as the approximate slope of the load deflection curve for a bearing assembly, obtained experimentally for the neoprene material, and shown in Appendix F.

7.5 Comparison of Computed and Measured Results

7.5.1 Failure loads

The predicted maximum loads for the test specimens, computed from the ACI model, AASHTO model, and yield line theory are summarized in Table 7.1 for the interior tests and Table 7.2 for the corner tests and edge tests. The boundary restraining factors, computed for the observed punching loads in Section 7.3 using the Kinnunen and Nylander model, are also listed in the tables.

7.5.2 Maximum Load Capacity and Restraining Factors

7.5.2.1 Interior Tests

Considering the restraining factors for the tests carried out at midspan, the restraining factor for the first specimen (S/T=18.4) was ρ=25% while that for the second specimen (S/T=20.4) was ρ=33%. This, of course, is the opposite of what one might expect. There are, however other differences between the two specimens that could cause this result. The first specimen was loaded only by single and double imprint wheel loads, while the second

Table 7.1 Summary of Maximum Loads at Interior Tests (Theoretical and Experimental)

		Test Results				Theoretical Equations			
Position	Load Pattern (Number of imprints)	Specimen	Test	Maximum Load (Kips)	Failure?	ACI Formula (Kips)	AASHTO Formula (Kips)	Yield-line (Kips)	Kinnunen & Nylander % of Rest (*)
	Single	1	1	48.0	Yes	37	16	33.6	25.0
	Double	1	4	72.0	Yes	53	22	34.3	26.0
	Quadruple	2	1	70.0	No	103	42	38.6	31.0
Interior	Quadruple	2	3	70.0	No	103	42	38.6	34.0
Midspan	Quadruple	3	1	52.5	Yes	71	30	27.0	30.0
	Quadruple	3	3	54.5	Yes	71	30	27.0	30.0
	Quadruple	4	1	68.0	Yes	109	45	35.6	23.5
	Quadruple	4	3	74.0	Yes	109	45	38.6	28.6
	Quadruple	5	1	85.0	Yes	105	44	48.3	40.0
	Single	1	6	37.5	Yes	37	16	33.6	16.5
	Double	1	5	46.0	Yes	53	22	34.3	13.7
Interior	Quadruple	2	5	70.0	Yes	103	42	38.6	28.5
(1/6 of	Quadruple	2	6	58.0	Yes	103	42	38.6	27.5
total	Quadruple	3	5	45.0	Yes	71	30	27.0	28.0
span	Quadruple	3	7	47.5	Yes	71	30	27.0	37.0
from end)	Quadruple	4	6	42.0	Yes	109	45	35.6	31.3
	Quadruple	4	7	62.0	Yes	109	45	35.6	22.7
	Quadruple	5	5	85.0	No	105	44	48.3	35.0
Interior End	Quadruple	5	7	38.0	Yes	81	34	35.5	-

* Restraining factor "Factor to estimate the influence of practical boundary conditions"
Note: 100% Fully restrained
0% No restraignment

Table 7.2 Summary of Maximum Loads at Edge and Corner (Theoretical and Experimental)

Position	Load Pattern (Number of imprints)	Test Results: Specimen	Test	Maximum Load (Kips)	Failure?	Theoretical Equations: ACI Formula (Kips)	AASHTO Formula (Kips)	Yield-line (Kips)
Free Edge	Single	1	2	37.5	Yes	28.72	15.50	37.8
	Quadruple	2	2	50.0	No	79.00	35.00	47.0
	Quadruple	3	8	48.0	Yes	54.00	24.00	32.0
	Quadruple	4	2	55.0	No	84.00	37.00	47.0
	Quadruple	5	2	55.0	Yes	79.00	35.00	44.5
Free Corner	Single	1	8	19.5	Yes	16.00	7.00	18.5
	Quadruple	2	5	58.0	Yes	61.00	27.00	40.0
	Quadruple	3	6	30.0	Yes	42.00	18.00	24.4
	Quadruple	4	5		Yes(**	65.00	29.00	40.0
	Quadruple	5	4	23.5	Yes	62.00	27.00	23.0
Parapet Edge	Single	1	3	50.0	No	34.00	15.00	78.0
	Single	1	7	50.0	No	34.00	15.00	76.0
	Quadruple	2	4	60.0	No	122.00	54.00	49.5
	Quadruple	3	8	25.0	No(*)	84.00	37.00	30.5
	Quadruple	4	4	55.0	No	130.00	58.00	48.5
	Quadruple	5	3	45.0	No(*)	124.00	55.00	41.0
Parapet Corner	Single	1	8	44.0	Yes	20.00	9.00	38.0
	Quadruple	2	7	55.0	Yes	109.00	48.00	43.5
	Quadruple	3	4	35.0	Yes	70.00	31.00	24.0
	Quadruple	4	5	48.0	Yes	108.00	49.00	43.5
	Quadruple	5	8	56.0	No(*)	103.00	46.00	34.0

* Test stopped due to development of yield line for full length of specimen

** Test was not performed due to failure during dynamic testing

specimen was loaded only by four imprint tandem assembly loads. For the third specimen (S/T=22.5) there was a reduction in the restraining factor relative to the second specimen to η=30%. This, however, was still larger than the restraining factor for the first specimen. For tests carried out at 1/6 of the total span from the end of the bridge, the restraining factor increased from approximately η=15% in the first specimen to η=28% in the second specimen, probably reflecting the loading difference, as explained above. For the third specimen with the larger S/T ratio there was only an insignificant reduction in the restraining factor to η=26%, relative to the second specimen. The fourth specimen indicated smaller restraining factors than the similar second specimen, decreasing from η=33% to approximately η=25% for tests carried out at midspan, and from η=28% to η=16%, for tests carried out at 1/6 of the span length from the end of the bridge. These reductions were most likely related to the fact that specimen 4 was tested in fatigue before being loaded to failure. This prior damage undoubtedly reduced the capacity for restraint. The fifth specimen (S/T=17.6), the specimen with bulb-tee girders, indicated a restraining factor of approximately η=40% for tests carried out at midspan, and a value of η=35% for tests carried out at 1/6 of the total span from the end of the bridge, the largest restraining factors computed for the entire study.

Note that S/T=17.6 given above for the fifth specimen, reflects the transverse span of the slab from flange tip to flange tip of the bulb-tee girders. This reduced span was considered appropriate because during testing the strength and stiffness of the flanges limited the punching failure mechanism to this reduced area. The reduced effective span is reflected in the increase in the restraining factors.

From Table 7.1, it is observed that the ACI formula based on the punching shear model underestimated the punching loads for single and double point loading on the slab interior at midspan. For single and double point load at 1/6 of the total span from the end it either closely predicted the test result or slightly overestimated it, while for quadruple point load, it consistently overestimated the punching loads. The AASHTO formula always predicted a lower strength than the ACI formula, and grossly underpredicted the observed failure loads, except for one case, where it slightly overpredicted a failure load. It should be noted that this one case was a test at a location that had suffered considerable damage in previous fatigue testing. The yield-line theory, underpredicted slab strength, to various degrees, in all the cases.

7.5.2.2 Free edge, Parapet edge and Corner tests

Because the Kinnunen & Nylander punching shear model was meant to analyze slabs where failure may occur by "punching" along a truncated cone, completely surrounding a

concentrated load or reaction area, this model could not be used for exterior edge and corner tests. Hence, interpretation of test results was limited to yield-line theory, and the ACI and AASHTO formulas. As shown in Table 7.2, the yield-line theory gave good predictions of the observed failure load for the single imprint tests at the free edge and free corner and underpredicted the failure load for the single imprint test at the parapet corner. For the quadruple point loadings, it consistently underpredicted the observed failure loads, for all the cases where the slab failed during the test. The exception was the fifth specimen, for free edge, parapet edge and parapet corner tests, where the yield line theory gave close predictions of observed strength. Hence, the yield line theory seemed to be better at predicting failure loads for exterior portions than for interior portions. The ACI formula underestimated the observed failure load in the case of all the single imprint tests and overestimated the failure load in the case of all the quadruple imprint loads. This was largely similar to the results for interior tests. The AASHTO formula always predicted a lower strength than the ACI formula, and underpredicted the observed failure loads for the test carried out on the free edge and free corner and except for single imprint loading, gave good predictions of the failure load for cases in which the parapet corner failed. For the single imprint loading, it grossly underpredicted the observed failure

load. Again, the result is similar to that for interior loading.

In Summary, the ACI formula gave unconservative predictions for quadruple imprint loading, when the critical crack pattern is assumed to surround the entire tandem load assembly, and underestimated the punching loads for single imprint loading. The yield line theory gave reasonable predictions or, underpredicted for single imprint loadings, and underpredicted the punching loads for quadruple imprint loading. The AASHTO formula in general, for almost all the cases, underpredicted test results.

7.5.3 Maximum deflections

7.5.3.1 Maximum deflections on the slab

The observed slab deflections were compared with the computed results of the Kinnunen and Nylander theory described in Section 7.3, using Equation 7.10. As listed in Table 7.3, for the single imprint loadings, the predicted deflections were far less than the corresponding observed deflections. For double imprint loading, there was an underprediction of approximately 25% for the test carried out at midspan, while there was an overprediction of approximately 39% for the test carried out at 1/6 of the total span from the end of the bridge. In the case of four imprint loading the model gave very variable predictions of deflections. As listed in Table 7.3, in some cases there was an overprediction while in others there was an underprediction.

Table 7.3 Summary of Maximum Slab Deflections (Theoretical and Experimental)

Position	Load Pattern (Number of imprints)	Test Results: Specimen	Test	Maximum Load (Kips)	Failure?	Maximum Test Defl (Inches)	Theoretical values: Kinnunen & Nylander % of Rest (*)	Maximum Defl In	% of Defl Discrepancy (**)
	Single	1	1	46.0	Yes	1.47	25.0	0.40	-73
	Double	1	4	72.0	Yes	2.05	26.0	1.51	28
	Quadruple	2	1	70.0	No	1.55	33.0	1.32	20
Interior	Quadruple	2	3	70.0	No	1.20	34.0	1.23	3
Midspan	Quadruple	3	1	52.5	Yes	1.74	30.0	1.95	12
	Quadruple	3	3	54.5	Yes	1.76	20.0	2.01	14
	Quadruple	4	1	66.0	Yes	1.91	23.6	1.90	5
	Quadruple	4	3	74.0	Yes	2.38	28.6	1.63	32
	Quadruple	5	1	95.0	Yes	1.72	40.0	1.62	6
	Single	1	8	37.5	Yes	1.78	16.8	0.48	73
	Double	1	5	45.0	Yes	1.59	13.7	2.35	39
Interior	Quadruple	2	6	75.0	Yes	1.33	28.5	1.70	28
(1/6 of	Quadruple	2	8	69.0	Yes	1.49	27.5	1.62	8
total	Quadruple	3	5	45.0	Yes	1.98	28.0	2.18	10
span	Quadruple	3	7	47.5	Yes	1.88	27.0	2.12	13
from end)	Quadruple	4	6	42.0	Yes	2.28	[illegible]	3.02	34
	Quadruple	4	7	62.0	Yes	2.21	22.7	[illegible]	-8
	Quadruple	5	5	55.0	No	0.93	35.0	1.74	87
Interior End	Quadruple	5	7	38.0	Yes	0.58			

* Restraining factor "Factor to estimate the influence of practical boundary conditions"
Note 100% Fully restrained
0% No restrainment

** $\frac{\text{Calculated-Measured}}{\text{Measured}}$

7.5.3.2 Maximum deflections on the girders

The observed girder deflections were compared with the computed results from the Finite Element Elastic Model described in Section 7.4. As listed in Table 7.4, for the interior tests at midspan, the maximum overprediction of the experimental results was 29%, while the maximum underprediction was 16%. Hence, the model gave very variable predictions of deflection. For interior tests carried out at 1/6 of the total span from the end of the bridge, as indicated in Table 7.4, the model consistently overpredicted deflections, with extremely large overprediction for the only single imprint test and for specimen 5, the bulb-tee specimen. Much of the discrepancy between observed and computed deflections may be ascribed to the modeling of the bearing pads. While the stiffness of these pads was estimated and included in the analytical model, the actual stiffness of the pads was affected by many variables, making it difficult to obtain a reliable stiffness for use in the model. These variables included loading rate and fundamental nonlinearity.

7.5.4 Boundary restraining forces

The restraining forces, obtained using the Kinnunen and Nylander theory are indicated in Table 7.5. Note that these results can vary somewhat from those for restraining factors, as total boundary force represents the product of restraining factor and maximum restraining force. This latter parameter can vary from one specimen to another.

Table 7.4 Summary of Maximum Deflections on the Beam (Theoretical and Experimental)

Position	Load Pattern (Number of imprints)	Specimen	Test	Maximum Load (Kips)	Failure?	Measured Maximum Deflection (Inches)	Calculated* Maximum Deflection (Inches)	% of Defl Discrepancy (**)
	Single	1	1	46.0	Yes	0.195	0.217	11.3
	Double	1	4	72.0	Yes	0.351	0.329	6.3
	Quadruple	2	1	70.0	No	0.362	0.340	6.1
Interior	Quadruple	2	3	70.0	No	0.337	0.320	-5.0
Midspan	Quadruple	3	1	52.5	Yes	0.191	0.247	29.3
	Quadruple	3	3	54.5	Yes	0.278	0.249	10.4
	Quadruple	4	1	56.0	Yes	0.352	0.312	-11.4
	Quadruple	4	3	74.0	Yes	0.400	0.338	-15.5
	Quadruple	5	1	95.0	Yes	0.455	0.549	20.6
	Single	1	6	37.5	Yes	0.004(***)	0.118	-
	Double	1	5	46.0	Yes	0.091	0.142	56.0
Interior	Quadruple	2	6	70.0	Yes	0.146	0.221	51.4
(1/8 of	Quadruple	2	8	68.0	Yes	0.128	0.217	69.5
total	Quadruple	3	5	45.0	Yes	0.110	0.141	28.2
span	Quadruple	3	7	47.5	Yes	0.133	0.150	12.8
from end)	Quadruple	4	6	42.0	Yes	0.07[illegible]	0.132	65.0
	Quadruple	4	7	62.0	Yes	0.146	0.194	32.8
	Quadruple	5	3	55.0	No	0.082	0.204	149
Interior End	Quadruple	5	7	38.0	Yes	0.020	0.089	345

* From Finite Element model described in Section 7.4

** $\frac{\text{Calculated-Measured}}{\text{Measured}}$

*** LVDT Position offset from the centerline of the girder

Table 7.5 Summary of Theoretical Boundary Restraining Forces

Position	Load Pattern (Number of imprints)	Test Results: Specimen	Test	Maximum Load (Kips)	Failure?	Theoretical values Using Kinnunen & Nylander Model: % of Rest. *,	Boundary R. Force (Lb/in)	Boundary R. Moment (Lb-in/in)
	Single	1	1	45.0	Yes	25.0	1500.0	1050.0
	Double	1	4	72.0	Yes	28.0	1500.0	1000.0
	Quadruple	2	1	70.0	No	33.0	1750.0	1350.0
Interior	Quadruple	2	3	78.0	No	34.0	1800.0	1400.0
Midspan	Quadruple	3	1	52.5	Yes	30.0	1300.0	900.0
	Quadruple	3	3	54.5	Yes	29.0	1250.0	880.0
	Quadruple	4	1	66.0	Yes	23.5	1250.0	950.0
	Quadruple	4	3	74.0	Yes	28.5	1400.0	1100.0
	Quadruple	5	1	95.0	Yes	40.5	2200.0	1550.0
	Single	1	8	37.5	Yes	18.6	1000.0	700.0
	Double	1	5	45.0	Yes	13.7	800.0	600.0
Interior	Quadruple	2	8	70.0	Yes	28.5	1500.0	1150.0
(1/6 of	Quadruple	2	9	69.0	Yes	27.5	1450.0	1100.0
total	Quadruple	3	5	45.0	Yes	25.0	1100.0	800.0
span	Quadruple	3	7	47.5	Yes	27.0	1150.0	850.0
from end)	Quadruple	4	6	42.0	Yes	11.3	800.0	400.0
	Quadruple	4	7	82.0	Yes	22.7	1200.0	900.0
	Quadruple	5	5	65.0	No	35.0	1900.0	1470.0
Interior End	Quadruple	5	7	38.0	Yes	-		-

* Restraining factor "Factor to estimate the influence of practical boundary conditions"
Note 100% Fully restrained
0% No restrainment

Comparing the boundary forces and moments implied by the tests carried out at midspan, the boundary force and boundary moment for the first specimen (S/T=18.4) were approximately 1500 lb/in. and 1000 lb-in/in. respectively, while for the second specimen (S/T=20.4) they were approximately 1750lb/in. and 1350 lb-in/in. respectively. This, of course, is the opposite of what one might expect and the reasons are the same as in the case of the restraining factors given in Section 7.5.2. For the third specimen there was a reduction in the boundary force and boundary moment to approximately 1250 lb/in. and 900 lb-in/in. Note that these forces are smaller than those for specimen 1, a pattern that is somewhat different than that for restraining factors and more in line with what one might initially expect.

For tests carried out at 1/6 of the total span from the end of the bridge, the boundary force and boundary moment increased from approximately 900 lb/in. and 650 lb-in/in. respectively in the first specimen to approximately 1450 lb/in. and 1100 lb-in/in. respectively in the second specimen, reflecting the loading difference, as explained in Section 7.5.2. For the third specimen with the larger S/T ratio there was a reduction in the boundary force and boundary moment to 1100 lb/in. and 800 lb-in/in. respectively, relative to the second specimen.

The fourth specimen indicated smaller boundary forces and boundary moments than the similar second specimen,

decreasing from approximately 1750 lb/in. and 1350 lb-in/in. to approximately 1300 lb/in. and 1000 lb-in/in. for tests carried out at midspan, and from approximately 1450 lb/in. and 1100 lb-in/in., to approximately 900 lb/in. and 650 lb-in/in. respectively. Again these reductions were most likely related to the fact that specimen 4 was tested in fatigue before being loaded to failure as discussed in Section 7.5.2. The fifth specimen (S/T=17.6), the specimen with bulb-tee girders indicated a boundary force and boundary moment of approximately 2200 lb/in. and 1680 lb-in/in., for tests carried out at midspan, and 1900 lb/in. and 1470 lb-in/in. for tests carried out at 1/6 of the total span from the end of the bridge, the largest boundary force and boundary moment computed for the entire study.

7.5.5 Stresses in Bracing

Figures 7.26 and 7.28 show the locations of the braces while Figures 7.27, and 7.29 show the typical cross section. Table 7.6, shows the maximum strain values obtained from the Finite Element Model along with some experimental values obtained. The corresponding maximum strains compared relatively well with experimental values, except for tests at midspan on the second and fifth specimens,where there was a discrepancy of more than 40%. Table 7.7 shows that the contribution of the boundary restraining forces to the bracing forces was comparatively small compared to that of the vertical forces. Note that

Table 7.6 Summary of Maximum Strains on the Bracing (Theoretical and Experimental)

Position	Load Pattern (Number of imprints)	Test Results: Specimen	Test	Maximum Load (Kips)	Failure?	Measured Maximum Strain (Mic In/In)	Calculated* Maximum Strain (Microinches Inches)	% of Strain Discrepancy (**)
	Single	1	1	48 0	Yes	-	230	-
	Double	1	4	72 0	Yes		374	-
	Quadruple	2	1	70 0	No	230	303	31.7
Interior	Quadruple	2	3	70 0	No	220	315	43.2
Midspan	Quadruple	3	1	52 5	Yes	200	228	14 0
	Quadruple	3	3	54 5	Yes	250	246	-1 8
	Quadruple	4	1	68 0	Yes	270	281	4 1
	Quadruple	4	3	74 0	Yes	300	327	9 0
	Quadruple	5	1	85 0	Yes	204	273	33 8
	Single	1	8	37 5	Yes		87	
	Double	1	9	45.0	Yes		99	
Interior	Quadruple	2	6	70 0	Yes	-	219	
(1/8 of	Quadruple	2	8	59 0	Yes	-	211	-
total	Quadruple	3	5	45 0	Yes	-	138	-
span	Quadruple	3	7	47 5	Yes		147	
from end)	Quadruple	4	5	42 0	Yes		127	
	Quadruple	4	7	62 0	Yes		168	
	Quadruple	5	5	65.0	No	214	198	-7 5
Interior End	Quadruple	5	7	36 0	Yes	140	114	-18 6

* From Finite Element model described in Section 7 4

** $\frac{\text{Calculated-Measured}}{\text{Measured}}$

Table 7.7 Summary of Maximum Strains on the Bracing (Experimental)

Position	Load Pattern (Number of imprints)	Test Results: Specimen	Test Results: Test	Test Results: Maximum Load (Kips)	Test Results: Failure?	Calculated Maximum Strain Due to Vertical Forces* (Microinches/Inches)	Maximum Strain Due to Boundary Rest Forces* (Mic In/In)
	Single	1	1	48.0	Yes	215	15
	Double	1	4	72.0	Yes	345	28
	Quadruple	2	1	70.0	No	280	25
Interior	Quadruple	2	3	70.0	No	288	27
Midspan	Quadruple	3	1	52.5	Yes	211	17
	Quadruple	3	3	54.5	Yes	224	22
	Quadruple	4	1	66.0	Yes	285	18
	Quadruple	4	3	74.0	Yes	304	23
	Quadruple	5	1	93.0	Yes	245	30
	Single	1	8	37.5	Yes	86	1
	Double	1	5	48.0	Yes	98	1
Interior	Quadruple	2	6	70.0	Yes	196	23
(1/5 of	Quadruple	2	8	59.0	Yes	209	2
total	Quadruple	3	5	45.0	Yes	135	1
span	Quadruple	3	7	47.5	Yes	153	14
from end)	Quadruple	4	6	42.0	Yes	186	1
	Quadruple	4	7	62.0	Yes	174	14
	Quadruple	5	5	65.0	No	182	18
Interior End	Quadruple	5	7	38.0	Yes	113	1

* From Finite Element model described in Section 7.4

additional tables from calculations for the finite element procedure are shown in Appendix K. Tables in Appendix K, show that for any particular pair of bracing, one had higher bending strains, while the other had higher axial strains.

CHAPTER 8
SUMMARY, CONCLUSIONS AND RECOMMENDATIONS

8.1 Summary

A series of laboratory tests on approximately one-half scale models of concrete bridge decks were performed using 0.3% isotropic reinforcement following the Ontario empirical design approach. Four specimens with slabs cast on steel girders were constructed, and three of them were tested statically, while the fourth specimen was subjected to a large number of cyclic loads and then subjected to static loading to failure. Additionally one specimen was cast on standard size bulb-tee girders, as recently adopted in Florida and was tested statically. The purpose of these tests was to understand better the behavior of lightly reinforced isotropic bridge decks on steel and bulb-tee girders, under static and fatigue loading conditions, with span to thickness ratios beyond the Ontario Code limitations and following American standard practice with regards to bridge deck construction.

8.2 Conclusions and Recommendations

1) For loading on slab interiors, away from parapets and free edges, isotropically reinforced slabs, detailed in accordance with the Ontario Highway Bridge Design

provisions do appear to have considerable reserve strength beyond yielding, even for larger transverse spans with span to thicknesses ratios as high as 22. Note that this is considerably in excess of the maximum of 15 in the Ontario Code.

2) Considerable reserve strength beyond yielding was also observed for portions of the slab adjacent to free edges and on the parapet edges. For tests adjacent to parapets, strong interaction between parapet and slab was observed.
3) Excessive overhang reduced the parapet slab interaction. Specimen 1, with the lowest ratio of overhang to slab thickness, indicated greater deflection for the girder adjacent to the parapet, indicating that the parapet drew some load from the adjacent slab. For specimens with larger overhangs, such as specimens 2, 3, 4 and 5, the deflection of the two adjacent beams were approximately equal, indicating that this transfer of load to the parapet was no longer as significant.
4) Excessive overhang increased the possibility of the development of a negative moment yield line over the full length of the specimen as observed in the third and fifth specimens, which had the highest ratios of overhang to slab thicknesses.
5) The presence of the parapet seemed to significantly affect slab strength for lower overhang to thicknesses ratios. For specimen 1, with the lowest overhang to

thickness ratio, the punching load for the interior span adjacent to the parapet was approximately 40% higher than for the interior span adjacent to the free edge. For the other specimens, with their larger overhang to thickness ratios, the parapet did not have such an effect upon the boundary conditions of the interior spans, as the punching loads for the interior span adjacent to the parapet was approximately equal to that for the interior span adjacent to the free edge.

6) The observed strains in the bracing, close to the neutral axis, were always in the elastic range. This somewhat conflicted with the observation that the welds between bracing and girder fractured during testing for several specimens. Calculations did not indicate that the strains at the maximum distance from the neutral axis would include sufficient bending strain to fail the welds. Because of the local geometry in the region of the welds, it was difficult to obtain a flawless weld and this may have accounted for the fractures.
7) Observation of the deflection response of the slab in cases where the welds in the bracing failed indicated a considerable increase in the deflection of the slab after the bracing failed without increasing the load.
8) For load on the interior span adjacent to the free edge, the two adjacent girders indicated approximately equal load distribution until the welds in the bracing for the loaded span failed. After the welds in the bracing had

failed, the deflection of the inner girder became greater than the deflection of the girder adjacent to the free edge, indicating a redistribution of load toward the interior of the slab. Hence, the bracing affected load distribution. For loading on the interior span adjacent to the parapet, however, the relative deflection of the two girders adjacent to the load was not affected by the failure of the welds in the bracing.

9) For the specimen on bulb-tee girders, the failure patterns for all the interior tests were confined to the portion of the slab between the flange tips. This was apparently due to the strengthening effect of the flange and the composite action between the deck of the slab and the girder. Consequently the effective transverse span (S/T) for slabs on bulb-tee girders appears to be limited to the region between the two interior flange tips. For the specimen tested the new S/T computed using this criteria was 17.6

10) Comparison of the maximum load recorded for all the interior tests at midspan for all the specimens on steel girders with different S/T ratios ranging from S/T=18.4 to S/T=22.5 (Table 3.1) with the maximum load recorded for the specimen on bulb-tee girder (Table 6.1) indicated that the specimen on bulb-tee girder exhibited a failure load consistent with the reduced S/T ratio of 17.6.

11) For the specimen on bulb-tee girders, the failure patterns for the parapet edge and free edge were confined to the portion of the slab between the exterior flange tip and the parapet or free edge, while for the case of the corner tests the failure pattern included the girder flange.

12) One test carried out at the end of the specimen on bulb-tee girders, did not indicate a large increase in load beyond that associated with yield, but this load was still higher than the AASHTO ultimate load and the heaviest vehicle load including the corresponding safety factors. This failure was by punching, but it is reasonable to think that confinement could be much less significant at this discontinuous end.

13) Comparison of the maximum loads attained on the damaged specimen (after the dynamic loading was applied) with those attained on the undamaged specimen indicated a reduction in the load capacity of no more than 10%, except for one test carried out at 1/6 of the total length of the bridge, which had suffered considerable damage during dynamic loading, the bracing having failed, causing the specimen to respond inelastically during the process of dynamic loading. In general the isotropically reinforced slabs performed well after cyclic loading, with their strength not being severely diminished.

14) The boundary restraining forces and boundary restraining moments, as well as the restraining factors, were strongly influenced by the transverse span to thicknesses ratios. For the same imprint loadings, this values decreased for larger span to thicknesses ratios.
15) The ACI formula underestimated the punching loads for single imprint loading while consistently overestimated the punching loads for quadruple imprint loads.
16) The AASHTO formula always underestimated the punching loads, except for one case, where it slightly overpredicted a failure load, but it should be noted that this one case was a test at a location that had suffered considerable damage in previous fatigue testing.
17) For loading on slab interiors, away from parapet and free edges, the yield line theory, underpredicted slab strength, to various degrees, in all cases.
18) For free edge, free corner, parapet edge and parapet corner, the yield line theory gave either a reasonable strength prediction or an underprediction when the load was of the single imprint type. For quadruple imprint loading, for all test locations, the yield line theory underpredicted strength in all cases.

APPENDIX A

LVDT LOCATIONS FOR TESTS

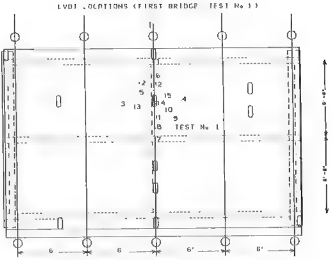

Figure A.1 LVDT Locations (First Bridge - Test No 1)

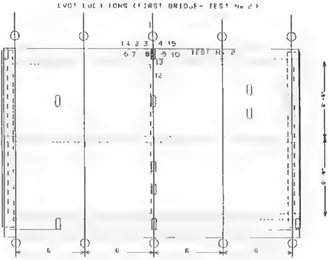

Figure A.2 LVDT Locations (First Bridge - Test No 2)

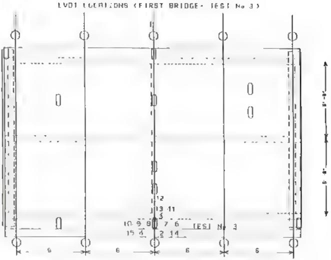

Figure A.3 LVDT Locations (First Bridge - Test No 3)

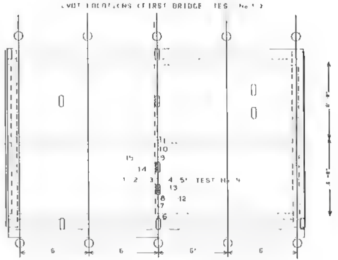

Figure A.4 LVDT Locations (First Bridge - Test No 4)

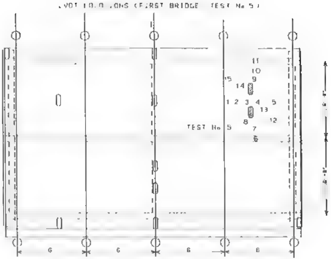

Figure A.5 LVDT Locations (First Bridge - Test No 5)

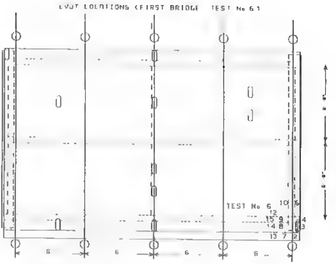

Figure A.6 LVDT Locations (First Bridge - Test No 6)

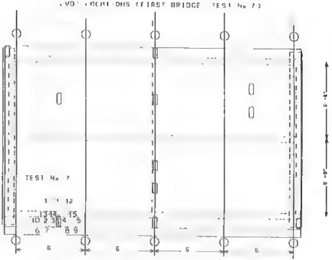

Figure A.7 LVDT Locations (First Bridge - Test No 7)

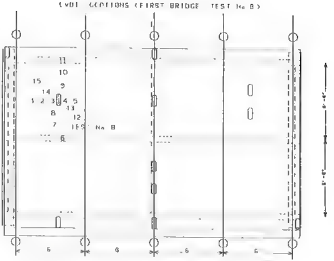

Figure A.8 LVDT Locations (First Bridge - Test No 8)

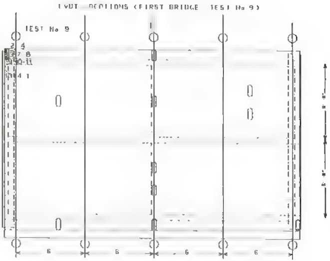

Figure A.9 LVDT Locations (First Bridge - Test No 9)

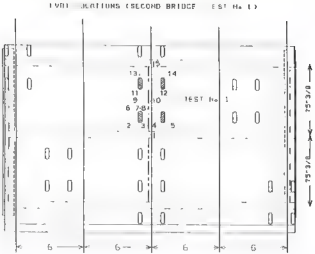

Figure A.10 LVDT Locations (Second Bridge - Test No 1)

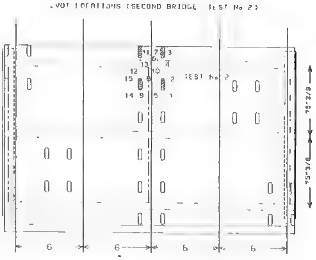

Figure A.11 LVDT Locations (Second Bridge - Test No 2)

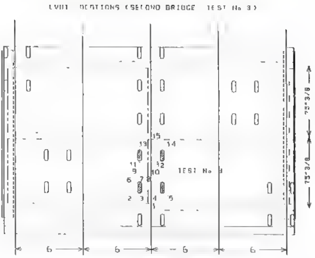

Figure A.12 LVDT Locations (Second Bridge - Test No 3)

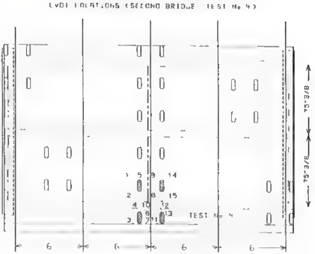

Figure A.13 LVDT Locations (Second Bridge - Test No 4)

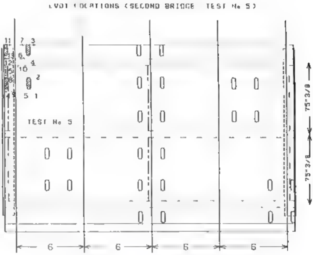

Figure A.14 LVDT Locations (Second Bridge - Test No 5)

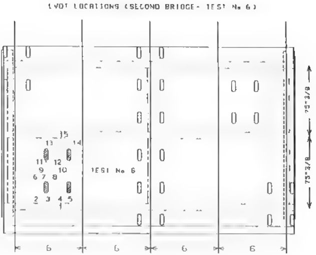

Figure A.15 LVDT Locations (Second Bridge - Test No 6)

LVDT LOCATIONS (SECOND BRIDGE TEST No 7)

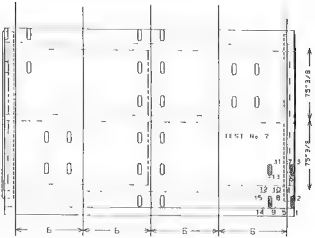

Figure A.16 LVDT Locations (Second Bridge - Test No 7)

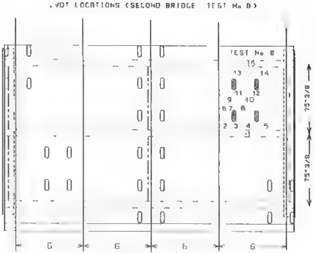

Figure A.17 LVDT Locations (Second Bridge - Test No 8)

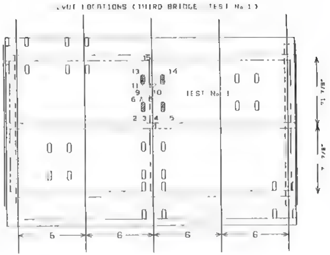

Figure A.18 LVDT Locations (Third Bridge - Test No 1)

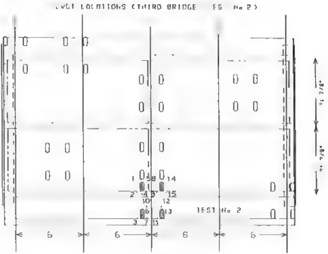

Figure A.19 LVDT Locations (Third Bridge - Test No 2)

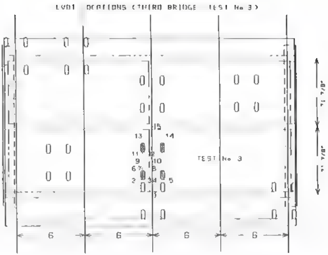

Figure A.20 LVDT Locations (Third Bridge - Test No 3)

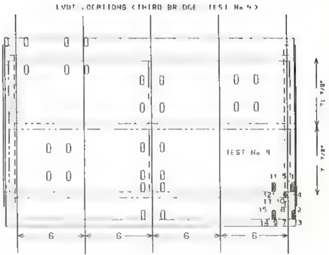

Figure A.21 LVDT Locations (Third Bridge - Test No 4)

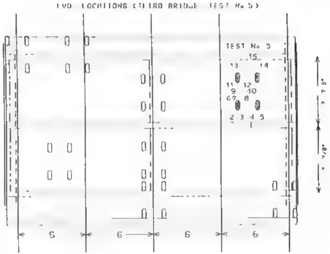

Figure A.22 LVDT Locations (Third Bridge - Test No 5)

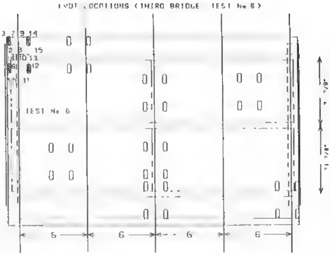

Figure A.23 LVDT Locations (Third Bridge - Test No 6)

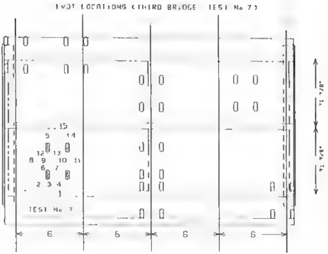

Figure A.24 LVDT Locations (Third Bridge - Test No 7)

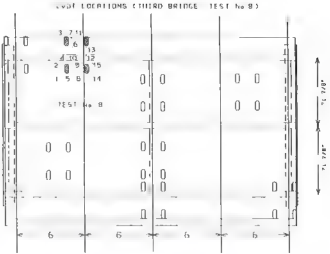

Figure A.25 LVDT Locations (Third Bridge - Test No 8)

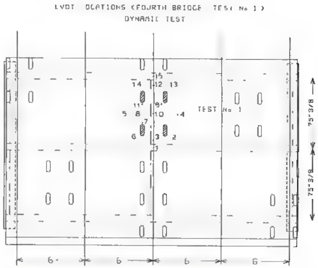

Figure A.26 LVDT Locations (Fourth Bridge - Test No 1 - Dynamic Test)

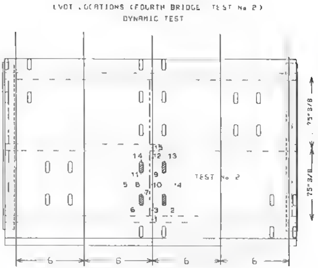

Figura A.27 LVDT Locations (Fourth Bridge - Test No 2 - Dynamic Test)

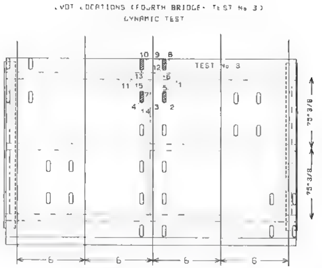

Figure A.28 LVDT Locations (Fourth Bridge - Test No 3 - Dynamic Test)

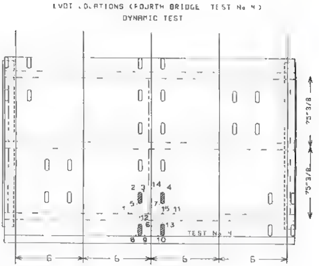

Figure A.29 LVDT Locations (Fourth Bridge - Test No 4 - Dynamic Test)

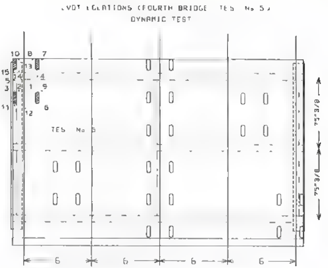

Figure A.30 LVDT Locations (Fourth Bridge - Test No 5 - Dynamic Test)

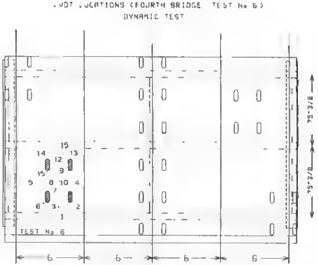

Figure A.31 LVDT Locations (Fourth Bridge - Test No 6 - Dynamic Test)

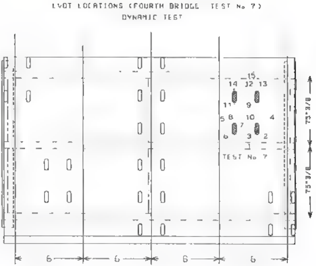

Figure A.32 LVDT Locations (Fourth Bridge - Test No 7 - Dynamic Test)

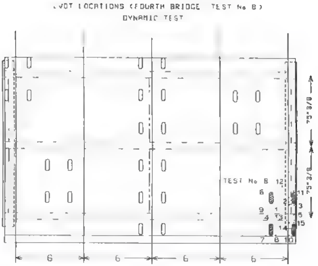

Figure A.33 LVDT Locations (Fourth Bridge - Test No 8 - Dynamic Test)

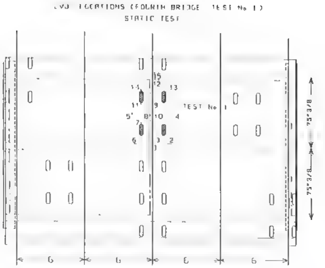

Figure A.34 LVDT Locations (Fourth Bridge - Test No 1 - Static Test)

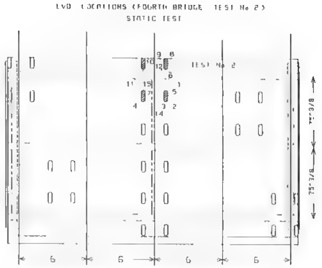

Figure A.35 LVDT Locations (Fourth Bridge - Test No 2 - Static Test)

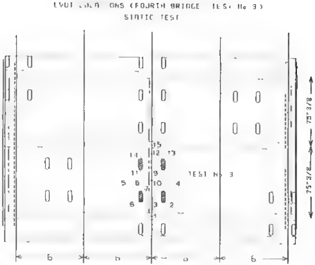

Figure A.36 LVDT Locations (Fourth Bridge - Test No 3 - Static Test)

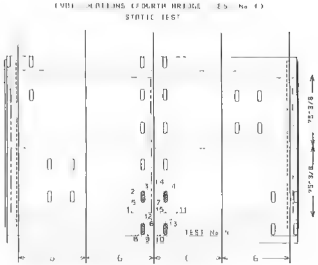

Figure A.37 LVDT Locations (Fourth Bridge - Test No 4 - Static Test)

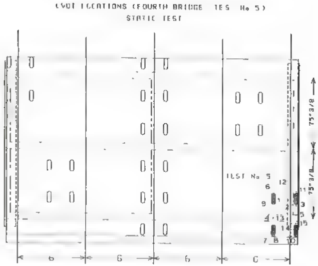

Figure A.36 LVDT Locations (Fourth Bridge - Test No 5 - Static Test)

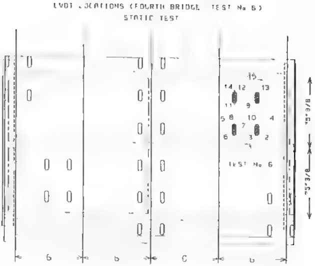

Figure A.39 LVDT Locations (Fourth Bridge - Test No 6 - Static Test)

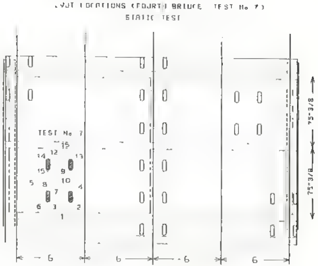

Figure A.40 LVDT Locations (Fourth Bridge - Test No 7 - Static Test)

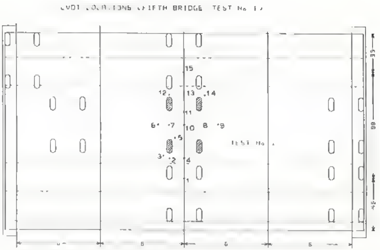

Figure A.42 LVDT Locations (Fifth Bridge - Test No 1)

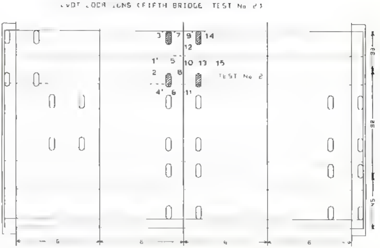

Figure A.43 LVDT Locations (Fifth Bridge - Test No 2)

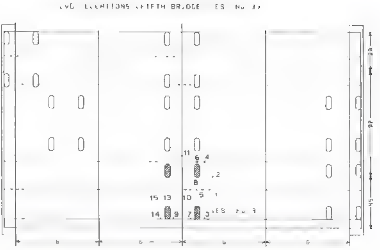

Figure A.44 LVDT Locations (Fifth Bridge - Test No 3)

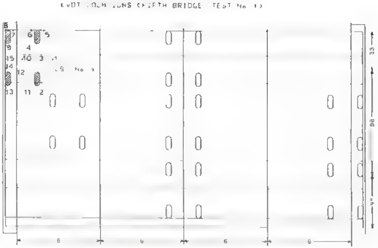

Figure A.45 LVDT Locations (Fifth Bridge - Test No 4)

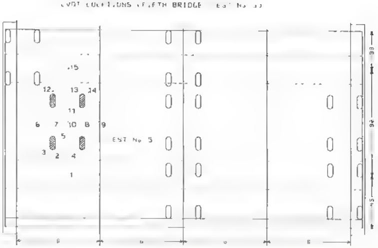

Figure A.46 LVDT Locations (Fifth Bridge - Test No 5)

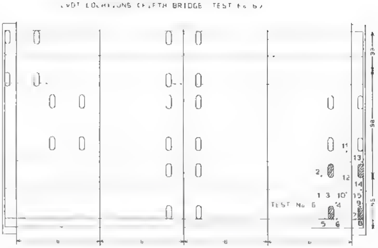

Figure A.47 LVDT Locations (Fifth Bridge - Test No 6)

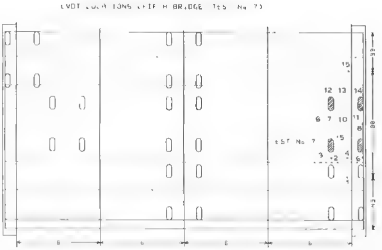

Figure A.48 LVDT Locations (Fifth Bridge - Test No 7)

APPENDIX B

COMPLETE LOAD DEFLECTION PLOTS

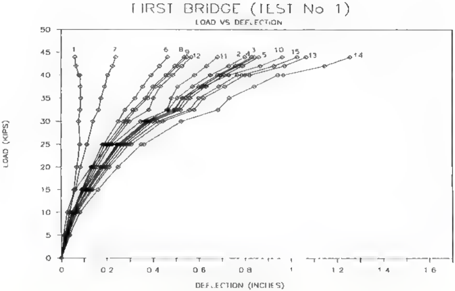

Figure B.1 Load-Deflection Curves (First Bridge - Test No 1)

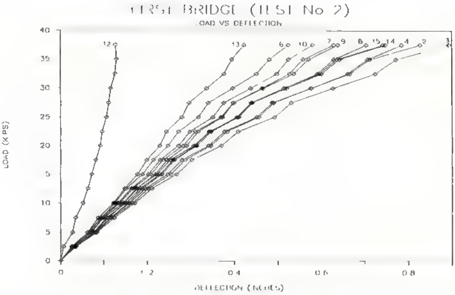

Figure B 2 Load-Deflection Curves (First Bridge - Test No 2)

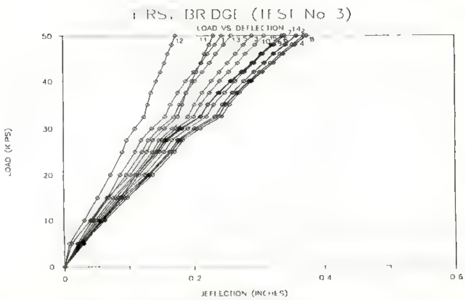

Figure B.3 Load-Deflection Curves (First Bridge - Test No 3)

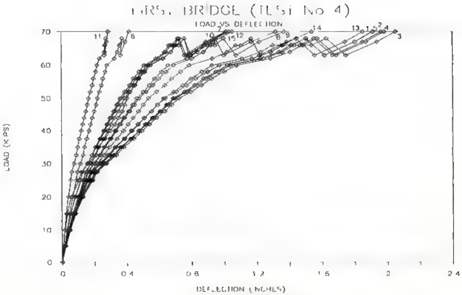

Figure B.4 Load-Deflection Curves (First Bridge - Test No 4)

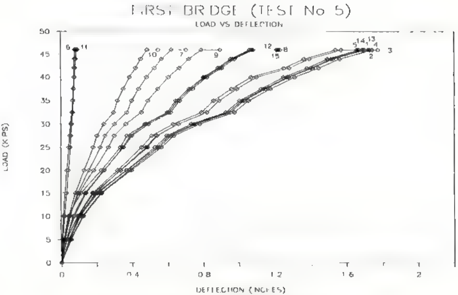

Figure B.5 Load-Deflection Curves (First Bridge - Test No 5)

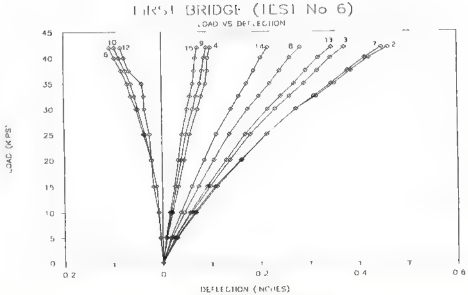

Figure B.6 Load-Deflection Curves (First Bridge - Test No 6)

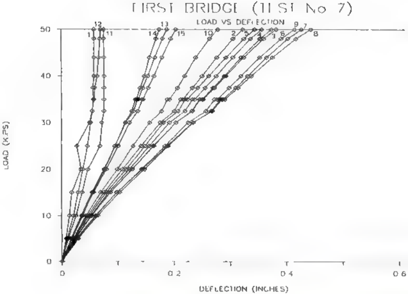

Figure B.7 Load-Deflection Curves (First Bridge - Test No 7)

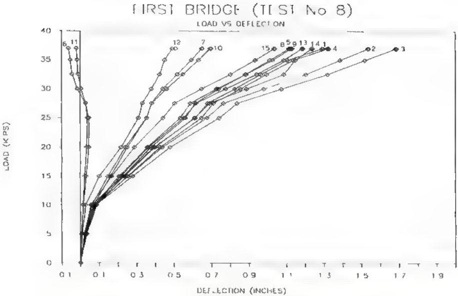

Figure B.8 Load-Deflection Curves (First Bridge - Test No 8)

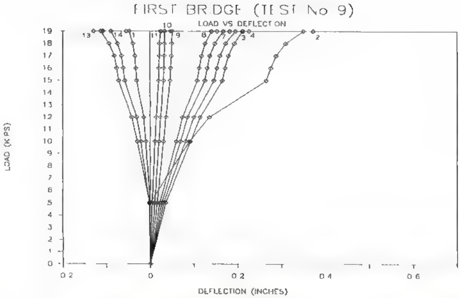

Figure B.9 Load-Deflection Curves (First Bridge - Test No 9)

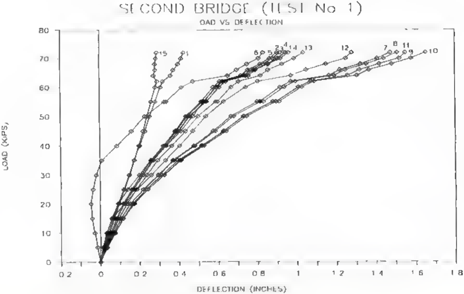

Figure B.10 Load-Deflection Curves (Second Bridge - Test No 1)

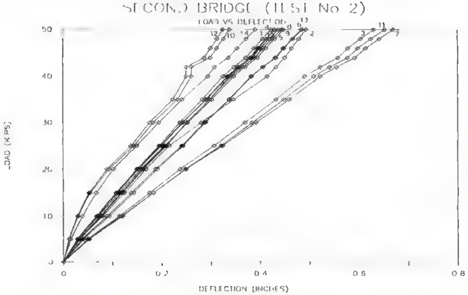

Figure B.11 Load-Deflection Curves (Second Bridge - Test No 2)

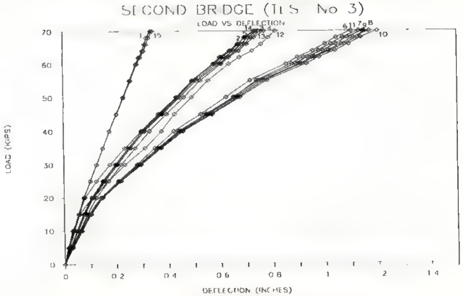

Figure B.12 Load-Deflection Curves (Second Bridge - Test No 3)

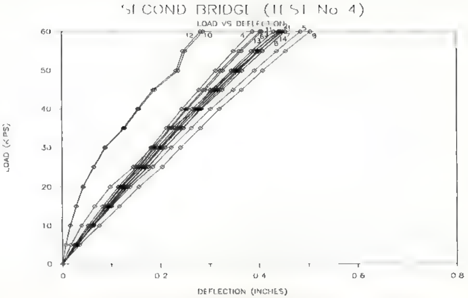

Figure B.13 Load-Deflection Curves (Second Bridge - Test No 4)

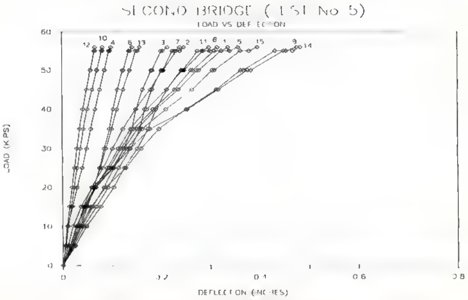

Figure B.14 Load-Deflection Curves (Second Bridge - Test No 5)

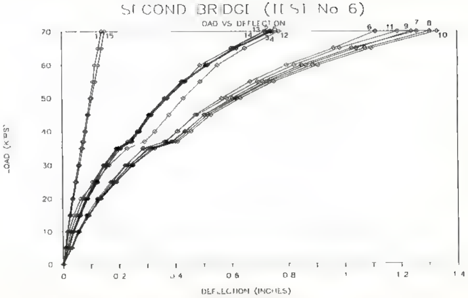

Figure B.15 Load-Deflection Curves (Second Bridge - Test No 6)

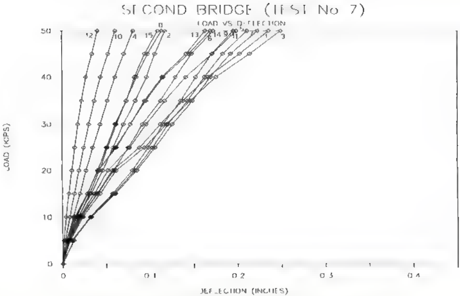

Figure B.16 Load-Deflection Curves (Second Bridge - Test No 7)

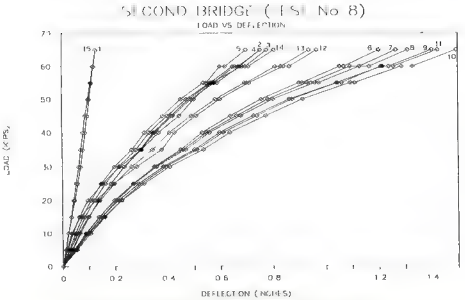

Figure B.17 Load-Deflection Curves (Second Bridge - Test No 8)

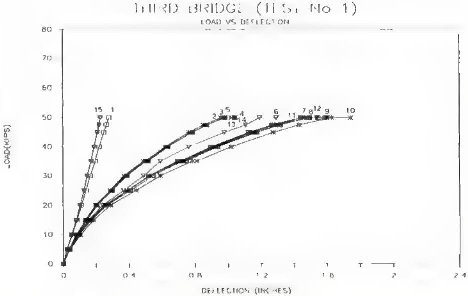

Figure B.1B Load-Deflection Curves (Third Bridge - Test No 1)

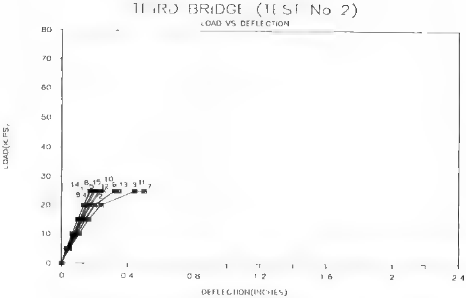

Figure B.19 Load-Deflection Curves (Third Bridge - Test No 2)

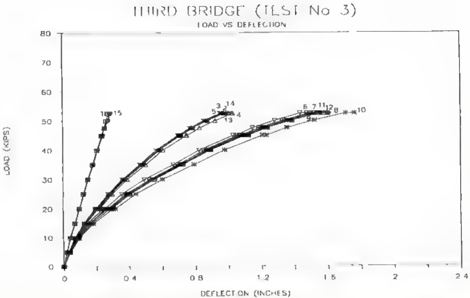

Figure B.20 Load-Deflection Curves (Third Bridge - Test No 3)

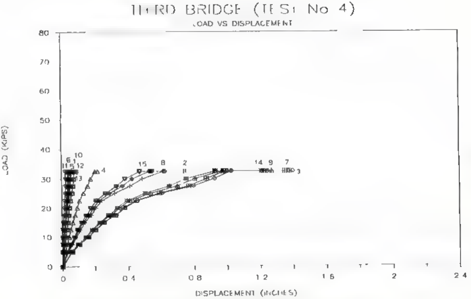

Figure B.21 Load-Deflection Curves (Third Bridge - Test No 4)

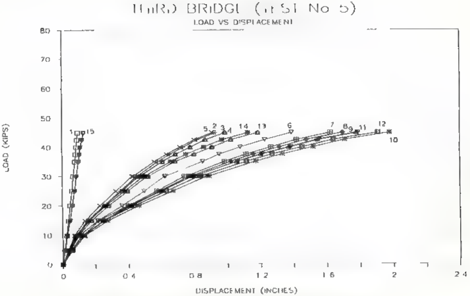

Figure B.22 Load-Deflection Curves (Third Bridge - Test No 5)

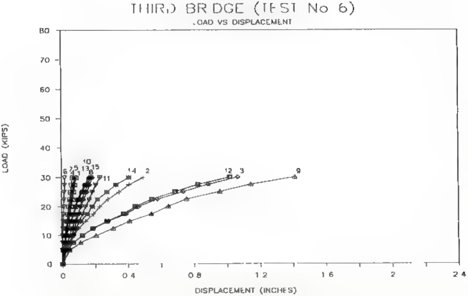

Figure B.23 Load-Deflection Curves (Third Bridge - Test No 6)

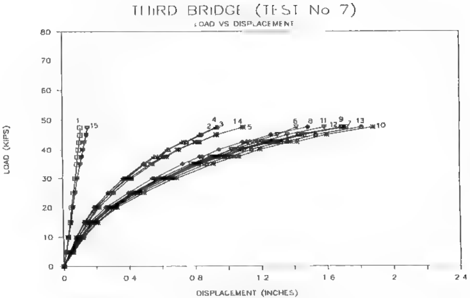

Figure B.24 Load-Deflection Curves (Third Bridge - Test No 7)

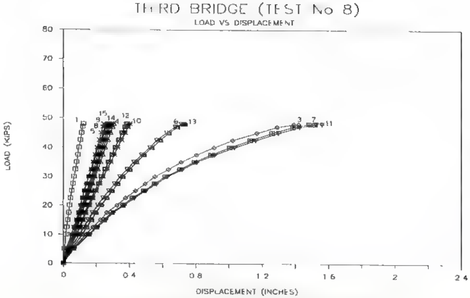

Figure B.25 Load-Deflection Curves (Third Bridge - Test No 8)

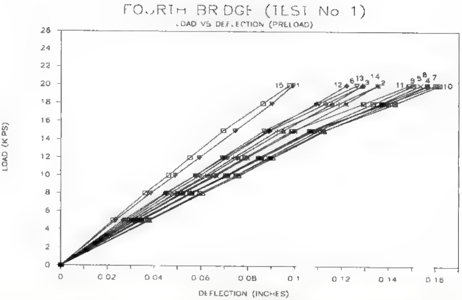

Figure B.26 Load-Deflection Curves (Fourth Bridge - Test No 1 -Preload)

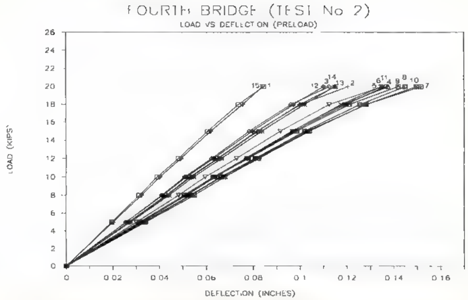

Figure B.27 Load-Deflection Curves (Fourth Bridge - Test No 2 -Preload)

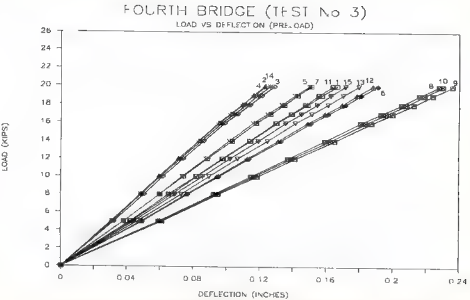

Figure B.28 Load-Deflection Curves (Fourth Bridge - Test No 3 -Preload)

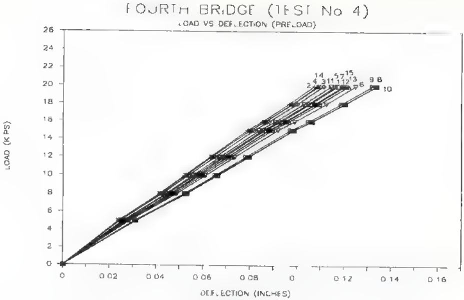

Figure B.29 Load-Deflection Curves (Fourth Bridge - Test No 4 -Preload)

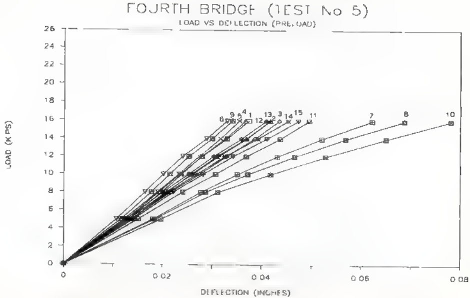

Figure B.30 Load-Deflection Curves (Fourth Bridge - Test No 5 -Preload)

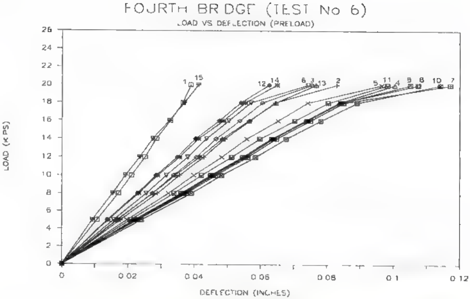

Figure B.31 Load-Deflection Curves (Fourth Bridge - Test No 6 -Preload)

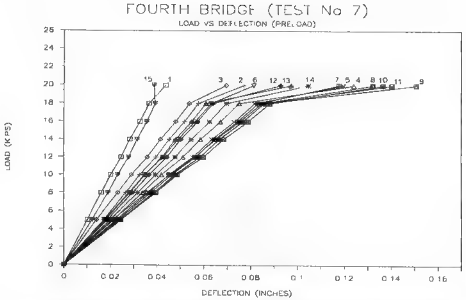

Figure B.32 Load-Deflection Curves (Fourth Bridge - Test No 7 -Preload)

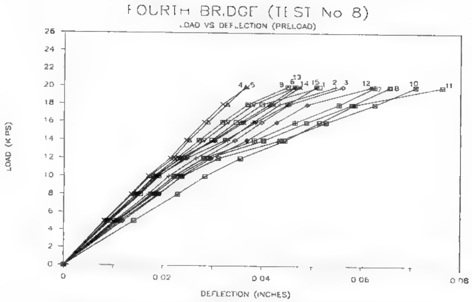

Figure B.33 Load-Deflection Curves (Fourth Bridge - Test No 8 -Preload)

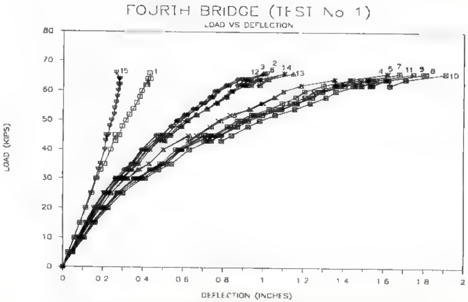

Figure B.34 Load-Deflection Curves (Fourth Bridge - Test No 1)

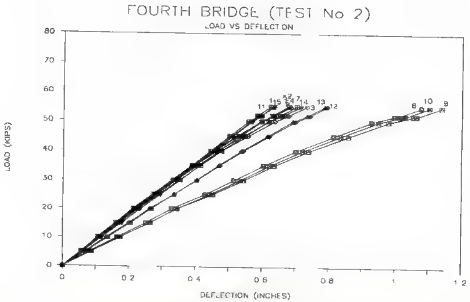

Figure B.35 Load-Deflection Curves (Fourth Bridge - Test No 2)

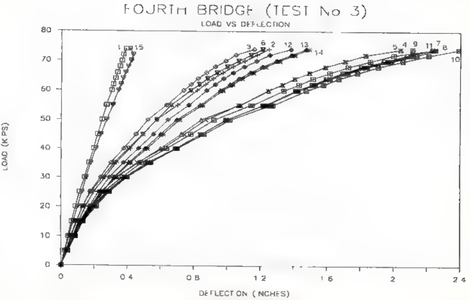

Figure B.36 Load-Deflection Curves (Fourth Bridge - Test No 3)

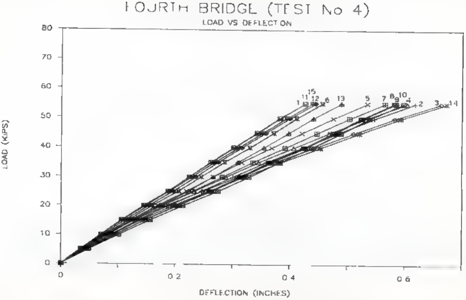

Figure B.37 Load-Deflection Curves (Fourth Bridge - Test No 4)

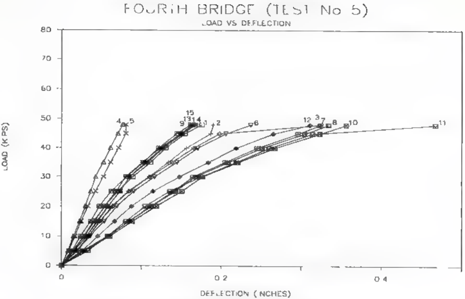

Figure B.38 Load-Deflection Curves (Fourth Bridge - Test No 5)

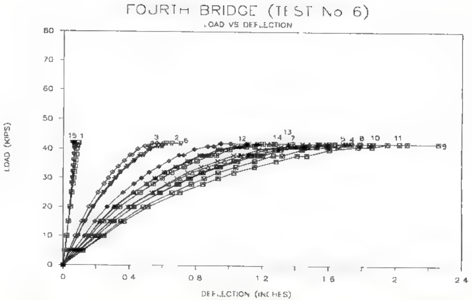

Figure B.39 Load-Deflection Curves (Fourth Bridge - Test No 6)

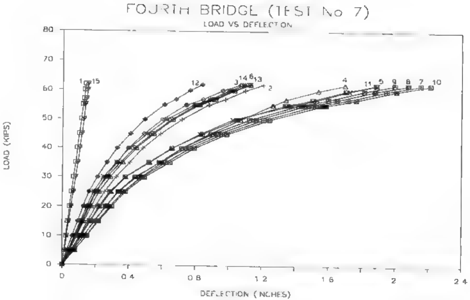

Figure B.40 Load-Deflection Curves (Fourth Bridge - Test No 7)

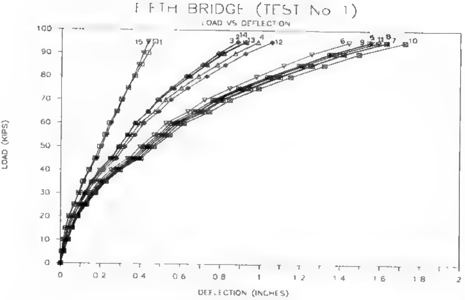

Figure B.41 Load-Deflection Curves (Fifth Bridge - Test No 1)

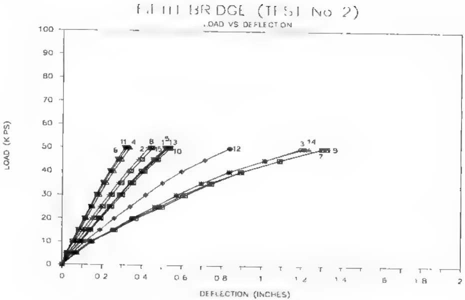

Figure B.42 Load-Deflection Curves (Fifth Bridge - Test No 2)

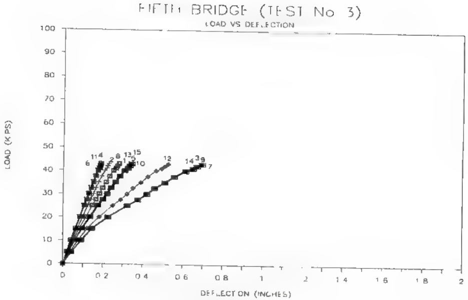

Figure B.43 Load-Deflection Curves (Fifth Bridge - Test No 3)

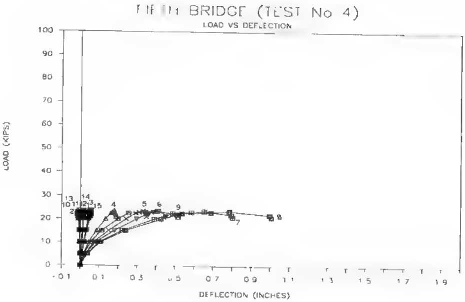

Figure B.44 Load-Deflection Curves (Fifth Bridge - Test No 4)

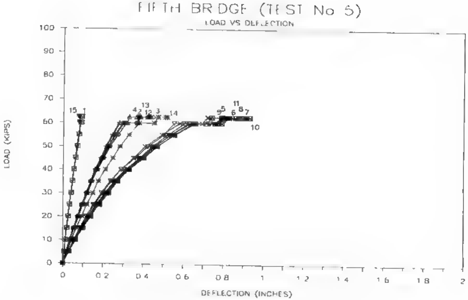

Figure B.45 Load-Deflection Curves (Fifth Bridge - Test No 5)

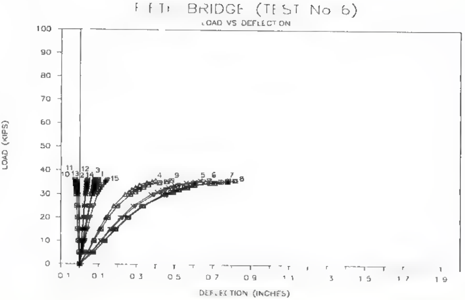

Figure B.46 Load-Deflection Curves (Fifth Bridge - Test No 6)

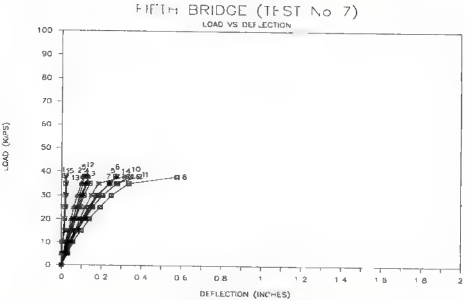

Figure B.47 Load-Deflection Curves (Fifth Bridge - Test No 7)

APPENDIX C

STRAIN GAGE LOCATIONS FOR TESTS

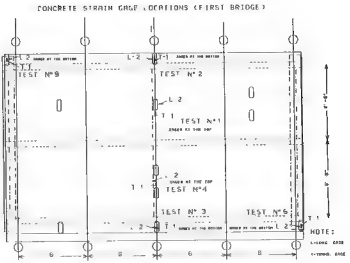

Figure C.1 Concrete Strain Gage Locations (First Bridge)

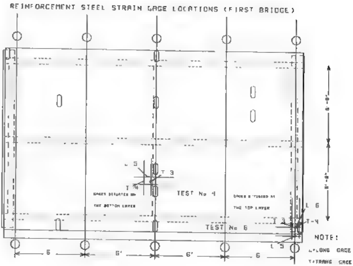

Figure C.2 Reinforcement Steel Strain Gage Locations (First Bridge)

CONCRETE STRAIN GAGE LOCATIONS (SECOND BRIDGE)

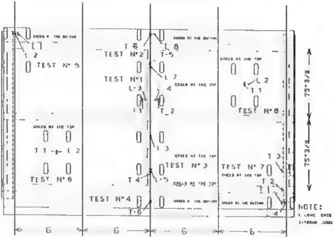

Figure C.3 Concrete Strain Gage Locations (Second Bridge)

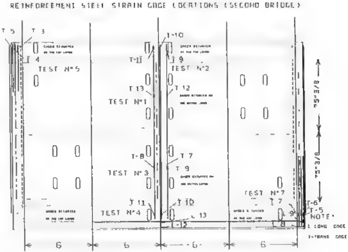

Figure C.4 Reinforcement Steel Strain Gage Locations (Second Bridge)

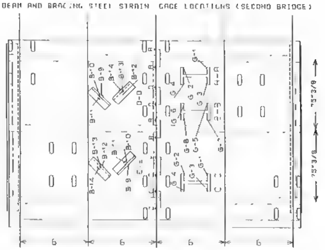

Figure C.5 Beam and Bracing Steel Strain Gage Locations (Second Bridge)

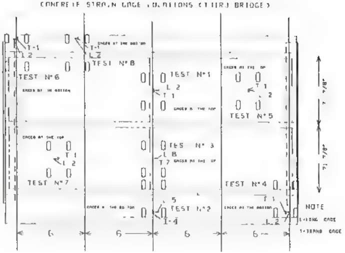

Figure C.6 Concrete Strain Gage Locations (Third Bridge)

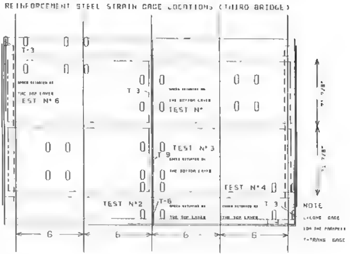

Figure C.7 Reinforcement Steel Strain Gage Locations (Third Bridge)

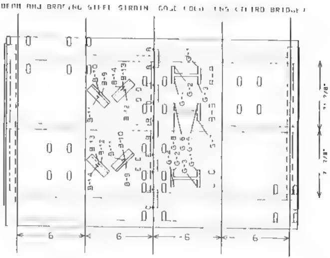

Figure C.8 Beam and Bracing Steel Strain Gage Locations (Third Bridge)

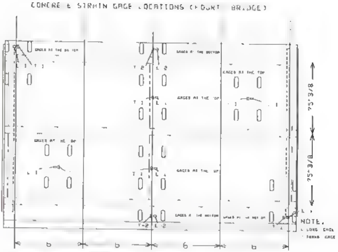

Figure C.9 Concrete Strain Gage Locations (Fourth Bridge)

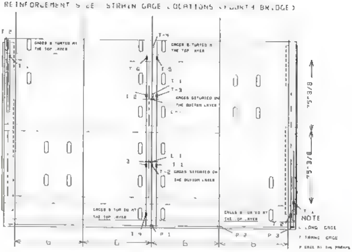

Figure C.10 Reinforcement Steel Strain Gage Locations (Fourth Bridge)

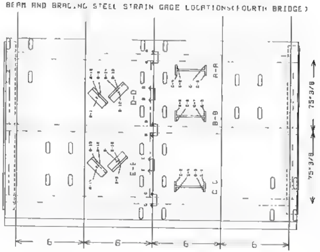

Figure C.11 Beam and Bracing Steel Strain Gage Locations (Fourth Bridge)

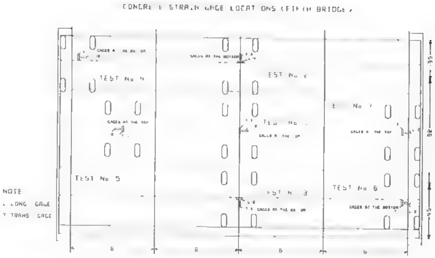

Figure C.12 Concrete Strain Gage Locations (Fifth Bridge)

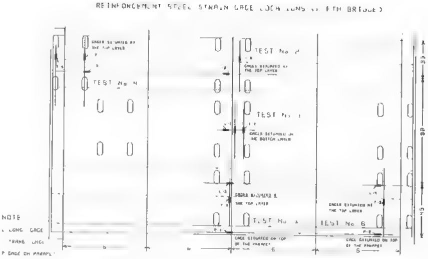

Figure C.13 Reinforcement Steel Strain Gage Locations (Fifth Bridge)

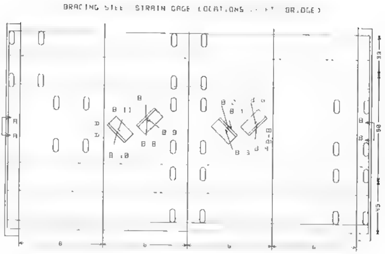

Figure C.14 Beam and Bracing Steel Strain Gage Locations (Fifth Bridge)

APPENDIX D

STRAIN GAGE PLOTS

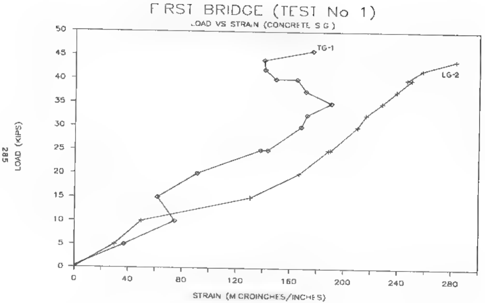

Figure D.1 Load-Strain Curves (First Bridge, Test No 1, Concrete S.G.)

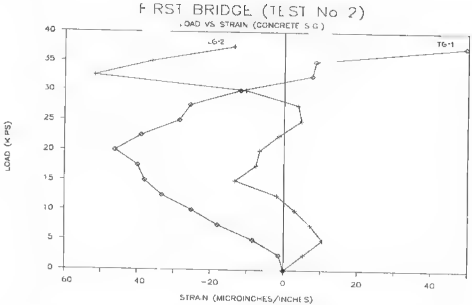

Figure D.2 Load-Strain Curves (First Bridge, Test No 2, Concrete S.G.)

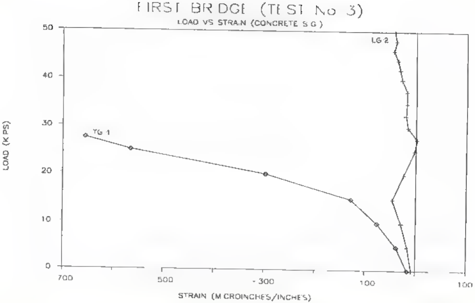

Figure D.3 Load-Strain Curves (First Bridge, Test No 3, Concrete S.G.)

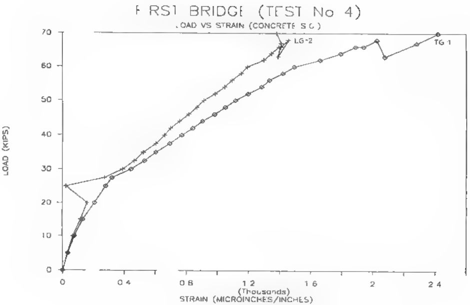

Figure D.4 Load-Strain Curves (First Bridge, Test No 4, Concrete S.G.)

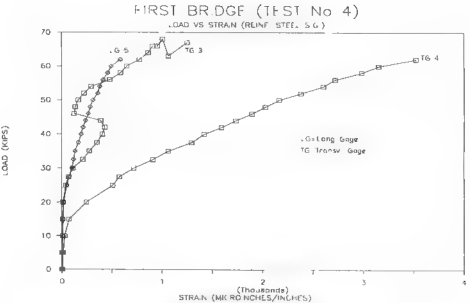

Figure D.5 Load-Strain Curves (First Bridge, Test No 4, Reinforced Steel S.G.)

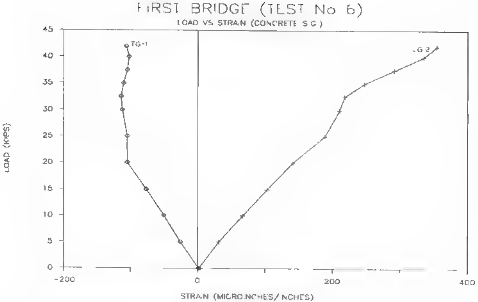

Figure D.6 Load-Strain Curves (First Bridge, Test No 6, Concrete S.G.)

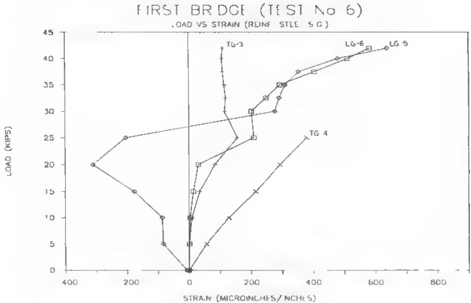

Figure D.7 Load-Strain Curves (First Bridge, Test No 6, Reinforced Steel S.G.)

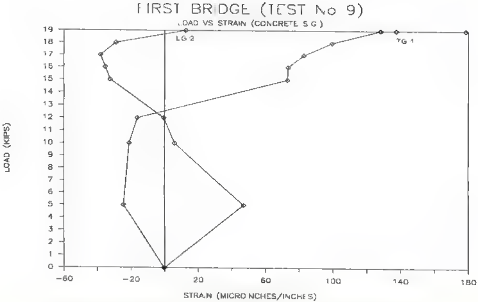

Figure D.8 Load-Strain Curves (First Bridge, Test No 9, Concrete S.G.)

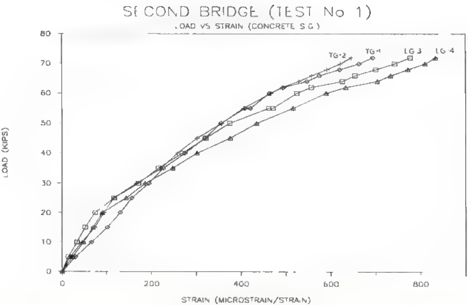

Figure D.9 Load-Strain Curves (Second Bridge, Test No 1, Concrete S.G.)

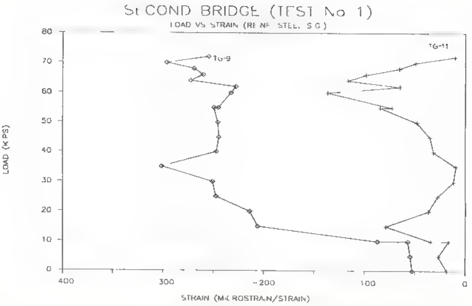

Figure D.10 Load-Strain Curves (Second Bridge, Test No 1, Reinforced Steel S.G.)

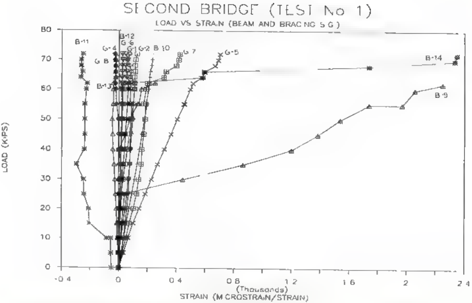

Figure D.11 Load-Strain Curves (Second Bridge, Test No 1, Beam and Bracing S.G.)

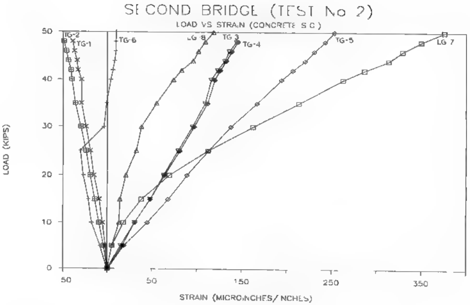

Figure D.12 Load-Strain Curves (Second Bridge, Test No 2, Concrete S.G.)

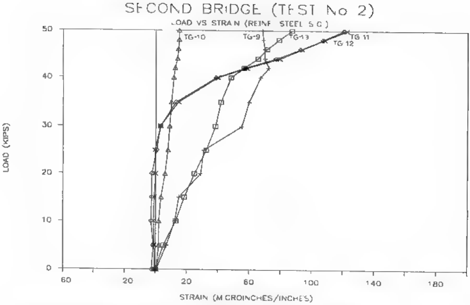

Figure D.13 Load-Strain Curves (Second Bridge, Test No 2, Reinforced Steel S.G.)

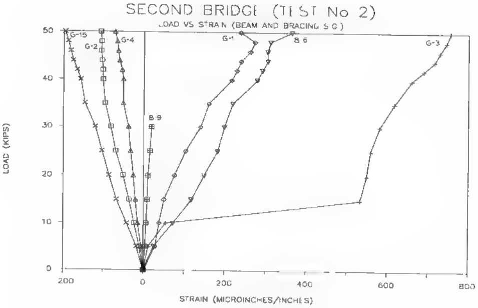

Figure D.14 Load-Strain Curves (Second Bridge, Test No 2, Beam and Bracing S.G.)

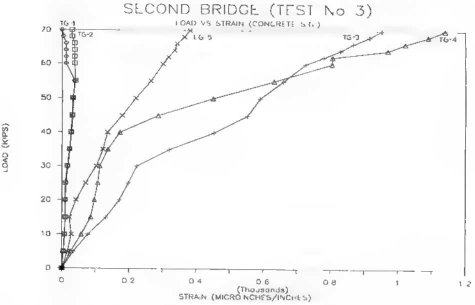

Figure D.15 Load-Strain Curves (Second Bridge, Test No 3, Concrete S.G.)

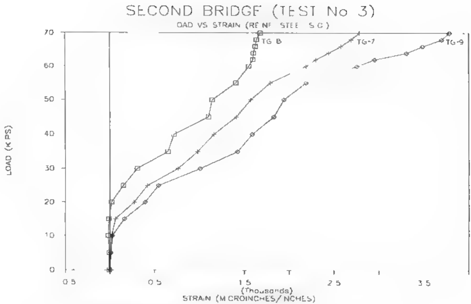

Figure D.16 Load-Strain Curves (Second Bridge, Test No 3, Reinforced Steel S.G.)

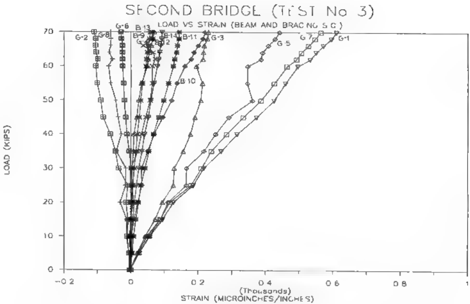

Figure D.17 Load-Strain Curves (Second Bridge, Test No 3, Beam and Bracing S.G.)

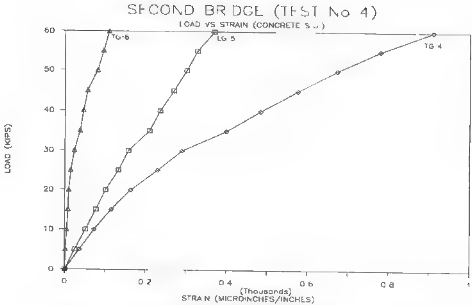

Figure D.18 Load-Strain Curves (Second Bridge, Test No 4, Concrete S.G.)

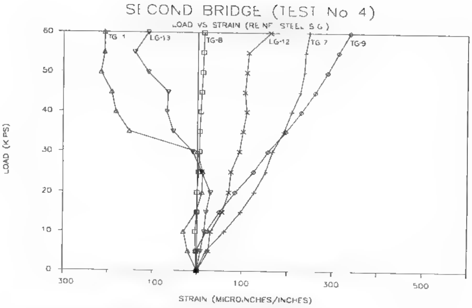

Figure D.19 Load-Strain Curves (Second Bridge, Test No 4, Reinforced Steel S.G.)

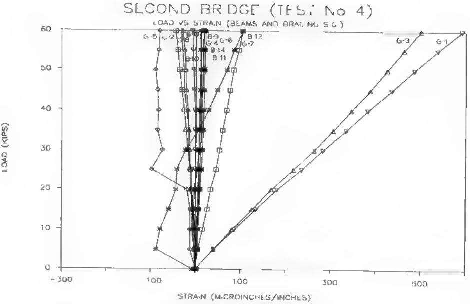

Figure D.20 Load-Strain Curves (Second Bridge, Test No 4, Beam and Bracing S.G.)

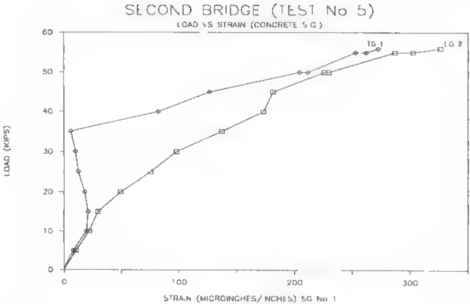

Figure D.21 Load-Strain Curves (Second Bridge, Test No 5, Concrete S.G.)

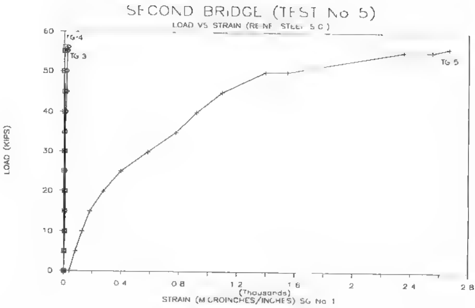

Figure D.22 Load-Strain Curves (Second Bridge, Test No 5, Reinforced Steel S.G.)

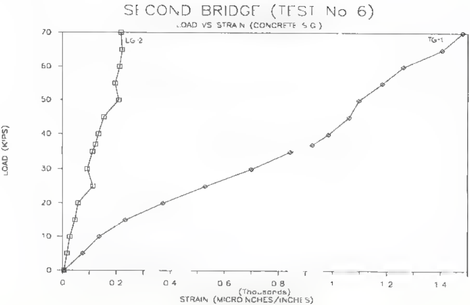

Figure D.23 Load-Strain Curves (Second Bridge, Test No 6, Concrete S.G.)

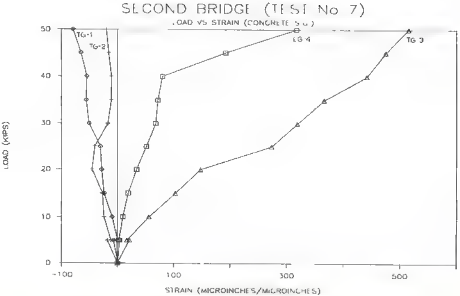

Figure D.24 Load-Strain Curves (Second Bridge, Test No 7, Concrete S.G.)

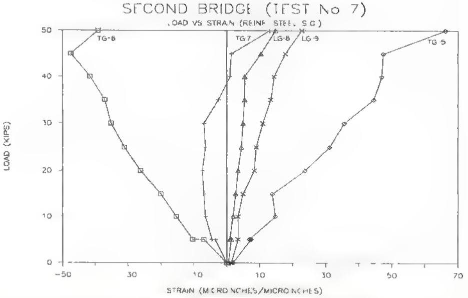

Figure D.25 Load-Strain Curves (Second Bridge, Test No 7, Reinforced Steel S.G.)

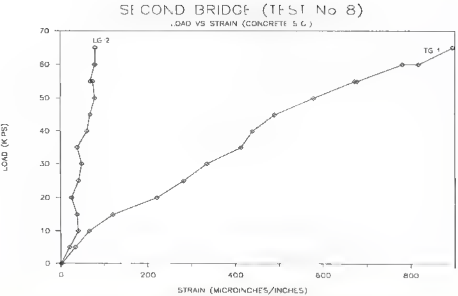

Figure D.26 Load-Strain Curves (Second Bridge, Test No 8, Concrete S.G.)

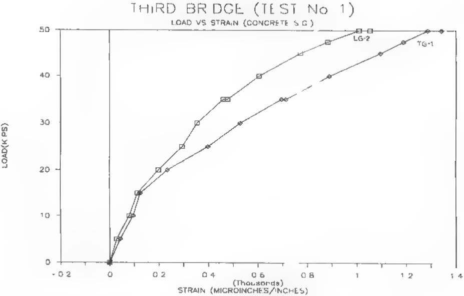

Figure D.27 Load-Strain Curves (Third Bridge, Test No 1, Concrete S.G.)

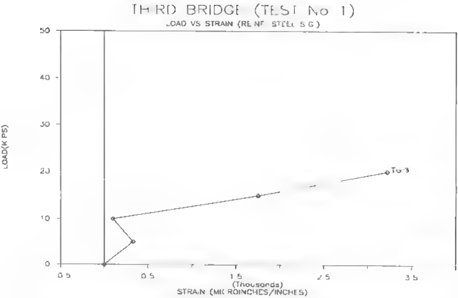

Figure D.28 Load-Strain Curves (Third Bridge, Test No 1, Reinforced Steel S.G.)

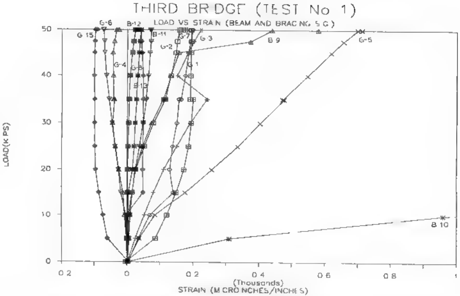

Figure D.29 Load-Strain Curves (Third Bridge, Test No 1, Beam and Bracing S.G.)

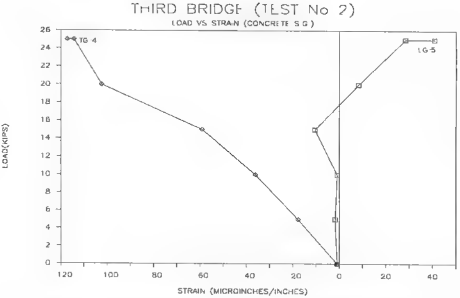

Figure D.30 Load-Strain Curves (Third Bridge, Test No 2, Concrete S.G.)

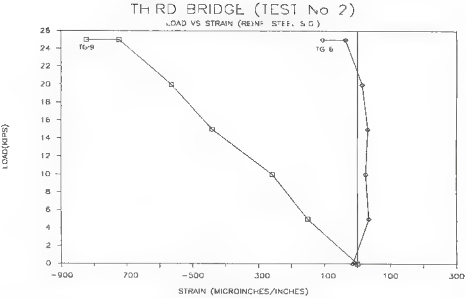

Figure D.31 Load-Strain Curves (Third Bridge, Test No 2, Reinforced Steel S.G.)

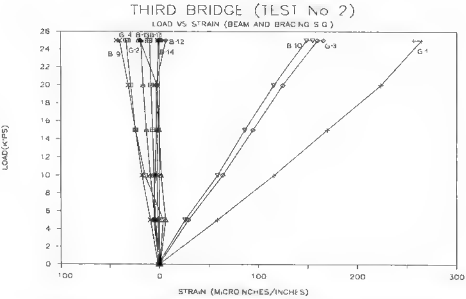

Figure D.32 Load-Strain Curves (Third Bridge, Test No 2, Beam and Bracing S.G.)

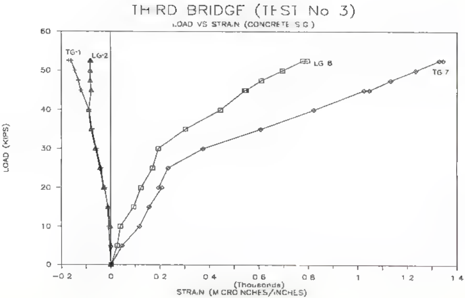

Figure D.33 Load-Strain Curves (Third Bridge, Test No 3, Concrete S.G.)

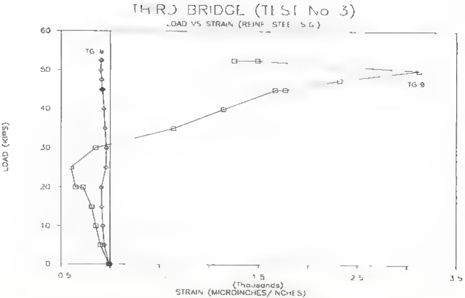

Figure D.34 Load-Strain Curves (Third Bridge, Test No 3, Reinforced Steel S.G.)

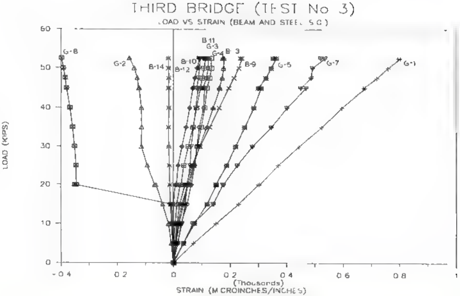

Figure D.35 Load-Strain Curves (Third Bridge, Test No 3, Beam and Bracing S.G.)

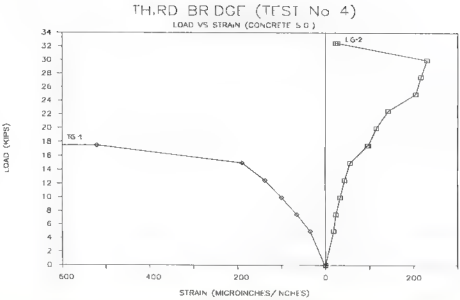

Figure D.36 Load-Strain Curves (Third Bridge, Test No 4, Concrete S.G.)

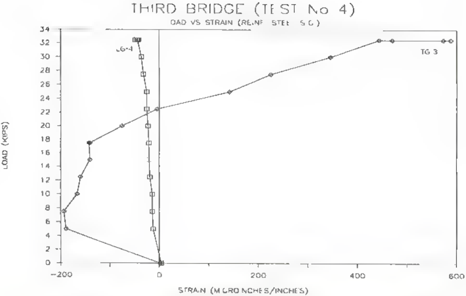

Figure D.37 Load-Strain Curves (Third Bridge, Test No 4, Reinforced Steel S.G.)

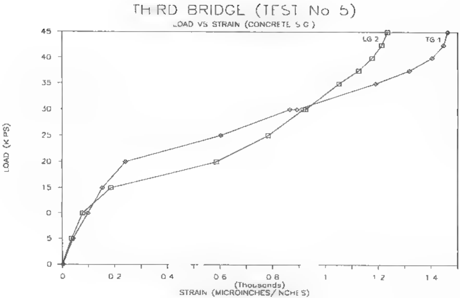

Figure D.38 Load-Strain Curves (Third Bridge, Test No 5, Concrete S.G.)

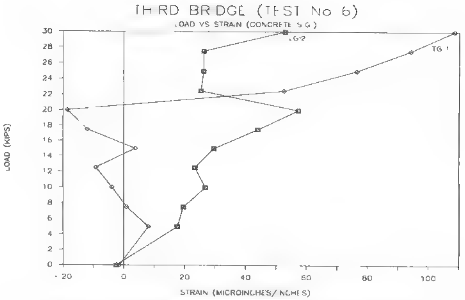

Figure D.39 Load-Strain Curves (Third Bridge, Test No 6, Concrete S.G.)

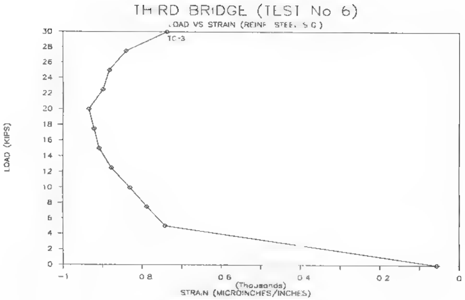

Figure D.40 Load-Strain Curves (Third Bridge, Test No 6, Reinforced Steel S.G.)

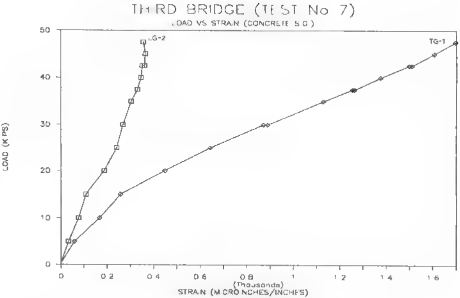

Figure D.41 Load-Strain Curves (Third Bridge, Test No 7, Concrete S.G.)

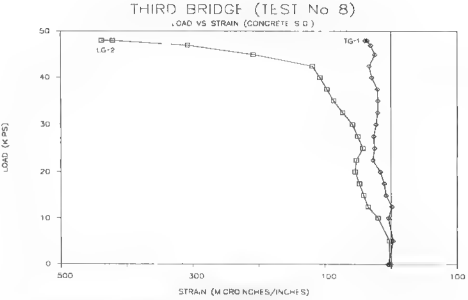

Figure D.42 Load-Strain Curves (Third Bridge, Test No 8, Concrete S.G.)

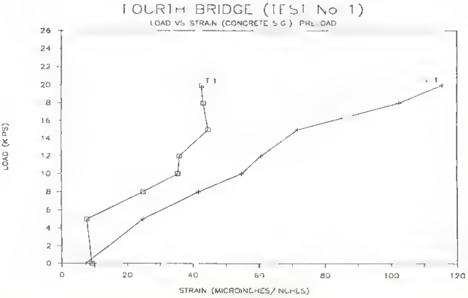

Figure D.43 Load-Strain Curves (Fourth Bridge, Test No 1, Concrete S.G., Preload)

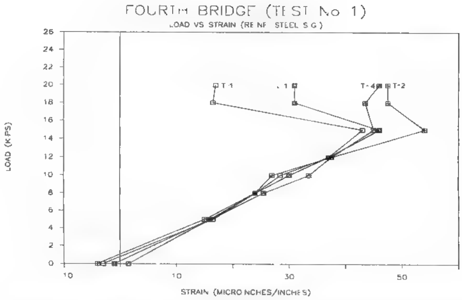

Figure D.44 Load-Strain Curves (Fourth Bridge, Test No 1, Reinforced Steel S.G., Preload)

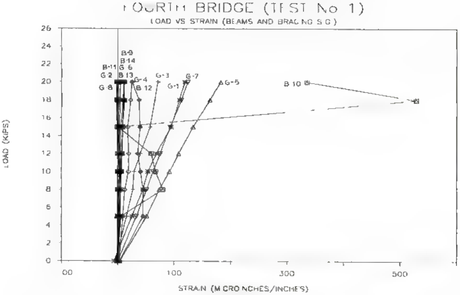

Figure D.45 Load-Strain Curves (Fourth Bridge, Test No 1, Beam and Bracing S.G., Preload)

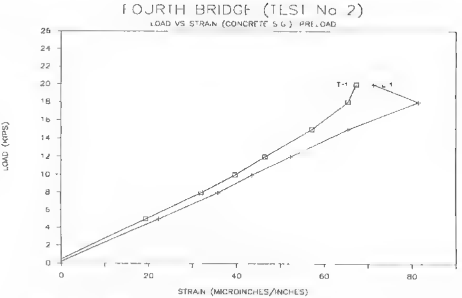

Figure D.46 Load-Strain Curves (Fourth Bridge, Test No 2, Concrete S.G., Preload)

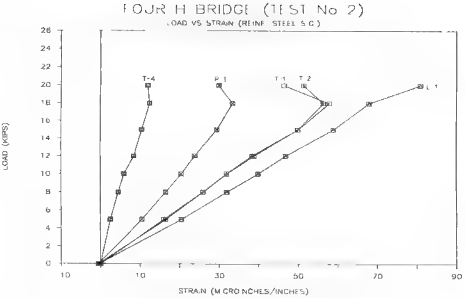

Figure D.47 Load-Strain Curves (Fourth Bridge, Test No 2, Reinforced Steel S.G., Preload)

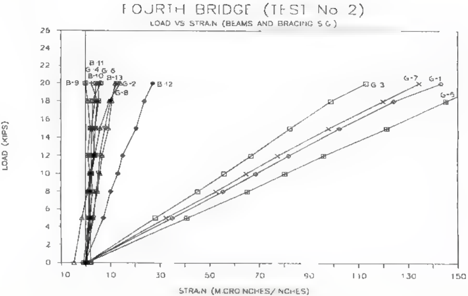

Figure D.48 Load-Strain Curves (Fourth Bridge, Test No 2, Beam and Bracing S.G., Preload)

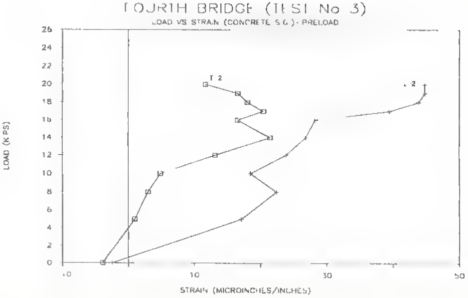

Figure D.49 Load-Strain Curves (Fourth Bridge, Test No 3, Concrete S.G., Preload)

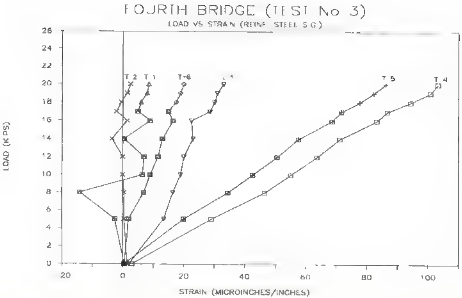

Figure D.50 Load-Strain Curves (Fourth Bridge, Test No 3, Reinforced Steel S.G., Preload)

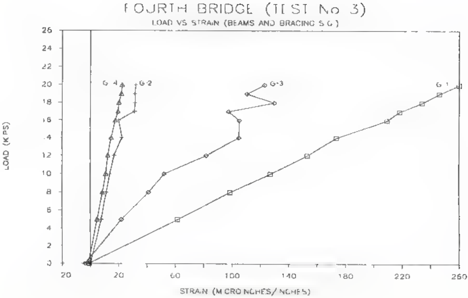

Figure D.51 Load-Strain Curves (Fourth Bridge, Test No 3, Beam and Bracing S.G., Preload)

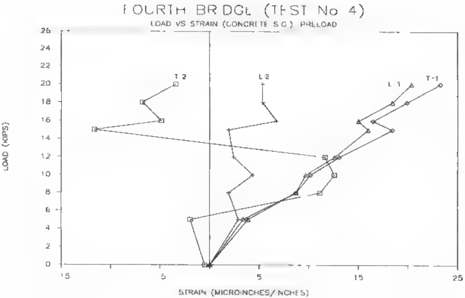

Figure D.52 Load-Strain Curves (Fourth Bridge, Test No 4, Concrete S.G., Preload)

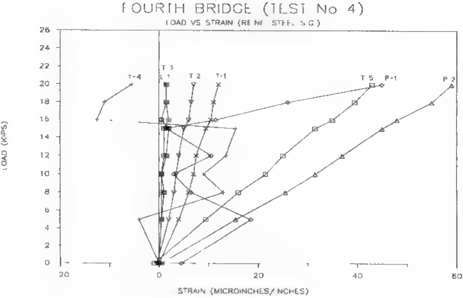

Figure D.53 Load-Strain Curves (Fourth Bridge, Test No 4, Reinforced Steel S.G., Preload)

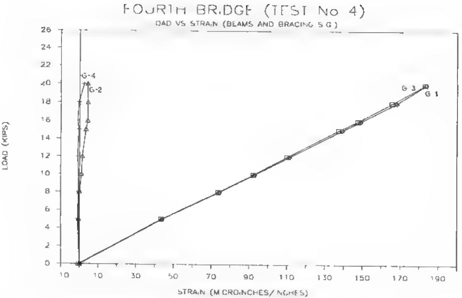

Figure D.54 Load-Strain Curves (Fourth Bridge, Test No 4, Beam and Bracing S.G., Preload)

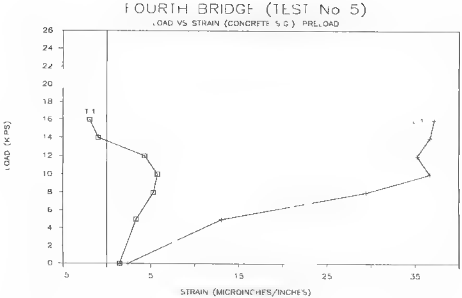

Figure D.55 Load-Strain Curves (Fourth Bridge, Test No 5, Concrete S.G., Preload)

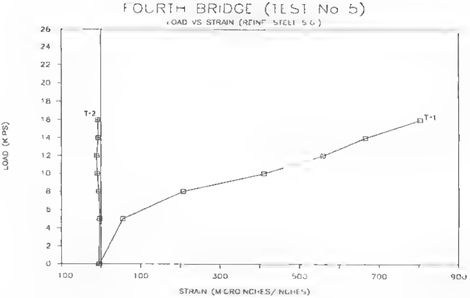

Figure D.56 Load-Strain Curves (Fourth Bridge, Test No 5, Reinforced Steel S.G., Preload)

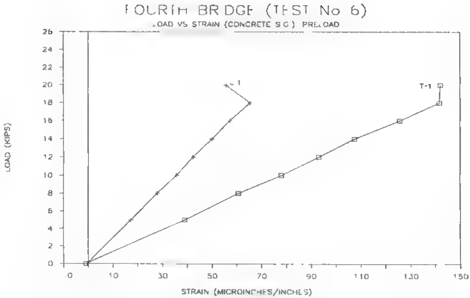

Figure D.57 Load-Strain Curves (Fourth Bridge, Test No 6, Concrete S.G., Preload)

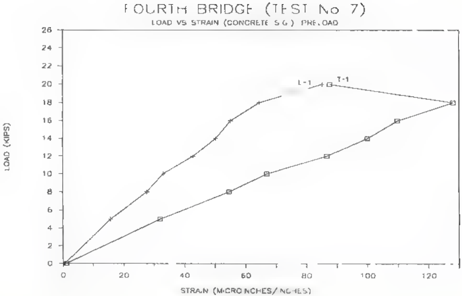

Figure D.58 Load-Strain Curves (Fourth Bridge, Test No 7, Concrete S.G., Preload)

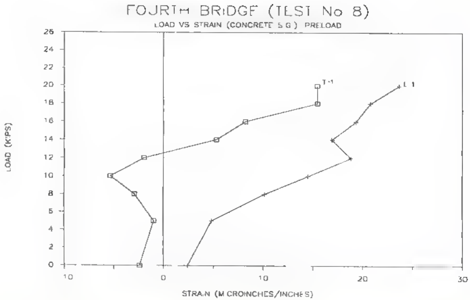

Figure D.59 Load-Strain Curves (Fourth Bridge, Test No 8, Concrete S.G., Preload)

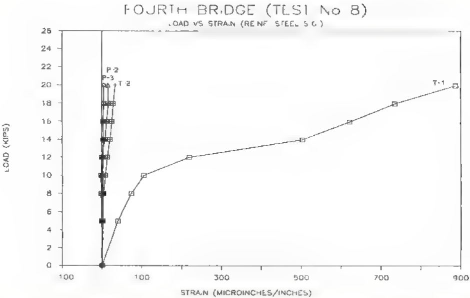

Figure D.60 Load-Strain Curves (Fourth Bridge, Test No 8, Reinforced Steel S.G., Preload)

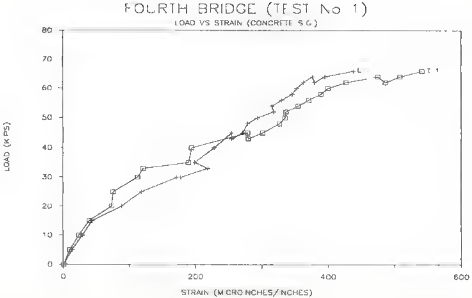

Figure D.61 Load-Strain Curves (Fourth Bridge, Test No 1, Concrete S.G.)

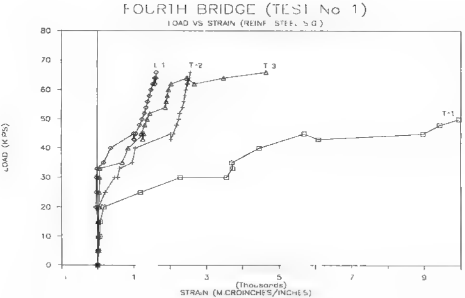

Figure D.62 Load-Strain Curves (Fourth Bridge, Test No 1, Reinforced Steel S.G.)

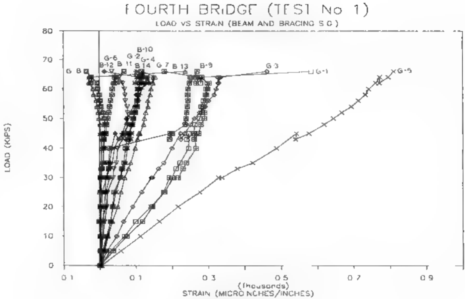

Figure D.63 Load-Strain Curves (Fourth Bridge, Test No 1, Beam and Bracing S.G.)

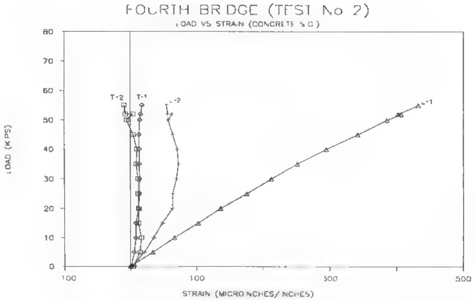

Figure D.64 Load-Strain Curves (Fourth Bridge, Test No 2, Concrete S.G.)

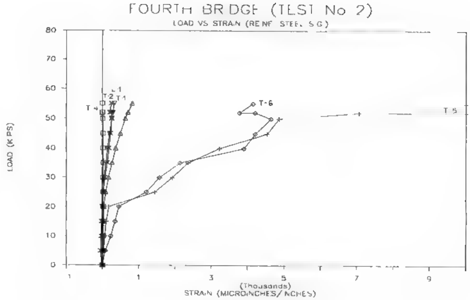

Figure D.65 Load-Strain Curves (Fourth Bridge, Test No 2, Reinforced Steel S.G.)

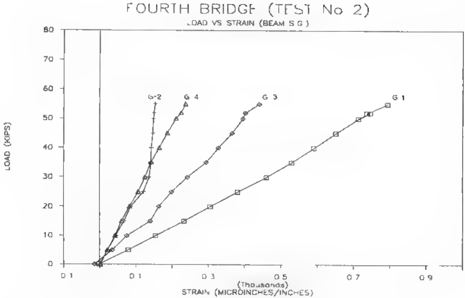

Figure D.66 Load-Strain Curves (Fourth Bridge, Test No 2, Beam and Bracing S.G.)

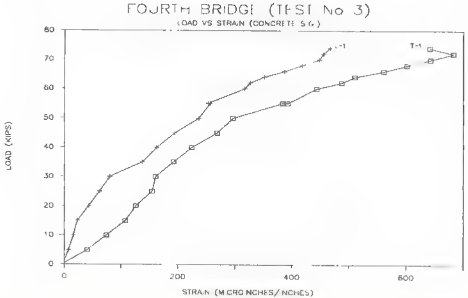

Figure D.67 Load-Strain Curves (Fourth Bridge, Test No 3, Concrete S.G.)

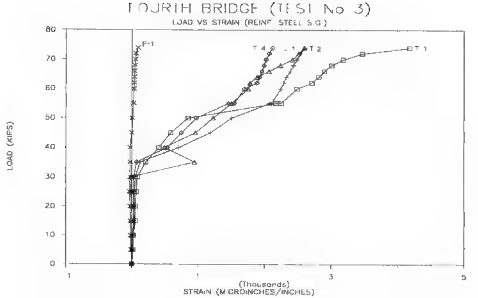

Figure D.68 Load-Strain Curves (Fourth Bridge, Test No 3, Reinforced Steel S.G.)

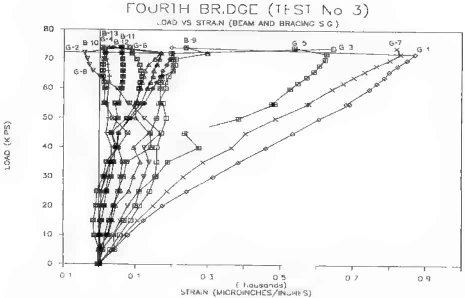

Figure D.69 Load-Strain Curves (Fourth Bridge, Test No 3, Beam and Bracing S.G.)

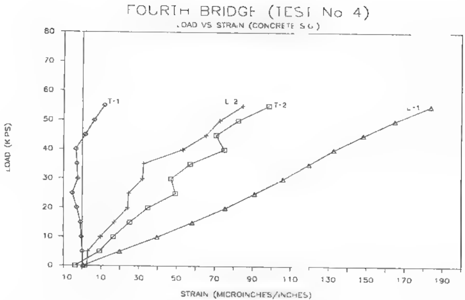

Figure D.70 Load-Strain Curves (Fourth Bridge, Test No 4, Concrete S.G.)

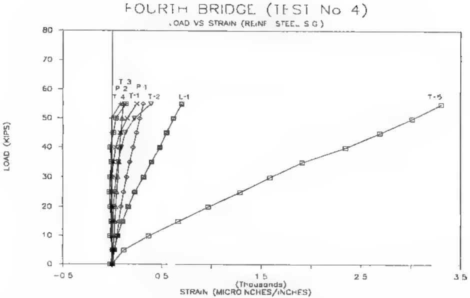

Figure D.71 Load-Strain Curves (Fourth Bridge, Test No 4, Reinforced Steel S.G.)

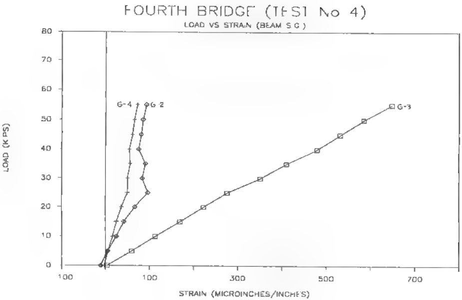

Figure D.72 Load-Strain Curves (Fourth Bridge, Test No 4, Beam S.G.)

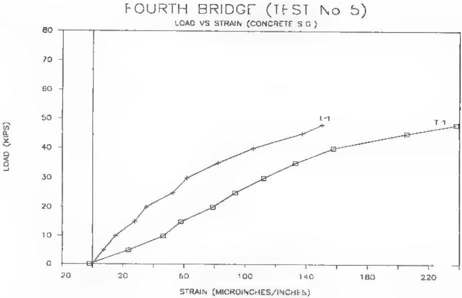

Figure D.73 Load-Strain Curves (Fourth Bridge, Test No 5, Concrete S.G.)

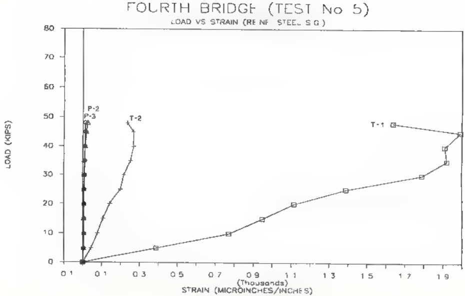

Figure D.74 Load-Strain Curves (Fourth Bridge, Test No 5, Reinforced Steel S.G.)

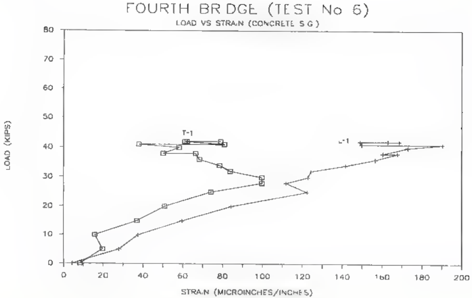

Figure D.75 Load-Strain Curves (Fourth Bridge, Test No 6, Concrete S.G.)

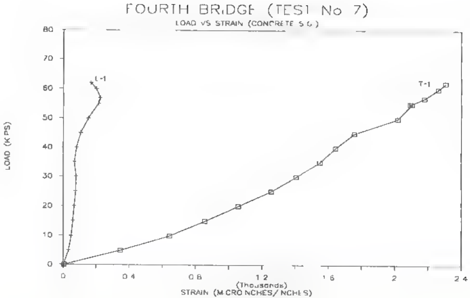

Figure D.76 Load-Strain Curves (Fourth Bridge, Test No 7, Concrete S.G.)

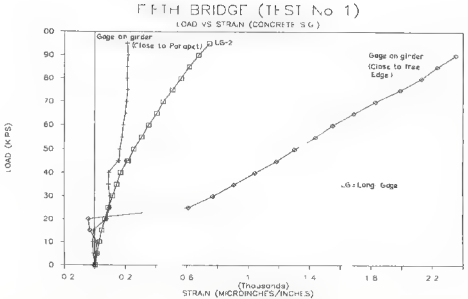

Figure D.77 Load-Strain Curves (Fifth Bridge, Test No 1, Concrete S.G.)

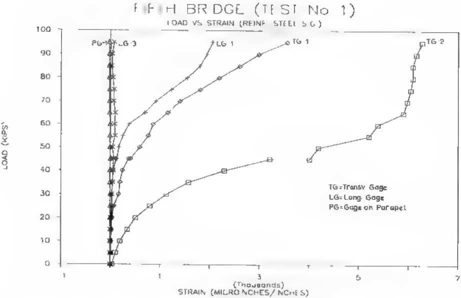

Figure D.78 Load-Strain Curves (Fifth Bridge, Test No 1, Reinforced Steel S.G.)

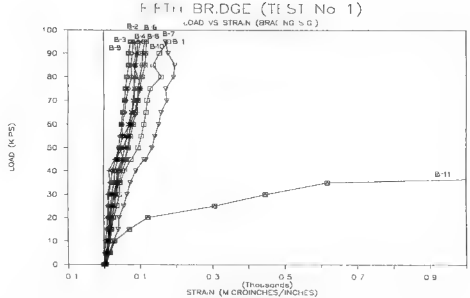

Figure D.79 Load-Strain Curves (Fifth Bridge, Test No 1, Beam and Bracing S.G.)

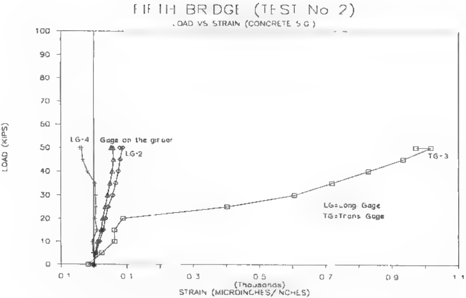

Figure D.80 Load-Strain Curves (Fifth Bridge, Test No 2, Concrete S.G.)

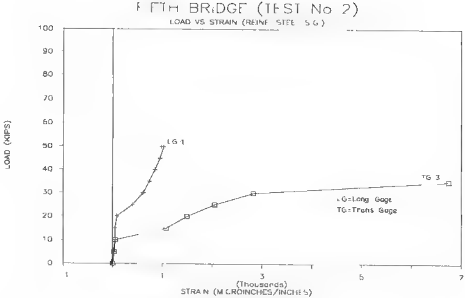

Figure D.81 Load-Strain Curves (Fifth Bridge, Test No 2, Reinforced Steel S.G.)

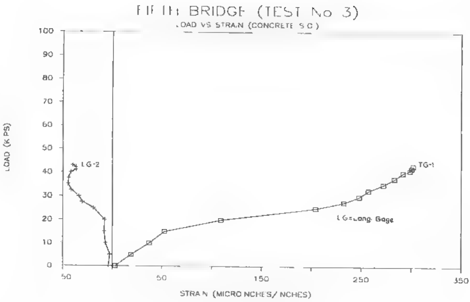

Figure D.82 Load-Strain Curves (Fifth Bridge, Test No 3, Concrete S.G.)

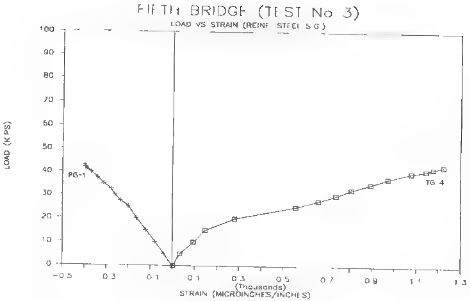

Figure D.83 Load-Strain Curves (Fifth Bridge, Test No 3, Reinforced Steel S.G.)

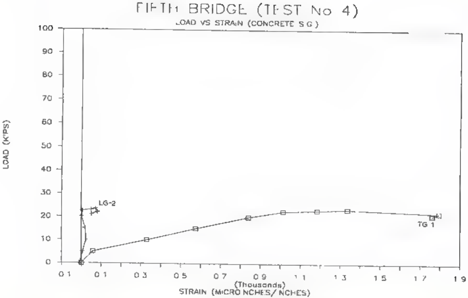

Figure D.84 Load-Strain Curves (Fifth Bridge, Test No 4, Concrete S.G.)

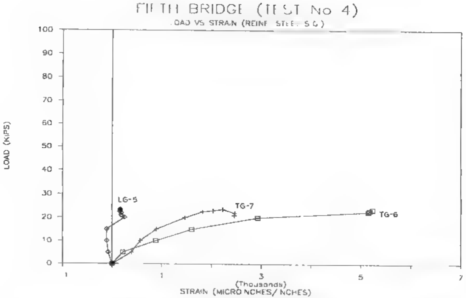

Figure D.85 Load-Strain Curves (Fifth Bridge, Test No 4, Reinforced Steel S.G.)

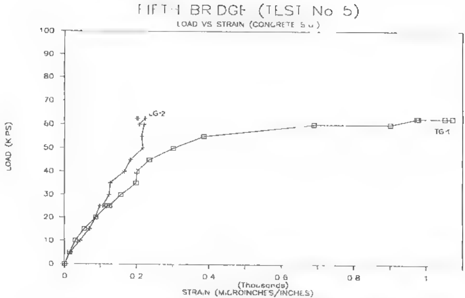

Figure D.86 Load-Strain Curves (Fifth Bridge, Test No 5, Concrete S.G.)

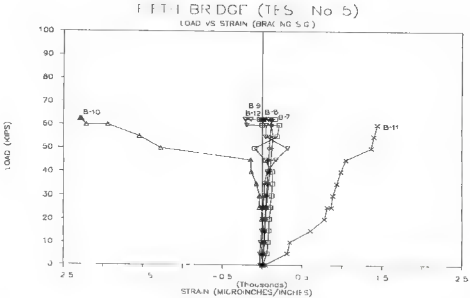

Figure D.87 Load-Strain Curves (Fifth Bridge, Test No 5, Beam and Bracing S.G.)

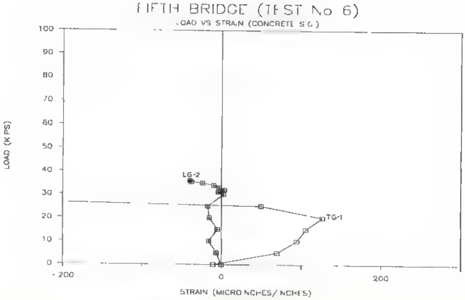

Figure D.88 Load-Strain Curves (Fifth Bridge, Test No 6, Concrete S.G.)

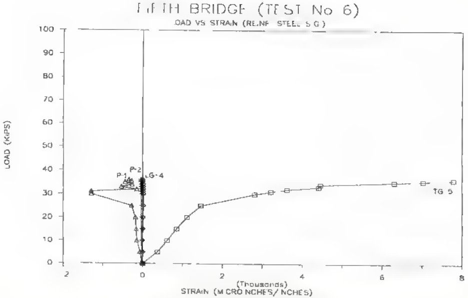

Figure D.89 Load-Strain Curves (Fifth Bridge, Test No 6, Reinforced Steel S.G.)

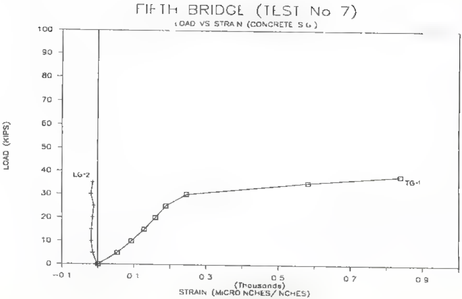

Figure D.90 Load-Strain Curves (Fifth Bridge, Test No 7, Concrete S.G.)

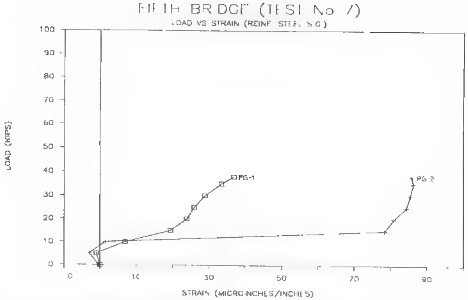

Figure D.91 Load-Strain Curves (Fifth Bridge, Test No 7, Reinforced Steel S.G.)

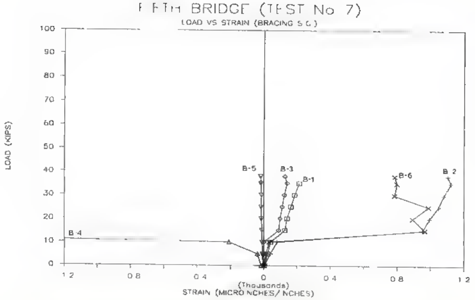

Figure D.92 Load-Strain Curves (Fifth Bridge, Test No 7, Bracing S.G.)

APPENDIX E

CRACK PATTERNS OBSERVED

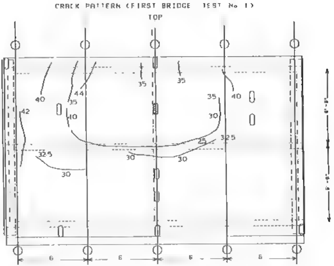

Figure E.1 Top Cracking Pattern (First bridge - Test No 1)

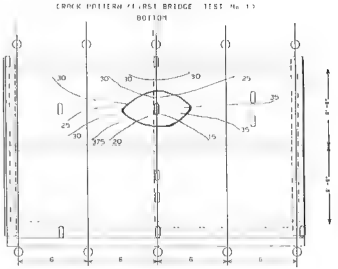

Figure E.2 Bottom Cracking Pattern (First Bridge - Test No 1)

CRACK PATTERN (FIRST BRIDGE TEST No 2)

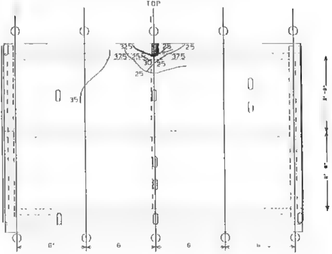

Figure E.3 Top Cracking Pattern (First Bridge - Test No 2)

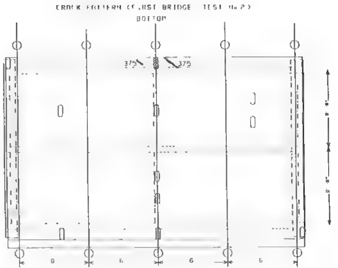

Figure E.4 Bottom Cracking Pattern (First Bridge - Test No 2)

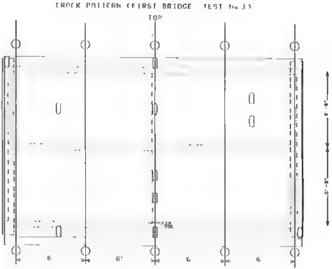

Figure E.5 Top Cracking Pattern (First Bridge - Test No 3)

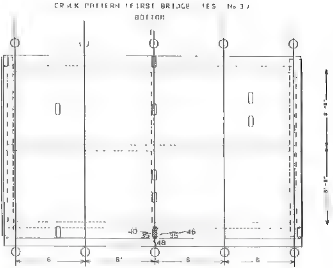

Figure E.6 Bottom Cracking Pattern (First Bridge - Test No 3)

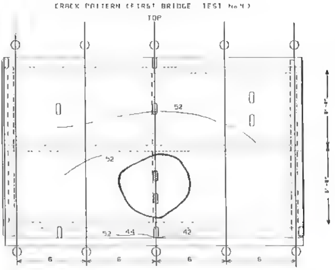

Figure E.7 Top Cracking Pattern (First Bridge - Test No 4)

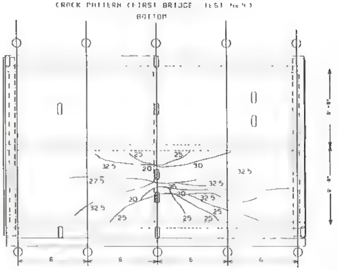

Figure E.8 Bottom Cracking Pattern (First Bridge - Test No 4)

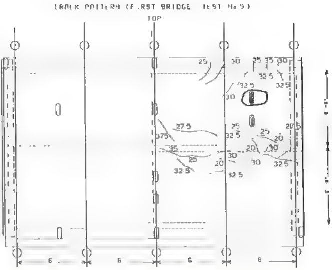

Figure E.9 Top Cracking Pattern (First Bridge - Test No 5)

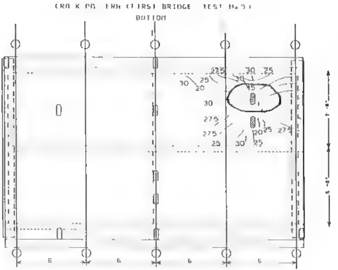

Figure E.10 Bottom Cracking Pattern (First Bridge - Test No 5)

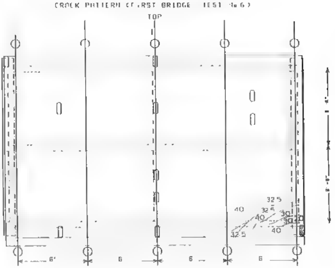

Figure E.11 Top Cracking Pattern (First Bridge - Test No 6)

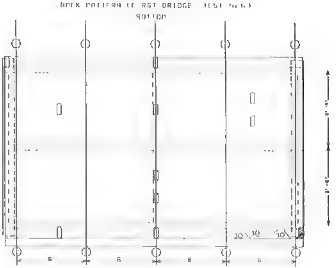

Figure E.12 Bottom Cracking Pattern (First Bridge - Test No 6)

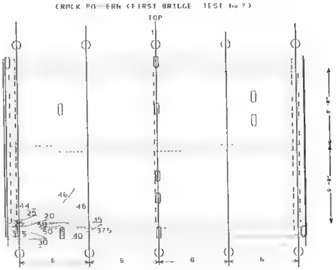

Figure E.13 Top Cracking Pattern (First Bridge - Test No 7)

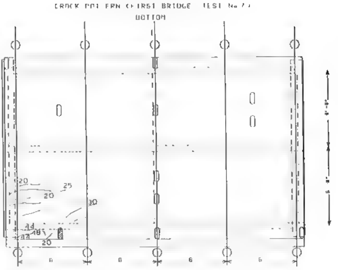

Figure E.14 Bottom Cracking Pattern (First Bridge - Test No 7)

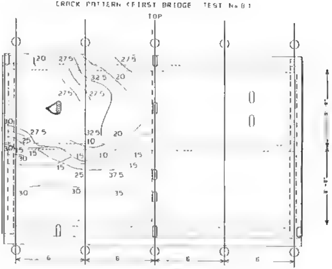

Figure E.15 Top Cracking Pattern (First Bridge - Test No 8)

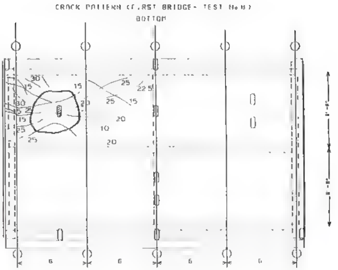

Figure E.16 Bottom Cracking Pattern (First Bridge - Test No 8)

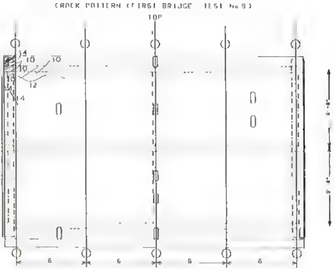

Figure E.17 Top Cracking Pattern (First Bridge - Test No 9)

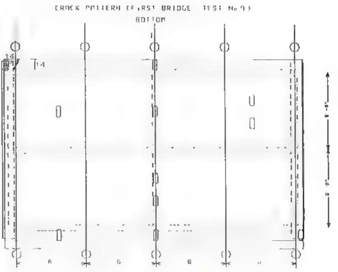

Figure E.18 Bottom Cracking Pattern (First Bridge - Test No 9)

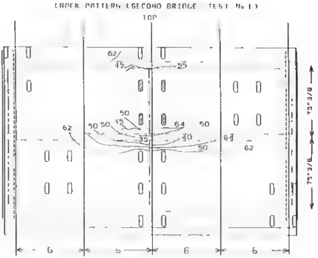

Figure E.19 Top Cracking Pattern (Second Bridge - Test No 1)

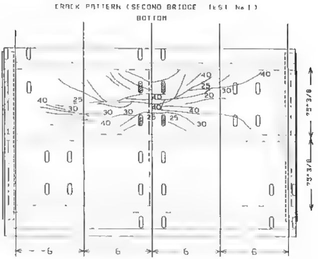

Figure E.20 Bottom Cracking Pattern (Second Bridge - Test No 1)

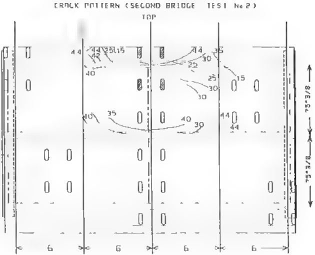

Figure E.21 Top Cracking Pattern (Second Bridge - Test No 2)

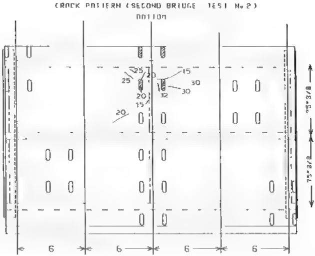

Figure E.22 Bottom Cracking Pattern (Second Bridge - Test No 2)

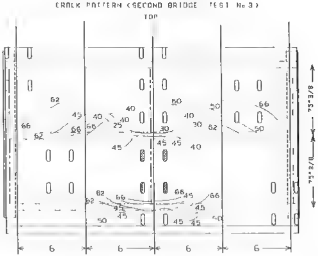

Figure E.23 Top Cracking Pattern (Second Bridge - Test No 3)

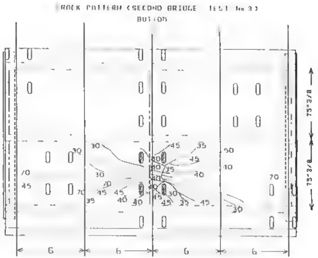

Figure E.24 Bottom Cracking Pattern (Second Bridge - Test No 3)

CRACK PATTERN (SECOND BRIDGE TEST No 4)

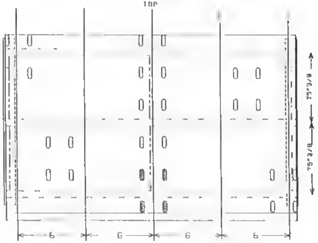

Figure E.25 Top Cracking Pattern (Second Bridge - Test No 4)

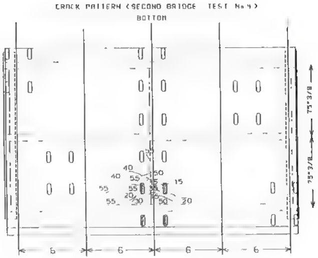

Figure E.26 Bottom Cracking Pattern (Second Bridge - Test No 4)

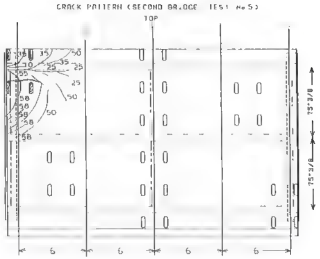

Figure E.27 Top Cracking Pattern (Second Bridge - Test No 5)

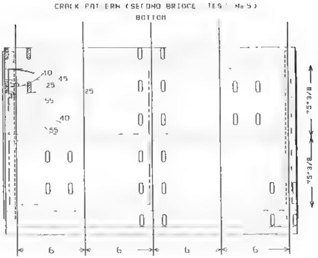

Figure E.28 Bottom Cracking Pattern (Second Bridge - Test No 5)

CRACK PATTERN (SECOND BRIDGE - TEST No 6)

TOP

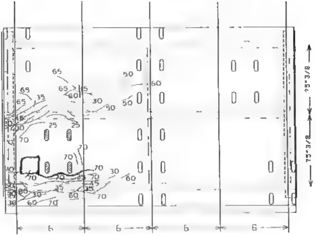

Figure E.29 Top Cracking Pattern (Second Bridge - Test No 6)

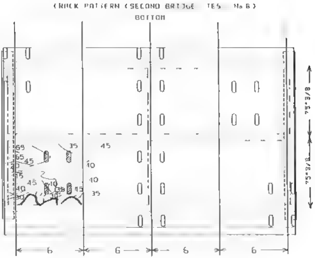

Figure E.30 Bottom Cracking Pattern (Second Bridge - Test No 6)

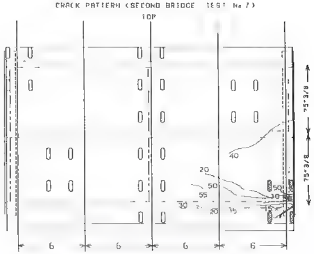

Figure E.31 Top Cracking Pattern (Second Bridge - Test No 7)

CRACK PATTERN (SECOND BRIDGE TEST No 7)
BOTTOM

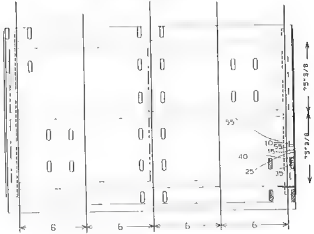

Figure E.32 Bottom Cracking Pattern (Second Bridge - Test No 7)

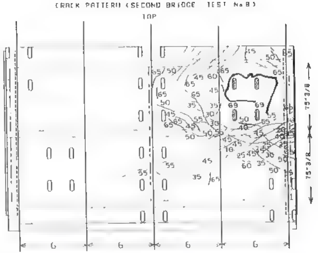

Figure E.33 Top Cracking Pattern (Second Bridge - Test No 8)

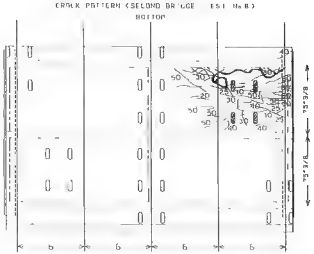

Figure E.34 Bottom Cracking Pattern (Second Bridge - Test No 8)

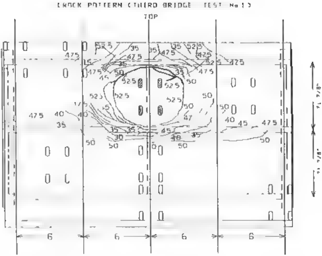

Figure E.35 Top Cracking Pattern (Third Bridge - Test No 1)

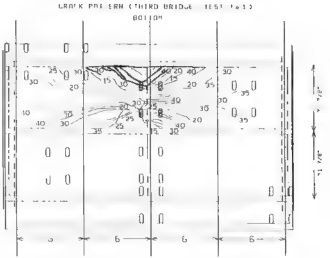

Figure E.36 Bottom Cracking Pattern (Third Bridge - Test No 1)

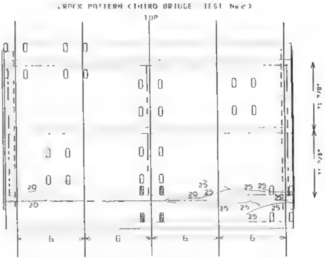

Figure E.37 Top Cracking Pattern (Third Bridge - Test No 2)

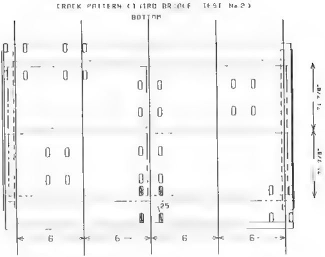

Figure E.38 Bottom Cracking Pattern (Third Bridge - Test No 2)

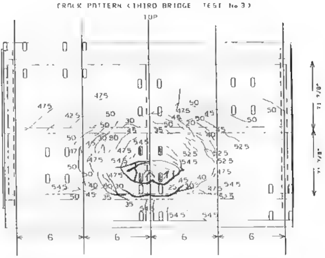

Figure E.39 Top Cracking Pattern (Third Bridge - Test No 3)

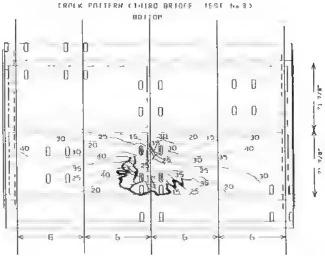

Figure E.40 Bottom Cracking Pattern (Third Bridge - Test No 3)

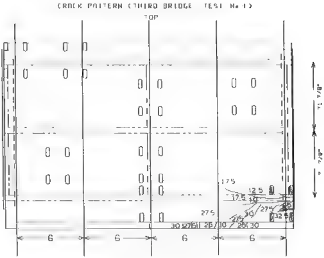

Figure E.41 Top Cracking Pattern (Third Bridge - Test No 4)

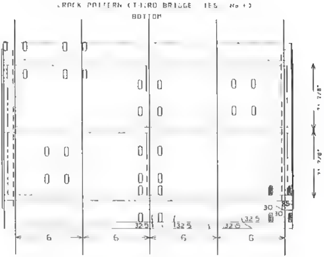

Figure E.42 Bottom Cracking Pattern (Third Bridge - Test No 4)

CRACK PATTERN (THIRD BRIDGE TEST No 5)

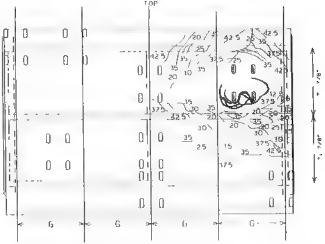

Figure E.43 Top Cracking Pattern (Third Bridge - Test No 5)

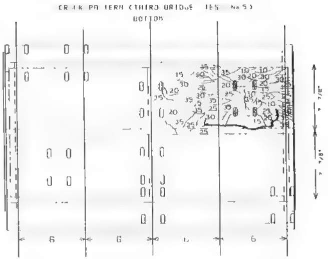

Figure E.44 Bottom Cracking Pattern (Third Bridge - Test No 5)

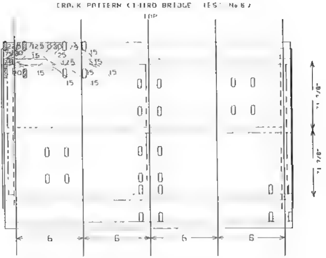

Figure E.45 Top Cracking Pattern (Third Bridge - Test No 6)

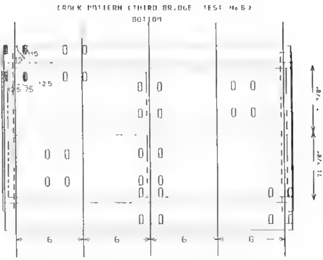

Figure E.46 Bottom Cracking Pattern (Third Bridge - Test No 6)

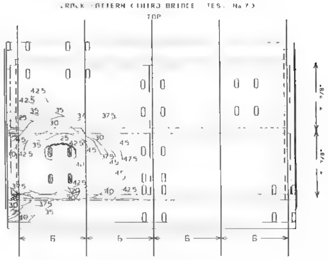

Figure E.47 Top Cracking Pattern (Third Bridge - Test No 7)

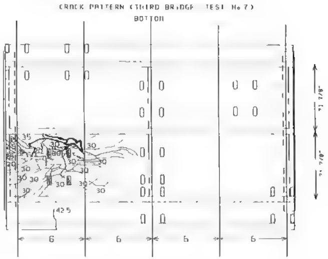

Figure E.48 Bottom Cracking Pattern (Third Bridge - Test No 7)

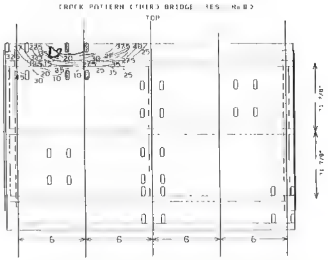

Figure E.49 Top Cracking Pattern (Third Bridge - Test No 8)

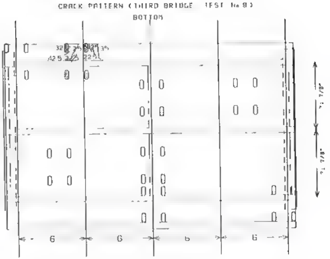

Figure E.50 Bottom Cracking Pattern (Third Bridge - Test No 8)

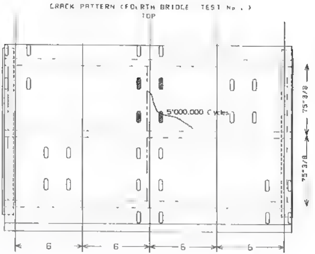

Figure E.51 Top Cracking Pattern (Fourth Bridge - Test No 1 - Dynamic Load)

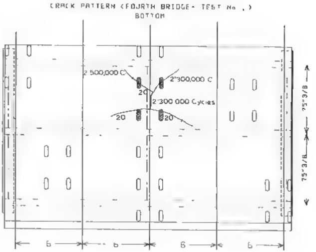

Figure E.52 Bottom Cracking Pattern (Fourth Bridge - Test No 1 - Dynamic Load)

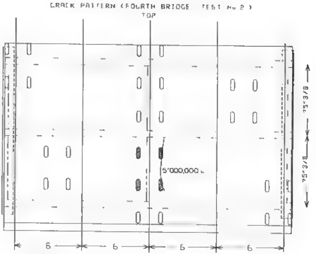

Figure E.53 Top Cracking Pattern (Fourth Bridge - Test No 2 - Dynamic Load)

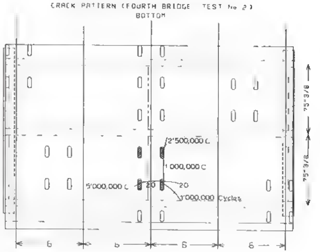

Figure E.54 Bottom Cracking Pattern (Fourth Bridge - Test No 2 - Dynamic Load)

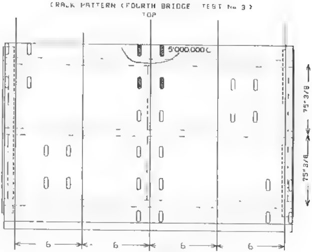

Figure E.55 Top Cracking Pattern (Fourth Bridge - Test No 3 - Dynamic Load)

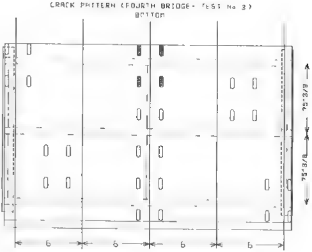

Figure E.56 Bottom Cracking Pattern (Fourth Bridge - Test No 3 - Dynamic Load)

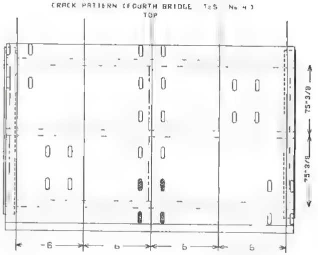

Figure E.57 Top Cracking Pattern (Fourth Bridge - Test No 4 - Dynamic Load)

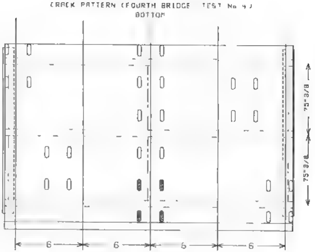

Figure E.58 Bottom Cracking Pattern (Fourth Bridge - Test No 4 - Dynamic Load)

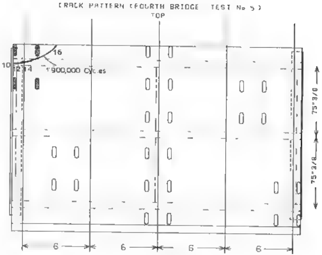

Figure E.59 Top Cracking Pattern (Fourth Bridge - Test No 5 - Dynamic Load)

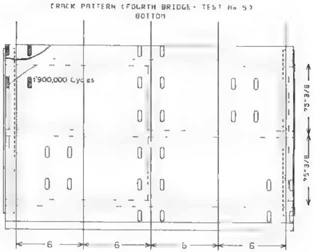

Figure E.60 Bottom Cracking Pattern (Fourth Bridge - Test No 5 - Dynamic Load)

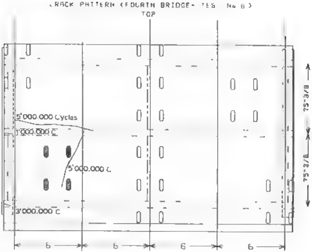

Figure E.61 Top Cracking Pattern (Fourth Bridge - Test No 6 - Dynamic Load)

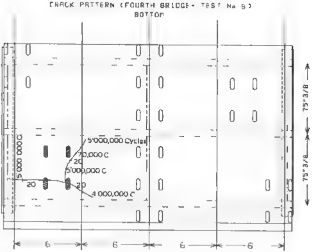

Figure E.62 Bottom Cracking Pattern (Fourth Bridge - Test No 6 - Dynamic Load)

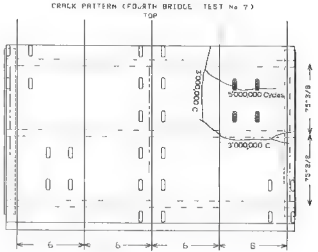

Figure E.63 Top Cracking Pattern (Fourth Bridge - Test No 7 - Dynamic Load)

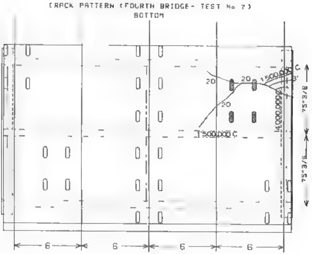

Figure E.64 Bottom Cracking Pattern (Fourth Bridge - Test No 7 - Dynamic Load)

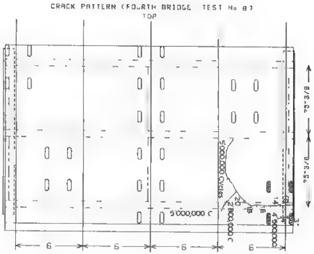

Figure E.65 Top Cracking Pattern (Fourth Bridge - Test No 8 - Dynamic Load)

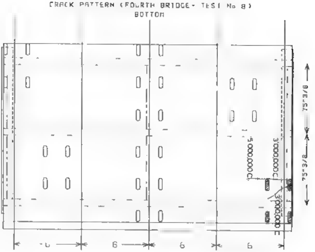

Figure E.66 Bottom Cracking Pattern (Fourth Bridge - Test No 8 - Dynamic Load)

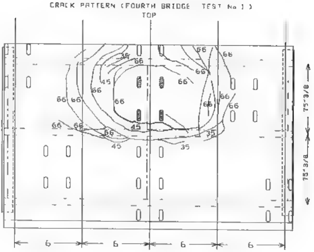

Figure E.67 Top Cracking Pattern (Fourth Bridge - Test No 1)

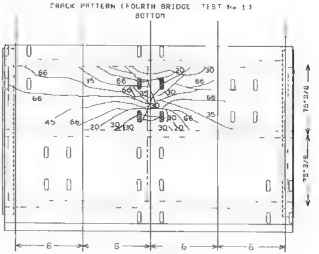

Figure E.68 Bottom Cracking Pattern (Fourth Bridge - Test No 1)

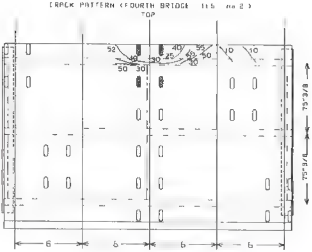

Figure E.69 Top Cracking Pattern (Fourth Bridge - Test No 2)

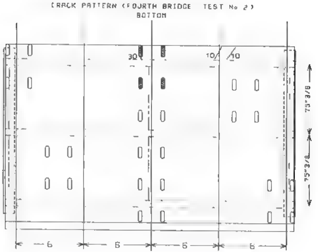

Figure E.70 Bottom Cracking Pattern (Fourth Bridge - Test No 2)

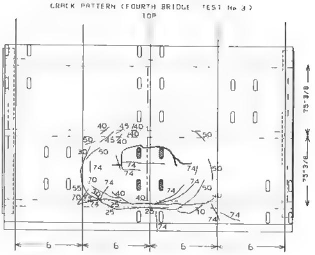

Figure E.71 Top Cracking Pattern (Fourth Bridge - Test No 3)

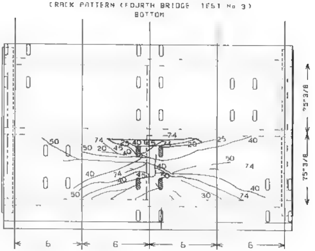

Figure E.72 Bottom Cracking Pattern (Fourth Bridge - Test No 3)

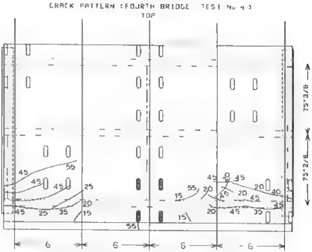

Figure E.73 Top Cracking Pattern (Fourth Bridge - Test No 4)

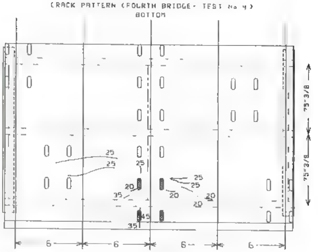

Figure E.74 Bottom Cracking Pattern (Fourth Bridge - Test No 4)

CRACK PATTERN (FOURTH BRIDGE TEST No 5)
TOP

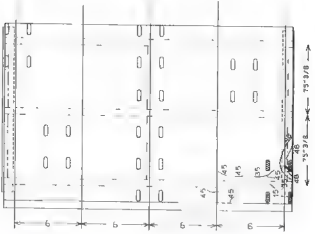

Figure E.75 Top Cracking Pattern (Fourth Bridge - Test No 5)

CRACK PATTERN (FOURTH BRIDGE TEST No 5)
BOTTOM

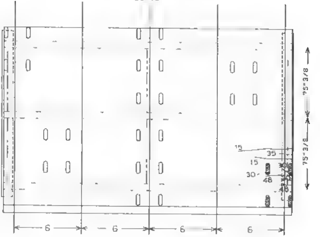

Figure E.76 Bottom Cracking Pattern (Fourth Bridge - Test No 5)

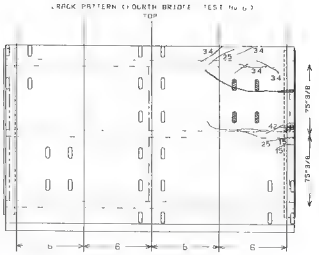

Figure E.77 Top Cracking Pattern (Fourth Bridge - Test No 6)

CRACK PATTERN (FOURTH BRIDGE- TEST No 6)
BOTTOM

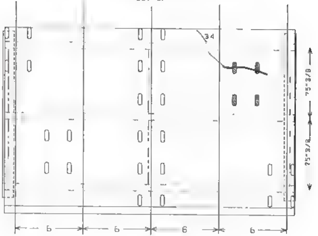

Figure E.78 Bottom Cracking Pattern (Fourth Bridge - Test No 6)

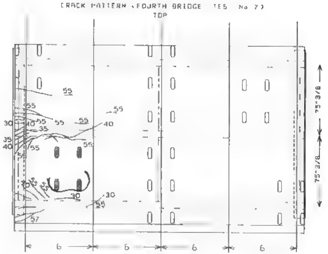

Figure E.79 Top Cracking Pattern (Fourth Bridge - Test No 7)

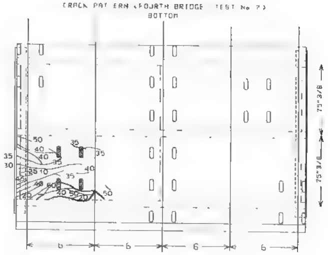

Figure E.80 Bottom Cracking Pattern (Fourth Bridge - Test No 7)

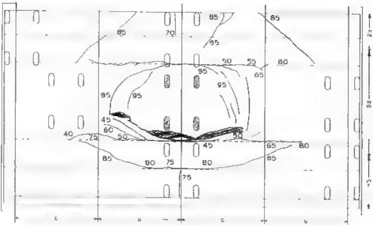

Figure E.81 Top Cracking Pattern (Fifth Bridge - Test No 1)

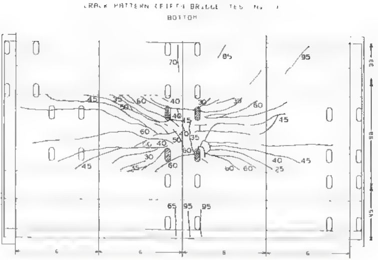

Figure E.82 Bottom Cracking Pattern (Fifth Bridge - Test No 1)

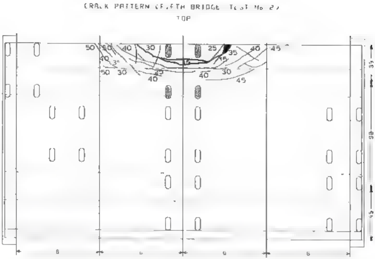

Figure E.83 Top Cracking Pattern (Fifth Bridge - Test No 2)

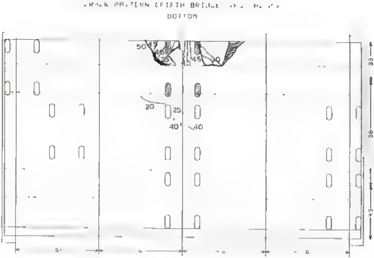

Figure E.84 Bottom Cracking Pattern (Fifth Bridge - Test No 2)

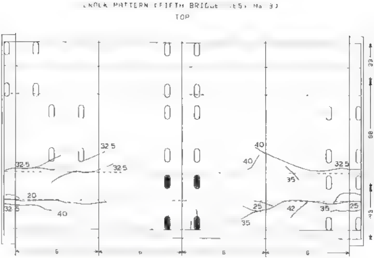

Figure E.65 Top Cracking Pattern (Fifth Bridge - Test No 3)

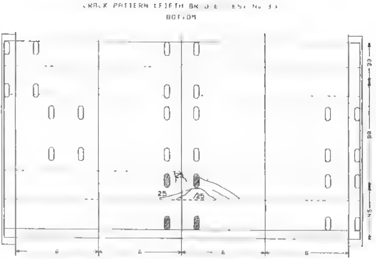

Figure E.86 Bottom Cracking Pattern (Fifth Bridge - Test No 3)

CRACK PATTERN OF FIFTH BRIDGE TEST No 4

TOP

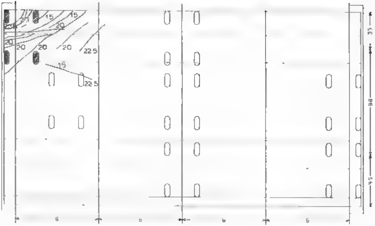

Figura E.87 Top Cracking Pattern (Fifth Bridge - Test No 4)

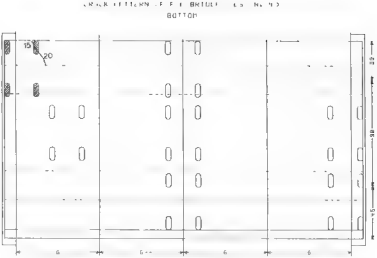

Figure E.88 Bottom Cracking Pattern (Fifth Bridge - Test No 4)

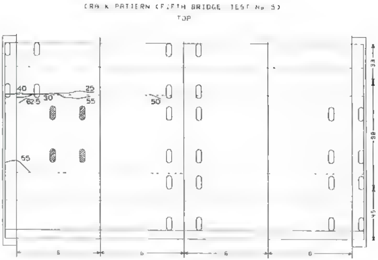

Figure E.89 Top Cracking Pattern (Fifth Bridge - Test No 5)

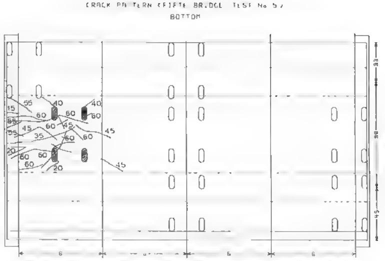

Figure E.90 Bottom Cracking Pattern (Fifth Bridge - Test No 5)

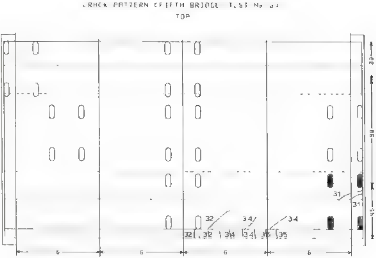

Figure E.91 Top Cracking Pattern (Fifth Bridge - Test No 6)

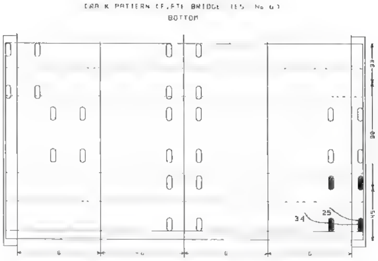

Figure E.92 Bottom Cracking Pattern (Fifth Bridge - Test No 6)

CRACK PATTERN (FIFTH BRIDGE TEST No 7)
TOP

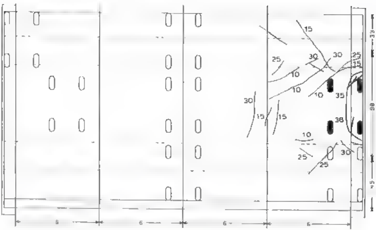

Figure E.93 Top Cracking Pattern (Fifth Bridge - Test No 7)

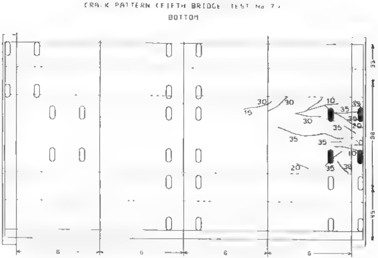

Figure E.94 Bottom Cracking Pattern (Fifth Bridge - Test No 7)

APPENDIX F

MATERIAL PROPERTIES

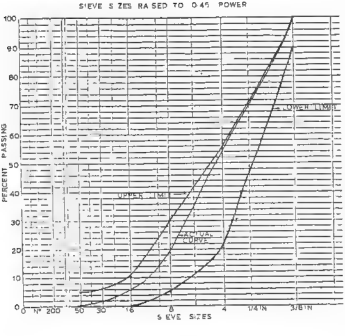

CONCRETE MIX
WEIGHT IN POUNDS OF AGGREGATE
(PER YARD)
1710 N°89 ROCK 5% MOISTURE
1270 SILICA SAND 5% MOISTURE
564 CEMENT TYPE 1
24 GAL WATER
17 ml OF AIR (MBLR)
45 ml OF RETARDER (MBL 80)

Figure F.1 Aggregate Gradation Chart and Concrete Mix

FIRST BRIDGE

Cast of the Slab .. 9/25/87

COMPRESSION TEST (Slab)

Days	Strength
6	4360
21	5100
28	5587
59	5122
74	5970
109	5810
115	6410

TENSION TEST (Slab)

Days	Strength
28	499
59	505
74	536
115	538

BEAM TEST (Slab)

Days	Strength
28	456
59	517
74	682
115	721

Cast of the Parapet .. 10/2/87

COMPRESSION TEST (Parapet)

Days	Strength
14	5500
28	6480
103	7710

TENSION TEST (Parapet)

Days	Strength
28	507
59	525
74	560
103	566

Figure F.2 Concrete Test Results (First Bridge)

SECOND BRIDGE

Cast of the slab.. 2/23/88

COMPRESSION TEST (Slab)

Days	Strength
13	5102
28	5980
63	6339
71	6550
78	6574

TENSION TEST (Slab)

Days	Strength
28	465
64	486
71	479
78	543

BEAM TEST (Slab)

Days	Strength
28	419
65	463
79	544

Cast of the Parapet ..3/2/88

COMPRESSION TEST (Parapet)

Days	Strength
5	5337
28	6450
55	7638
70	7692

Figure F.3 Concrete Test Results (Second Bridge)

THIRD BRIDGE

Cast of the slab.. 6/10/88

COMPRESSION TEST (Slab)

Days	Strength
28	5721
38	6137
40	5967
42	6020
45	5899
47	6366
49	6345
54	6382
56	6295
59	6369

TENSION TEST (Slab)

Days	Strength
28	498
54	502
56	495
59	505

BEAM TEST (Slab)

Days	Strength
28	528
49	589
59	630

Cast of the Parapet .. 6/17/88

COMPRESSION TEST (Parapet)

Days	Strength
28	5651
49	6142
52	5949

TENSION TEST (Parapet)

Days	Strength
28	530
49	545

BEAM TEST (Parapet)

Days	Strength
28	522
52	630

Figure F.4 Concrete Test Results (Third Bridge)

FOURTH BRIDGE

Cast of the slab.. 10/26/88

COMPRESSION TEST		TENSION TEST	BEAM TEST
Days	Strength	Strength	Strength
14	6129	460	675
28	6857	539	712
77	7544	676	752
92	7622	560	785
99	7551	657	739
112	7295	570	935
133	7464	612	893
166	7254	616	917
196	7434	611	1032
208	6982	586	912

Cast of the Parapet .. 11/04/88

COMPRESSION TEST		TENSION TEST	BEAM TEST
Days	Strength	Strength	Strength
14	5836	444	650
28	6189	480	674
77	6282	514	683
92	6357	531	756
99	6324	502	787
112	6158	536	886
133	6709	538	893
166	5981	588	916
196	6667	558	951
208	6207	545	917

Figure F.5 Concrete Test Results (Fourth Bridge)

FIFTH BRIDGE

Cast of the slab.. 08/14/89

COMPRESSION TEST		TENSION TEST	BEAM TEST
Days	Strength	Strength	Strength
7	4704	336	545
14	5213	389	528
28	6023	438	598
43	6380	529	647
60	6502	482	591

Cast of the Parapet .. 08/16/89

COMPRESSION TEST		TENSION TEST	BEAM TEST
Days	Strength	Strength	Strength
7	4008	403	662
28	5175	431	723
45	5439	392	581

Cast of the Bulb-Tee Girder .. 05/26/89

COMPRESSION TEST		TENSION TEST	BEAM TEST
Days	Strength	Strength	Strength
7	5698	485	703
14	5701	509	581
28	7369	484	586
120	6927	581	1014
150	7743	568	791

Figure F.6 Concrete Test Results (Fifth Bridge)

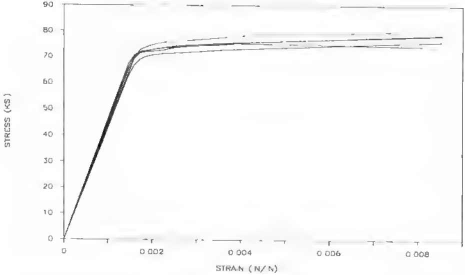

Figure F.7 Stress-Strain Curves for Deck Reinforcing Steel (Specimens 1, 2, 3, 4)

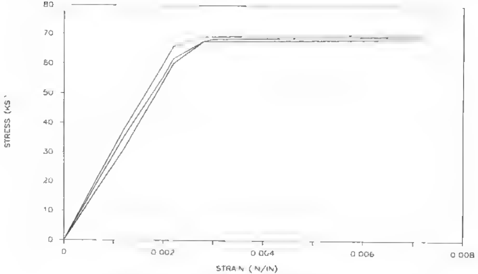

Figure F.8 Stress-Strain Curves for Deck Reinforcing Steel (Specimen 5)

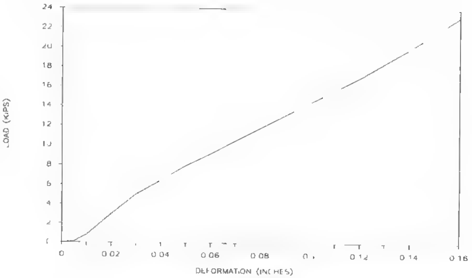

Figure F.9 Typical Load-Deformation Curve for Bearing Pads

APPENDIX G

MEASURED THICKNESSES OF DECK

BRIDGE No 1

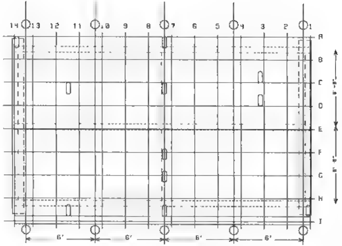

Figure G.1 Location of Reference Lines for Thickness Measurements (Bridge No 1)

Table G.1 Thickness Variation (First Bridge)

	1	2	3	4	5	6	7	8	9	10	11	12	13	14
A	4	4 3/32	4	4	4 1/16	4 5/32	4	4 1/8	4	4 1/8	4 5/32	4 5/32	4 1/32	4 3/16
B	4	4 7/32	4 5/16	4 9/32	4 9/32	4 17/32	4 11/32	4 13/32	4 11/32	4 11/32	4 13/32	4 13/32	4 7/16	4 3/16
C	4 7/32	4 3/8	4 13/32	4 3/8	4 13/32	4 15/32	4 15/32	4 9/16	4 1/2	4 19/32	4 17/32	4 15/32	4 3/8	4 3/16
D	4 5/16	4 1/2	4 1/2	4 7/16	4 17/32	4 5/8	4 19/32	4 3/4	4 23/32	4 23/32	4 7/16	4 17/32	4 3/8	4 3/16
E	4 5/16	4 3/8	4 7/16	4 11/32	4 13/32	4 19/32	4 15/32	4 9/16	4 5/8	4 9/16	4 9/16	4 1/8	4 5/16	4 7/32
F	4 1/4	4 7/32	4 3/8	4 13/32	4 19/32	4 3/4	4 21/32	4 5/8	4 11/16	4 13/32	4 19/32	4 1/2	4 1/4	4 1/8
G	4 1/8	4 9/32	4 11/32	4 15/32	4 19/32	4 5/8	4 5/8	4 1/2	4 19/32	4 11/32	4 15/32	4 3/16	4 1/16	4 3/32
H	4 5/32	4 1/4	4 5/16	4 11/32	4 21/32	4 5/8	4 21/32	4 11/32	4 13/16	4 5/32	4 1/32	4 1/16	4 1/32	4 5/32
I	4 1/8	4 1/16	4 1/16	4 1/8	4 5/16	4 3/16	4 3/16	4 3/16	4 1/4	4 1/8	4 1/16	4 1/16	4 1/8	4 3/16

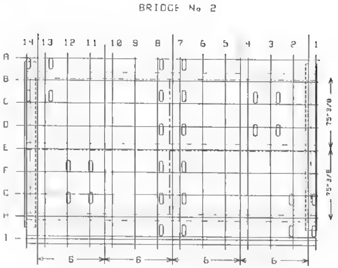

Figure G.2 Location of Reference Lines for Thickness Measurements (Bridge No 2)

Table G.2 Thickness Variation (Bridge No 2)

	1	2	3	4	5	6	7	8	9	10	11	12	13	14
A	3 13/16	3 3/4	3 3/4	3 3/4	3 3/4	3 13/16	3 13/16	3 3/4	3 3/4	3 13/16	3 7/8	3 3/4	3 13/16	3 3/4
B	3 13/16	3 13/16	3 11/16	3 5/8	3 9/16	3 9/16	3 1/2	3 5/8	3 5/8	3 1/2	3 9/16	3 11/16	3 13/16	3 3/4
C	3 3/4	3 13/16	3 3/4	3 5/8	3 1/2	3 1/2	3 5/8	3 9/16	3 11/16	3 11/16	3 3/4	3 3/4	3 13/16	3 7/8
D	3 3/4	3 3/4	3 5/8	3 3/4	3 13/16	3 7/8	3 3/4	3 11/16	3 11/16	3 13/16	3 13/16	3 13/16	3 3/4	3 13/16
E	3 3/4	3 11/16	3 5/8	3 9/16	3 9/16	3 1/2	3 9/16	3 9/16	3 11/16	3 5/8	3 11/16	3 11/16	3 11/16	3 3/4
F	3 7/8	3 5/8	3 5/8	3 9/16	3 1/2	3 7/16	3 7/16	3 9/16	3 5/8	3 11/16	3 11/16	3 11/16	3 13/16	3 13/16
G	3 7/8	3 13/16	3 11/16	3 3/4	3 11/16	3 11/16	3 5/8	3 3/4	3 15/16	3	3 15/16	3 7/8	3	3 7/8
H	3 13/16	3 11/16	3 11/16	3 5/8	3 5/8	3 9/16	3 1/2	3 9/16	3 11/16	3 5/8	3 11/16	3 3/4	3 13/16	3 13/16
I	3 7/8	3 5/8	3 9/16	3 1/2	3 1/2	3 11/16	3 7/16	3 9/16	3 3/4	3 7/8	3 15/16	3 3/4	3 13/16	3 3/4

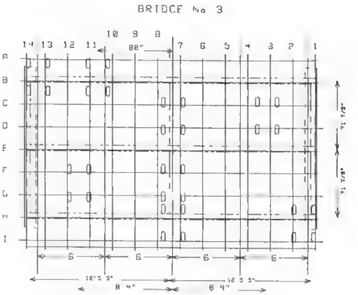

Figure G.3 Location of Reference Lines for Thickness Measurements (Bridge No 3)

Table G.3 Thickness Variation (Third Bridge)

	1	2	3	4	5	6	7	8	9	10	11	12	13	14
A	3 3/8	3 11/32	3 1/2	3 17/32	3 1/2	3 1/2	3 7/32	3 7/32	3 7/32	3 11/32	3 13/32	3 13/32	3 7/16	3 7/16
B	3 5/16	3 9/32	3 5/16	3 7/32	3 1/32	3	3 1/32	3 1/4	3 5/32	3 7/32	3 5/32	3 3/32	3 5/32	3 9/32
C	3 3/8	3 1/4	3 11/32	3 3/16	3 3/32	3 1/8	3 1/32	3 3/32	2 15/16	2 29/32	3 1/32	2 31/32	3 1/16	3 1/4
D	3 3/8	3 1/4	3 5/16	3 5/32	3 5/32	3 3/32	3 1/8	3 5/32	3 1/16	3	3 3/32	3 1/32	3 5/32	3 5/16
E	3 9/32	3 7/32	3 7/32	3 3/32	3 1/32	3 1/32	3 3/32	3 7/32	3 1/32	3 1/32	3 1/8	3 1/32	3 5/32	3 11/32
F	3 7/32	3 1/8	3 3/32	2 31/32	3	3	2 29/32	2 29/32	3	3 9/32	3 5/32	3 1/16	3 3/16	3 5/16
G	3 3/16	3 7/32	3 3/32	3 1/16	3 3/32	3 1/32	3	3	3 3/32	3 3/16	3 1/8	3 1/16	3 1/8	3 5/16
H	3 8/32	3 1/4	3 5/32	3 5/32	3 5/32	3 7/32	3 1/8	3 1/4	3 5/32	3 1/8	3 1/16	3 3/32	3 3/16	3 5/16
I	3 11/32	3 5/16	3 1/4	3 1/4	3 3/8	3 5/16	3 1/4	3 5/16	3 11/32	3 11/32	3 3/8	3 11/32	3 5/16	3 7/16

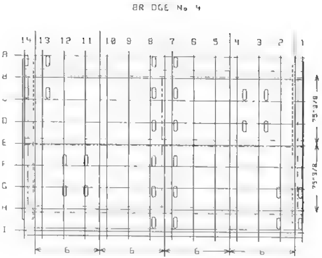

Figure G.4 Location of Reference Lines for Thickness Measurements (Bridge No 4)

Table G.4 Thickness Variation (Fourth Bridge)

	1	2	3	4	5	6	7	8	9	10	11	12	13	14
A	3 13/16	3 27/32	3 25/32	3 13/16	3 3/4	3 3/4	3 29/32	3 27/32	3 25/32	3 25/32	3 25/32	3 25/32	3 25/32	3 25/32
B	3 3/4	3 17/32	3 21/32	3 21/32	3 9/16	3 5/8	3 9/16	3 5/8	3 11/16	3 19/32	3 5/8	3 9/16	3 19/32	3 27/32
C	3 3/4	3 1/2	3 9/16	3 9/16	3 17/32	3 9/16	3 11/16	3 3/4	3 15/16	3 27/32	3 7/8	3 27/32	3 23/32	3 13/16
D	3 25/32	3 1/2	3 17/32	3 17/32	3 7/16	3 15/32	3 19/32	3 25/32	3 29/32	3 31/32	3 27/32	3 7/8	3 13/16	3 29/32
E	3 25/32	3 21/32	3 1/2	3 7/16	3 5/16	3 15/32	3 13/32	3 9/16	3 17/32	3 7/16	3 3/8	3 1/2	3 17/32	3 13/16
F	3 3/4	3 21/32	3 21/32	3 9/16	3 5/8	3 15/32	3 7/16	3 15/32	3 13/32	3 11/32	3 11/32	3 15/32	3 17/32	3 13/16
G	3 23/32	3 19/32	3 19/32	3 19/32	3 17/32	3 5/8	3 17/32	3 7/16	3 15/32	3 13/32	3 1/2	3 17/32	3 15/32	3 23/32
H	3 13/16	3 3/4	3 5/8	3 17/32	3 9/16	3 11/16	3 11/16	3 19/32	3 9/16	3 9/16	3 11/16	3 5/8	3 11/16	3 13/16
I	3 7/8	3 29/32	3 7/8	3 23/32	3 11/16	3 13/16	3 3/4	3 27/32	3 3/4	3 3/4	3 13/16	3 27/32	3 15/16	4 3/32

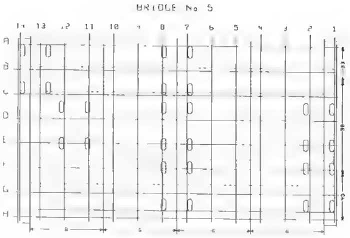

Figure G.5 Location of Reference Lines for Thickness Measurements (Bridge No 5)

Table G.5 Thickness Variation (Fifth Bridge)

	1	2	3	4	5	6	7	8	9	10	11	12	13	14
A	3 7/8	3 13/16	3 13/16	3 29/32	3 29/32	3 29/32	3 27/32	3 13/16	3 13/16	3 27/32	3 27/32	3 13/16	3 3/4	3 7/8
B	4 1/32	3 29/32	3 29/32	3 7/8	3 29/32	3 7/8	3 3/4	3 23/32	3 25/32	3 3/4	3 31/32	3 21/32	3 21/32	3 13/16
C	3 27/32	3 23/32	3 23/32	3 11/16	3 13/16	3 3/4	3 23/32	3 11/16	3 23/32	3 23/32	3 3/4	3 21/32	3 19/32	3 25/32
D	3 27/32	3 13/16	3 25/32	3 27/32	3 7/8	3 27/32	3 11/16	3 11/16	3 13/16	3 3/4	3 25/32	3 21/32	3 19/32	3 25/32
E	3 13/16	3 25/32	3 11/16	3 25/32	3 3/4	3 21/32	3 21/32	3 21/32	3 13/16	3 13/16	3 25/32	3 25/32	3 23/32	3 13/16
F	3 25/32	3 21/32	3 19/32	3 9/16	3 19/32	3 1/2	3 9/16	3 23/32	3 27/32	3 25/32	3 25/32	3 23/32	3 5/8	3 23/32
G	3 27/32	3 25/32	3 25/32	3 3/4	3 19/32	3 17/32	3 23/32	3 27/32	4	3 31/32	3 29/32	3 29/32	3 31/32	3 7/8
H	3 27/32	3 27/32	3 31/32	3 31/32	3 21/32	3 23/32	3 27/32	3 15/16	3 7/8	4	3 31/32	3 29/32	3 29/32	3 13/16

APPENDIX H

DEFLECTION BASINS

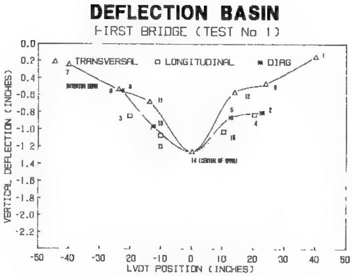

Figure H.1 Deflection Basin (First Bridge, Test No 1)

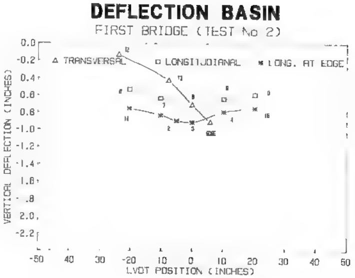

Figure H.2 Deflection Basin (First Bridge, Test No 2)

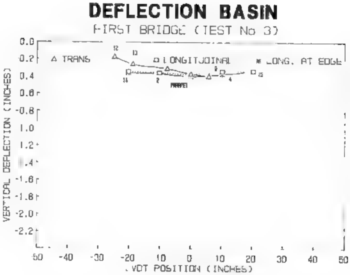

Figure H.3 Deflection Basin (First Bridge, Test No 3)

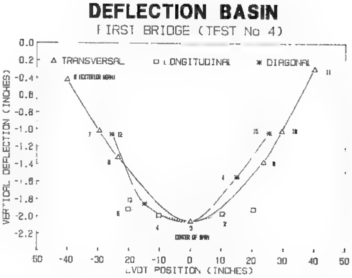

Figure H.4 Deflection Basin (First Bridge, Test No 4)

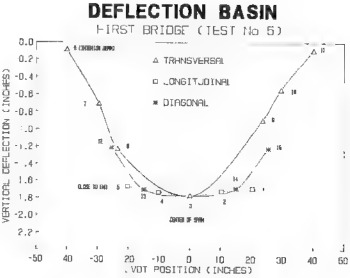

Figure H.5 Deflection Basin (First Bridge, Test No 5)

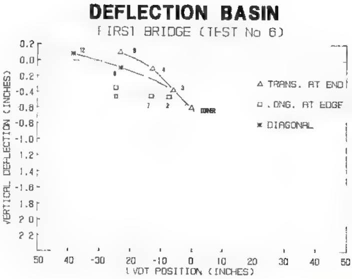

Figure H.6 Deflection Basin (First Bridge, Test No 6)

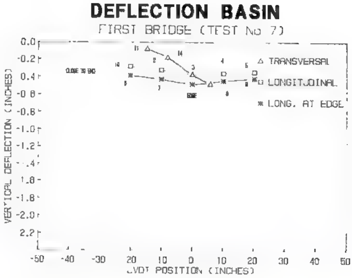

Figure H.7 Deflection Basin (First Bridge, Test No 7)

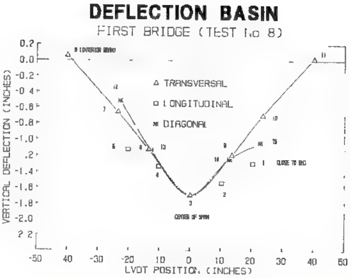

Figure H.8 Deflection Basin (First Bridge, Test No 8)

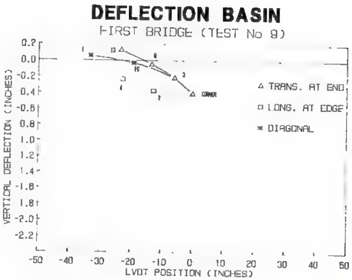

Figure H.9 Deflection Basin (First Bridge, Test No 9)

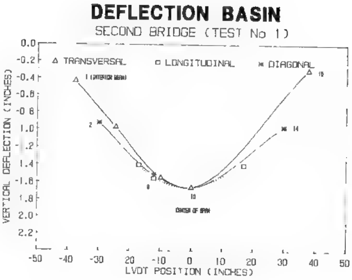

Figure H.10 Deflection Basin (Second Bridge, Test No 1)

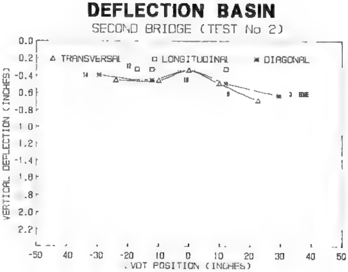

Figure H.11 Deflection Basin (Second Bridge, Test No 2)

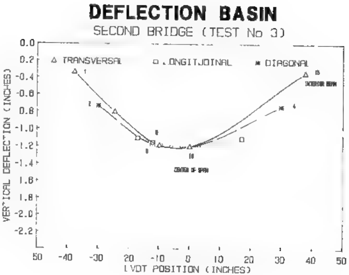

Figure H.12 Deflection Basin (Second Bridge, Test No 3)

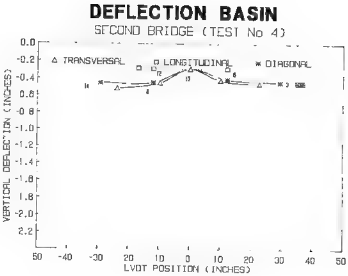

Figure H.13 Deflection Basin (Second Bridge, Test No 4)

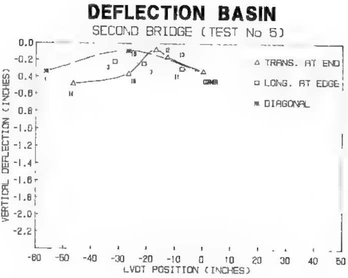

Figure H.14 Deflection Basin (Second Bridge, Test No 5)

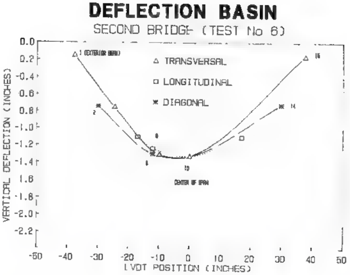

Figure H.15 Deflection Basin (Second Bridge, Test No 6)

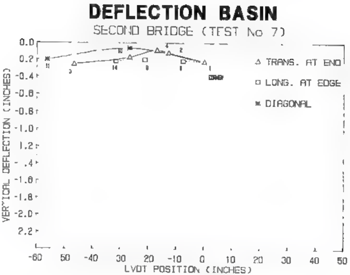

Figure H.16 Deflection Basin (Second Bridge, Test No 7)

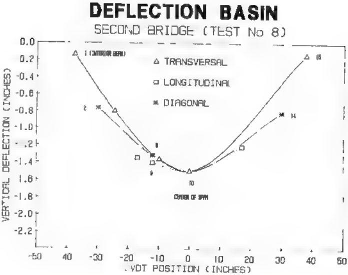

Figure H.17 Deflection Basin (Second Bridge, Test No 8)

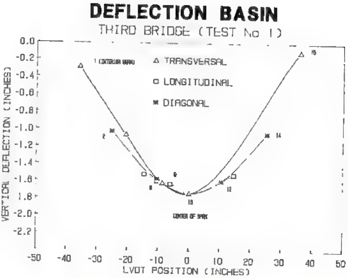

Figure H.18 Deflection Basin (Third Bridge, Test No 1)

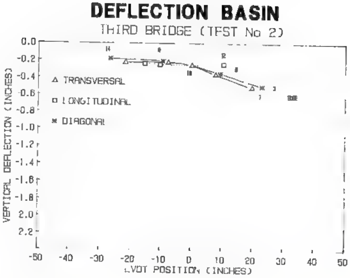

Figure H.19 Deflection Basin (Third Bridge, Test No 2)

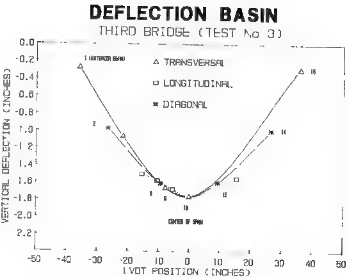

Figure H.20 Deflection Basin (Third Bridge, Test No 3)

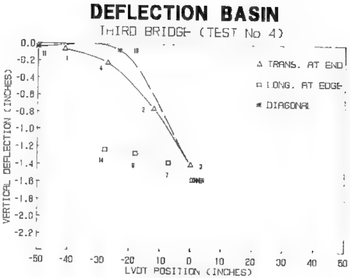

Figure H.21 Deflection Basin (Third Bridge, Test No 4)

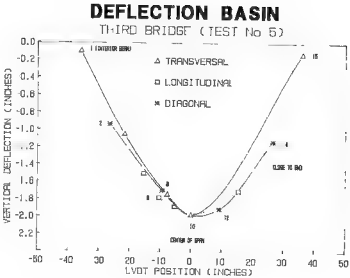

Figure H.22 Deflection Basin (Third Bridge, Test No 5)

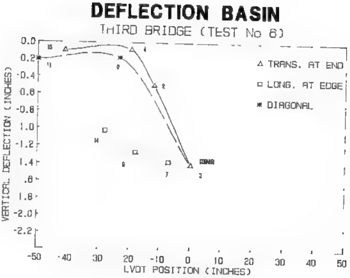

Figure H.23 Deflection Basin (Third Bridge, Test No 6)

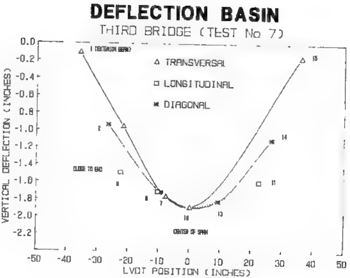

Figure H.24 Deflection Basin (Third Bridge, Test No 7)

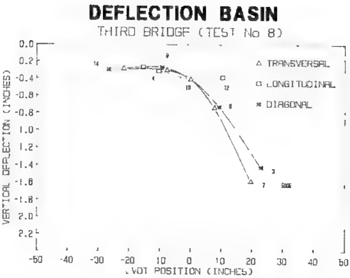

Figure H.25 Deflection Basin (Third Bridge, Test No 8)

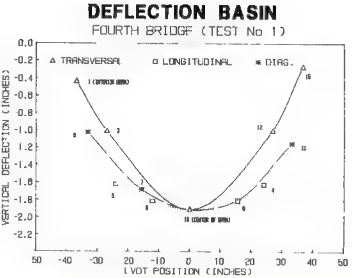

Figure H.26 Deflection Basin (Fourth Bridge, Test No 1)

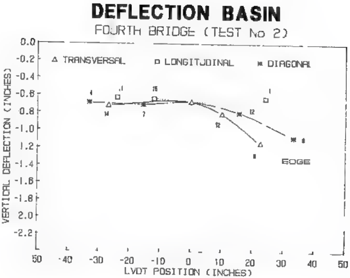

Figure H.27 Deflection Basin (Fourth Bridge, Test No 2)

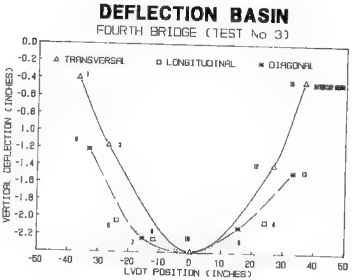

Figure H.28 Deflection Basin (Fourth Bridge, Test No 3)

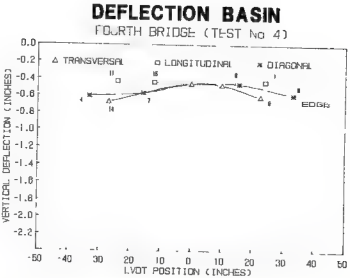

Figure H.29 Deflection Basin (Fourth Bridge, Test No 4)

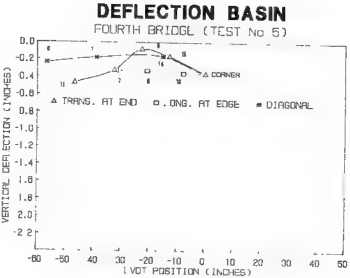

Figure H.30 Deflection Basin (Fourth Bridge, Test No 5)

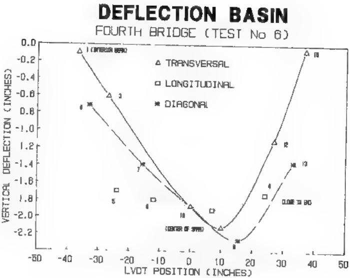

Figure H.31 Deflection Basin (Fourth Bridge, Test No 6)

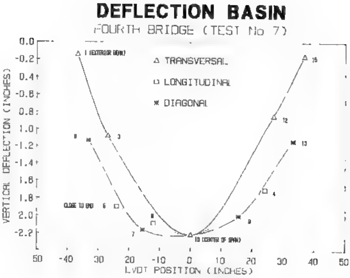

Figure H.32 Deflection Basin (Fourth Bridge, Test No 7)

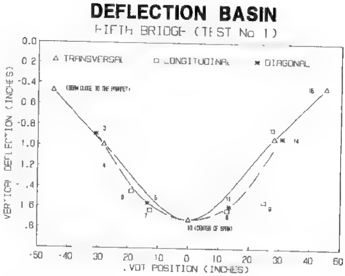

Figure H.33 Deflection Basin (Fifth Bridge, Test No 1)

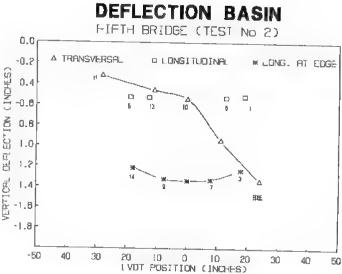

Figure H.34 Deflection Basin (Fifth Bridge, Test No 2)

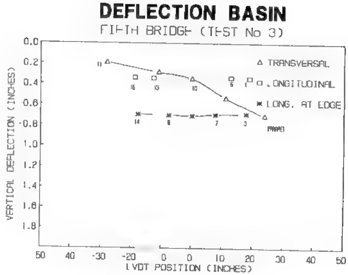

Figure H.35 Deflection Basin (Fifth Bridge, Test No 3)

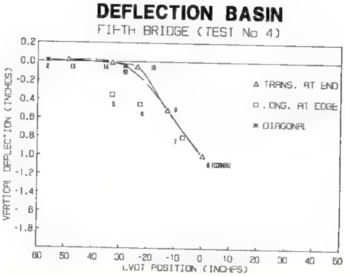

Figure H.36 Deflection Basin (Fifth Bridge, Test No 4)

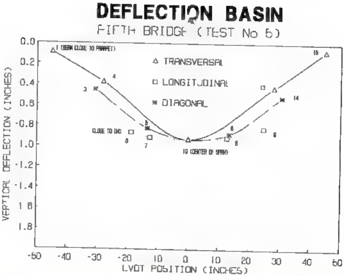

Figure H.37 Deflection Basin (Fifth Bridge, Test No 5)

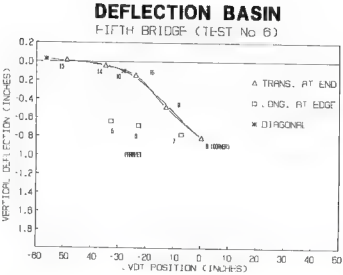

Figure H.38 Deflection Basin (Fifth Bridge, Test No 6)

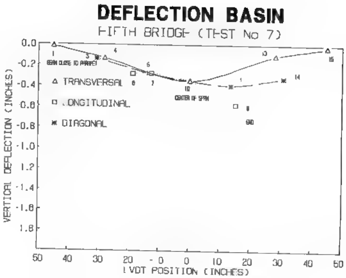

Figure H.39 Deflection Basin (Fifth Bridge, Test No 7)

APPENDIX I

PLOTS OF DYNAMIC TESTING

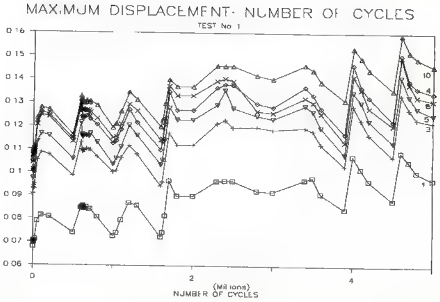

Figure I.1 Maximum Displacement-Number of Cycles (Test No 1)

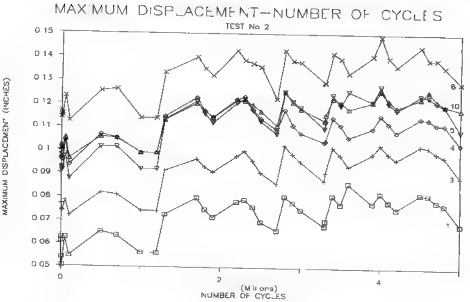

Figure I.2 Maximum Displacement-Number of Cycles (Test No 2)

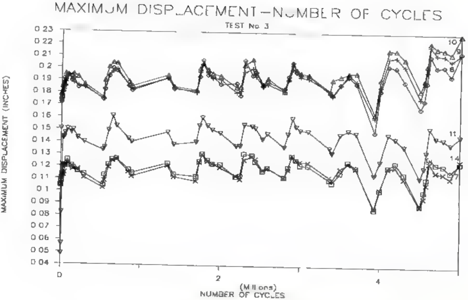

Figure I.3 Maximum Displacement-Number of Cycles (Test No 3)

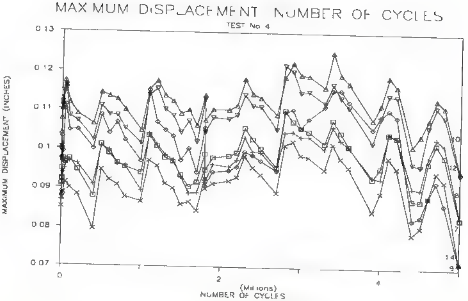

Figure I.4 Maximum Displacement-Number of Cycles (Test No 4)

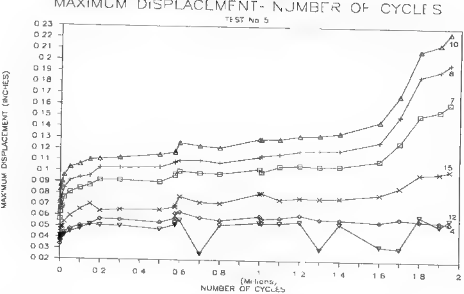

Figure I.5 Maximum Displacement-Number of Cycles (Test No 5)

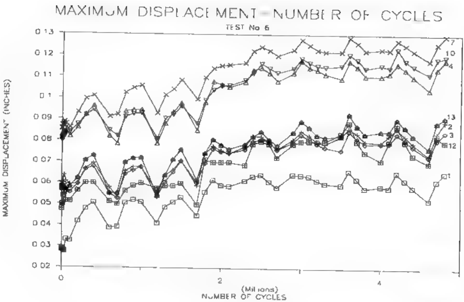

Figure I.6 Maximum Displacement-Number of Cycles (Test No 6)

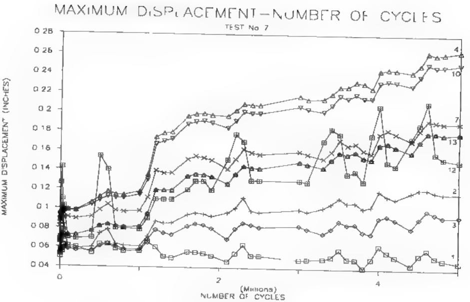

Figure I.7 Maximum Displacement-Number of Cycles (Test No 7)

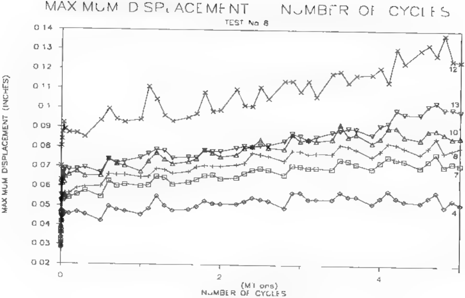

Figure I.8 Maximum Displacement-Number of Cycles (Test No 8)

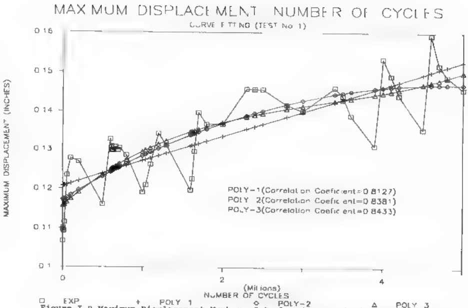

Figure I.9 Maximum Displacement-Number of Cycles (Curve Fitting, Test No 1)

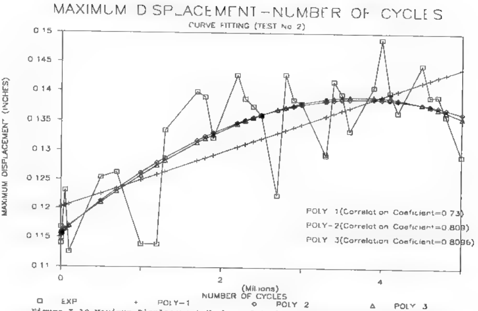

Figure I.10 Maximum Displacement-Number of Cycles (Curve Fitting, Test No 2)

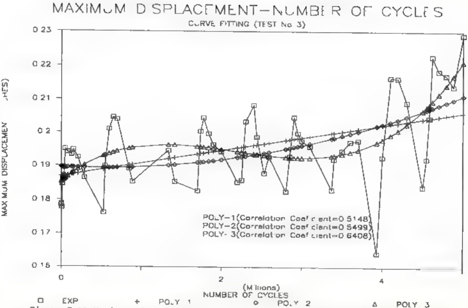

Figure I.11 Maximum Displacement-Number of Cycles (Curve Fitting, Test No 3)

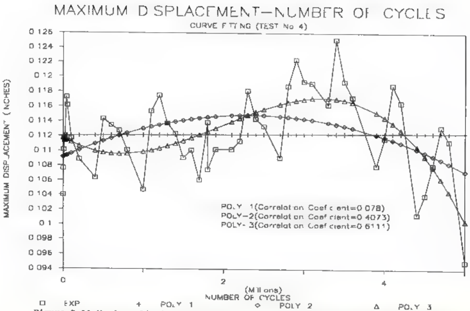

Figure I.12 Maximum Displacement-Number of Cycles (Curve Fitting, Test No 4)

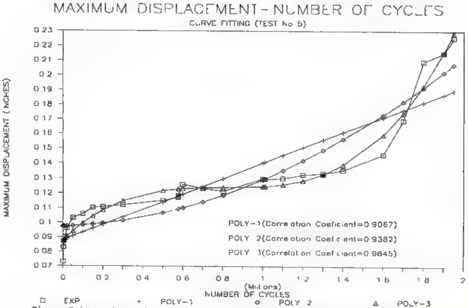

Figure I.13 Maximum Displacement-Number of Cycles (Curve Fitting, Test No 5)

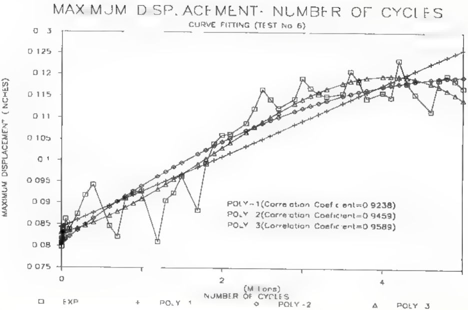

Figure I.14 Maximum Displacement-Number of Cycles (Curve Fitting, Test No 6)

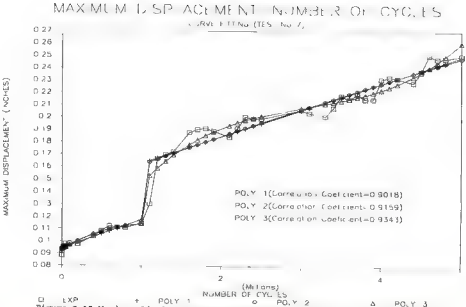

Figure I.15 Maximum Displacement-Number of Cycles (Curve Fitting, Test No 7)

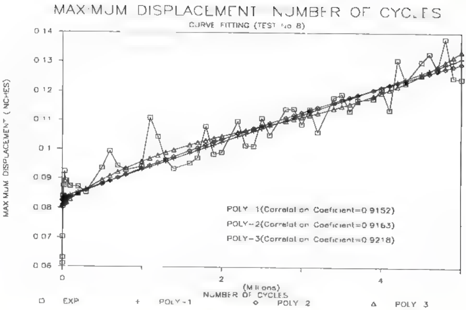

Figure I.16 Maximum Displacement-Number of Cycles (Curve Fitting, Test No 8)

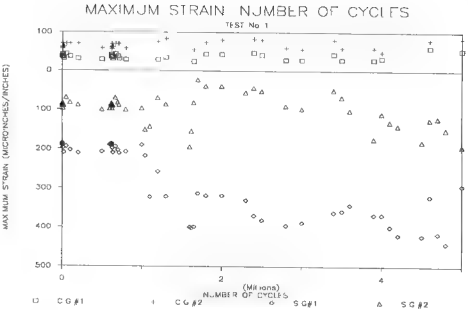

Figure I.17 Maximum Strain-Number of Cycles (Test No 1)

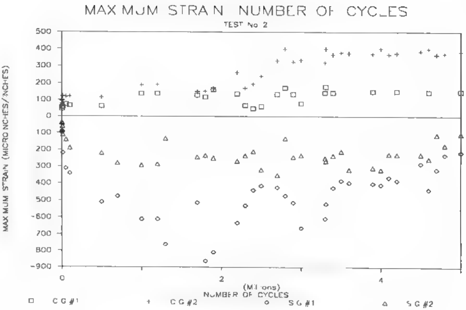

Figure I.18 Maximum Strain-Number of Cycles (Test No 2)

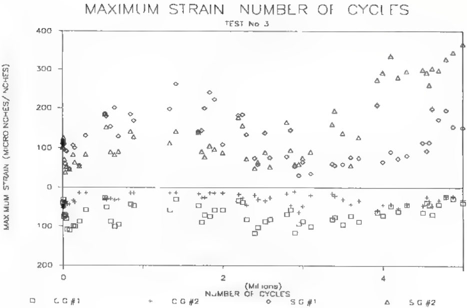

Figure I.19 Maximum Strain-Number of Cycles (Test No 3)

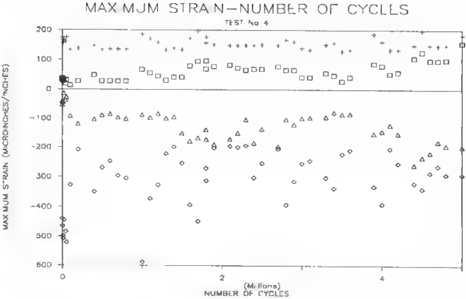

Figure I.20 Maximum Strain-Number of Cycles (Test No 4)

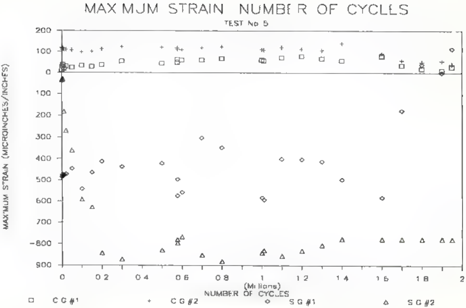

Figure I.21 Maximum Strain-Number of Cycles (Test No 5)

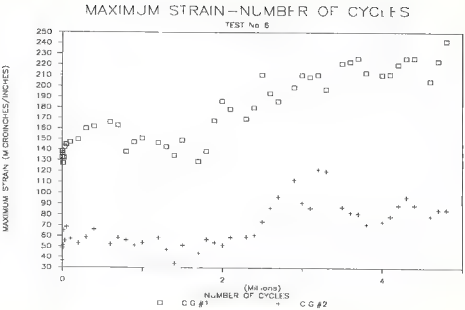

Figure I.22 Maximum Strain-Number of Cycles (Test No 6)

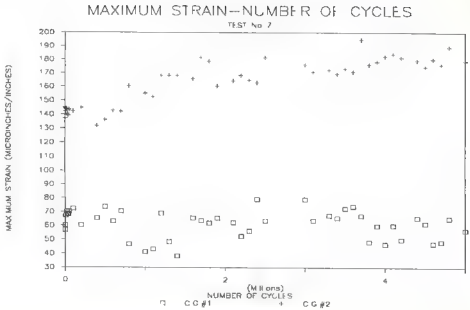

Figure I.23 Maximum Strain-Number of Cycles (Test No 7)

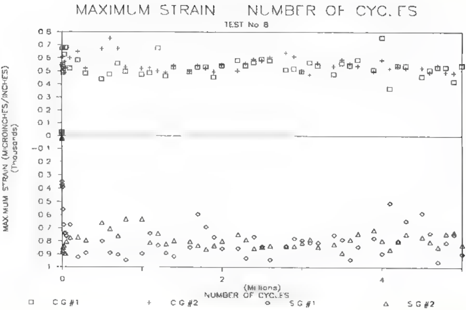

Figure I.24 Maximum Strain-Number of Cycles (Test No 8)

APPENDIX J

FORMULAS AND EXAMPLES FOR YIELD-LINE THEORY

YIELD LINE THEORY

1. FORMULAS

a) Interior Tests

$W_{ext}=P\delta$

$W_{in_1}=M_{yy}l_x\theta_x+M_{xx}l_y\theta_y$ (Rectangular shape)

$W_{in_2}=2\pi(M_{yy}+M_{xx})\delta$ (Circular shape)

$W_{ext}=W_{in_1}+W_{in_2}$

$M_{yy}=M(+)$

$M_{xx}=M(-)$

b) Free Edge (Single Imprint Test)

$W_{ext}=P\delta$

$W_{in_1}=\frac{1}{2}M_{yy}l_x\theta_x+\frac{1}{2}M_{xx}l_y\theta_y$ (Rectangular shape)

$W_{in_2}=\pi(M_{yy}+M_{xx})\delta$ (Circular shape)

$W_{ext}=W_{in_1}+W_{in_2}$

c) Free Corner (Single Imprint Test)

$W_{ext}=P\delta$

$W_{in_1}=\frac{1}{2}M_{yy}l_x\theta_x+\frac{1}{2}M_{xx}l_y\theta_y$ (Rectangular shape)

$W_{in_2}=\frac{1}{2}\pi(M_{yy}+M_{xx})\delta$ (Circular shape)

$W_{ext}=W_{in_1}+W_{in_2}$

d) <u>Free Edge (Tandem Load)</u>

$W_{ext} = P\delta$

$W_{int} = \frac{1}{2}(M_{xx} + M_{yy})\phi + M_{xx} l_y \theta_y$

$[1 - 2/3(a/R)]$

$W_{ext} = W_{int}$

f) <u>Parapet Edge</u>

$W_{ext} = P\delta$

$W_{int} = (M_{xx} + M_{yy})\phi + 2M_{xx}\sqrt{i}$

$[1 - 2/3(a/R)]$

$W_{ext} = W_{int}$

$i = M(+)/M(-)$

$\tan\phi = \sqrt{i}$

a=Radius of the distributed load

R=Radius of the yield line

e) <u>Free Corner (Tandem Load)</u>

$W_{ext} = P\delta$

$W_{int} = \frac{1}{4}(M_{xx} + M_{yy})\phi + M_{xx} l_y \theta_y$

$[1 - 2/3(a/R)]$

$W_{ext} = W_{int}$

f) <u>Parapet Edge</u>

$W_{ext} = P\delta$

$W_{int} = (M_{xx} + M_{yy})\pi [1 - 2/3(a/R)]$

$W_{ext} = W_{int}$

g) <u>Parapet Corner</u>

$W_{ext} = P\delta$

$W_{in_1} = \frac{1}{2}(M_{xx} + M_{yy})\pi [1 - 2/3(a/R)]$

$W_{in_2} = 2(M_{xx} + M_{yy})\phi [1 - 2/3(a/R)]$

$W_{ext} = W_{in_1} + W_{in_2}$

2. EXAMPLES

2.1 First Bridge

M_{yy}=29.6k-in/ft

M_{xx}=24.9k-in/ft

a) Interior Test (Single Imprint Load)

From Figure 7.3:

$$P=\frac{(29.6+24.9)}{12}\left(\frac{73}{12}\right)\left(\frac{1}{34.25}\right)(2)+\frac{2\pi}{2}\frac{(29.6+24.9)}{12}$$

P=33.6K.

b) Interior Test (Double Point Load)

From Figure 7.4

$$P=\frac{(29.6+24.9)}{12}\left(\frac{49.5}{12}\right)\left(\frac{1}{34.25}\right)(2)+\frac{2\pi}{2}\frac{(29.6+24.9)}{12}$$

P=34.25K.

c) Free Edge

From Figure 7.7

$$P=\frac{(29.6+42.3)}{12}\left(\frac{31.5}{12}\right)\left(\frac{1}{13.5}\right)(2)+\frac{\pi}{2}\frac{(29.6+24.9)}{12}$$

P=37.8K.

d) Free Corner

From Figure 7.7

$$P=\frac{1}{2}\frac{(29.6+42.3)}{12}\left(\frac{31.5}{12}\right)\left(\frac{1}{13.5}\right)(2)+\frac{1}{2}\frac{\pi}{2}\frac{(29.6+24.9)}{12}$$

P=18.5K.

e) Parapet Edge

From Figure 7.10:

$$0.574Po=\frac{(29.6+24.9)(\pi)}{12[1-2/3(11.5/13.50)]}$$

Po=37.95K.

P=75.90K.

f) Parapet Corner

From Figure 7.10:

$$0.574Po=\frac{\tfrac{1}{2}(29.6+24.9)(\pi)}{12[1-2/3(11.5/13.50)]}$$

Po=19.0K.
P=38.00K.

2.2 Second Bridge

M_{yy}=21.2k-in/ft

M_{xx}=21.2k-in/ft

a) Interior Test

From Figure 7.5:

$$P=\frac{(21.2+21.2)}{12}\frac{(58.6)}{12}\left(\frac{1}{15.06}\right)(2)+\frac{2\pi}{2}\frac{(21.2+21.2)}{12}$$

P=38.6K.

b) Free Edge

From Figure 7.8:

$$0.689Po=\frac{21.2(2.7)(1.833)}{12[1-2/3(11.5/30.34)]}+\frac{2(21.2)(1.3)}{12}$$

Po=23.64K.
P=47.29K.

c) Free Corner

From Figure 7.8:

$$0.689P=\frac{\tfrac{1}{2}21.2(2.7)(3.145)}{12[1-2/3(11.5/30.34)]}+\frac{(38.295)(21.2)}{(18.5)(12)}$$

Po=19.87K.
P=39.75K.

d) Parapet Edge

From Figure 7.11:

$$0.719Po=\frac{(21.2+21.2)(\pi)}{12[1-2/3(11.5/20.50)]}$$

Po=24.66K.
P=49.30K.

e) Parapet Corner

From Figure 7.11:

$$0.719P_o = \frac{\tfrac{1}{2}(21.2+21.2)(\pi+2.396)}{12[1-2/3(11.5/20.5)]}$$

P_o=21.73K.
P=43.50K.

2.3 Third Bridge

M_{yy}=16k-in/ft

M_{xx}=16k-in/ft

a) Interior Test

From Figure 7.3:

$$P = \frac{(16.0+16.0)}{12}\frac{(58.0)}{12}\left(\frac{1}{15.06}\right)(2) + \frac{2\pi}{2}\frac{(16.0+16.0)}{12}$$

P=27.0K.

b) Free Edge

From Figure 7.8:

$$0.7386P_o = \frac{16.0(2.7)(1.833)}{12[1-2/3(11.5/36.08)]} + \frac{2(16.0)(1.3)}{12}$$

P_o=16.03K.
P=32.07K.

c) Free Corner

From Figure 7.8:

$$0.689P_o = \frac{\tfrac{1}{2}16.0(2.7)(2.8578)}{12[1-2/3(11.5/36.08)]} + \frac{(40.975)(16)}{(22)(12)}$$

P_o=12.2K.
P=24.40K.

d) Parapet Edge

From Figure 7.11:

$$0.778P_o = \frac{(16.0+16.0)(\pi)}{12[1-2/3(11.5/13.0)]}$$

P_o=15.27K.
P=30.50K.

e) Parapet Corner

From Figure 7.11:

$$0.778P_o = \frac{\frac{1}{2}(16.0+16.0)(\pi+1.808)}{12[1-2/3(11.5/13.0)]}$$

P_o=12.0K.
P=24.0K.

2.4 Fourth Bridge

M_{yy}=21.2k-in/ft

M_{xx}=21.2k-in/ft

a) Interior Test

From Figure 7.5:

$$P = \frac{(21.2+21.2)}{12}\left(\frac{58.6}{12}\right)\left(\frac{1}{15.06}\right)(2) + \frac{2\pi}{2}\,\frac{(21.2+21.2)}{12}$$

P=38.6K.

b) Free Edge

From Figure 7.8:

$$0.689P_o = \frac{21.2(2.7)(1.833)}{12[1-2/3(11.5/30.34)]} + \frac{2(21.2)(1.3)}{12}$$

P_o=23.64K.
P=47.29K.

c) Free Corner

From Figure 7.8:

$$0.689P = \frac{\frac{1}{2}21.2(2.7)(3.145)}{12[1-2/3(11.5/30.34)]} + \frac{(38.295)(21.2)}{(18.5)(12)}$$

P_o=19.87K.
P=39.75K.

d) Parapet Edge

From Figure 7.12:

$$0.719P_o = \frac{(21.2+21.2)(\pi)}{12[1-2/3(11.5/20.50)]}$$

P_o=24.66K.
P=49.30K.

e) Parapet Corner

From Figure 7.11:

$$0.719P_o=\frac{\frac{1}{2}(21.2+21.2)(\pi+2.396)}{12[1-2/3(11.5/20.5)]}$$

$P_o=21.73K.$
$P=43.50K.$

2.5 Fifth Bridge

$M_{yy}=21.25\text{k-in/ft}$

$M_{xx}=21.25\text{k-in/ft}$

a) Interior Test

From Figure 7.6:

$$P=\frac{(21.25+21.25)}{12}\frac{(39.25)}{12}\left(\frac{1}{9.25}\right)(2)+\frac{2\pi}{2}\frac{(21.25+21.25)}{12}$$

$P=35.6K.$

b) Free Edge

From Figure 7.9:

$$0.726P_o=\frac{21.25(2.7)(1.833)}{12[1-2/3(11.5/34.44)]}+\frac{2(21.25)(1.3)}{12}$$

$P_o=22.2K.$
$P=44.5K.$

c) Free Corner

From Figure 7.9:

$$0.726P_o=\frac{\frac{1}{2}21.25(2.7)(2.6862)}{12[1-2/3(11.5/34.44)]}+\frac{(38.295)(21.25)}{(33.0)(12)}$$

$P_o=11.5K.$
$P=23K.$

d) Parapet Edge

From Figure 7.12:

$$0.719P_o=\frac{(21.25+21.25)(\pi)}{12[1-2/3(11.5/25.50)]}$$

$P_o=20.54K.$
$P=41.0K.$

e) Parapet Corner

From Figure 7.12:

$$0.719P_o=\frac{\frac{1}{2}(21.2+21.2)(\pi+2.396)}{12[1-2/3(11.5/20.5)]}$$

$P_o=17.10K.$

$P=34.20K.$

APPENDIX K

STRAINS IN BRACING

Table K.1 (a) Strains in Bracing (First Bridge)

		Test No 1			
		Strain due to Vertical Forces		Strain due to Boundary Restraining Forces	
		Bending	Axial	Bending	Axial
Location	Position	Strain	Strain	Strain	Strain
	1	155 6549	18 78277	-4 52883	2 423371
	2	95 5665	58 74840	1 639724	1 542145
END 1	3	158 2719	83 86328	-0 50298	0 208536
	4	136 066	148 7435	5 47242	2 886015
	1	-23 4715	223 6477	-4 65259	17 78000
	2	182 4151	15 67847	4 582231	0 818438
MIDDLE	3	58 34598	19 71743	-1 00594	29 30076
	4	230 365	213 2027	6 387882	15 25822
	1	-178 035	179 8804	5 0801	2 228400
	2	257 5272	104 9759	2 177913	1 376915
END 2	3	112 667	52 57881	1 156858	0 507235
	4	28 83758	29 85153	-4 83366	2 395833
		Test No 4			
		Strain due to Vertical Forces		Strain due to Boundary Restraining Forces	
		Bending	Axial	Bending	Axial
Location	Position	Strain	Strain	Strain	Strain
	1	-346.928	215 1148	9 692813	28 57774
	2	198 2945	114 1378	-3 48422	3 081723
END 1	3	115 891	81 28438	0 378148	0 205854
	4	210 8803	38 27588	5 030864	0 763888
	1	360 572	345 6321	-73 3127	28 23105
	2	78 10367	28 5977	1 970815	1 589185
MIDDLE	3	304 4138	21 20689	5 38849	32 41455
	4	-88 8048	381 1493	1 998851	28 33422
	1	15 2704	82 41378	0 477474	0 794801
	2	148 532	31 60918	1 28201	0 428448
END 2	3	385 2411	152 8735	4 06858	1 518981
	4	-260 326	285 3447	44 88165	21 80438

NOTE: The strains are in microinches inches
REFER TO FIGURES 2 1 AND 2 2

Table K.1 (b) Strains in Bracing (First Bridge)

Test No 5

Location	Position	Strain due to Vertical Forces: Bending Strain	Strain due to Vertical Forces: Axial Strain	Strain due to Boundary Restraining Forces: Bending Strain	Strain due to Boundary Restraining Forces: Axial Strain
	1	30 45518	4 437287	0 32774	0 327061
	2	120 974	47 85800	6 42238	0 488742
END-1	3	14 97969	0 076888	-0 01885	0 243333
	4	-49 5787	52 19061	-0 45535	0 403196
	1	-82 3021	157 5490	-6 46324	4 958763
	2	85.77978	3 157388	0 856043	0 067368
MIDDLE	3	78 32758	12 30569	-0 54188	7 245001
	4	157 002	155 7755	1 724039	4 375248
	1	-121 865	160 4806	1 37888	0 747173
	2	185 0138	97 97501	0 653411	0 509138
END-2	3	71 39481	61 18652	-0 28043	0 233768
	4	118 346	101 1590	7 728375	3 216843

Test No 6

Location	Position	Strain due to Vertical Forces: Bending Strain	Strain due to Vertical Forces: Axial Strain	Strain due to Boundary Restraining Forces: Bending Strain	Strain due to Boundary Restraining Forces: Axial Strain
	1	185 984	122 5733	2 598252	8 141885
	2	148 5966	88 20887	-1 31123	1 153782
END-1	3	24 11037	15 3558	-0 03838	0 018448
	4	22 63423	70 09893	0 269846	0 699461
	1	-135 313	139 6551	13 7936	5 703478
	2	70 85487	9.213356	0 817355	0 247345
MIDDLE	3	63 9822	4 795258	0 55845	3 664753
	4	80 2037	144 8275	1 143767	5 260253
	1	48 71278	7 058187	0 714768	0 044840
	2	73 8071	37 55387	-0 321	0 253323
END-2	3	39 8559	22 95258	-0 21045	0 113878
	4	105 78	68 42688	0 118415	2 824360

NOTE: The strains are in microinches/inches
REFER TO FIGURES 2 1 AND 2 2

Table K.2 (a) Strains in Bracing (Second Bridge)

		Test No 1			
		Strain due to Vertical Forces		Strain due to Boundary Restraining Forces	
		Bending	Axial	Bending	Axial
Location	Position	Strain	Strain	Strain	Strain
	1	54 14974	24 47318	1 71601	3 687739
	2	-31 0516	76 62835	0 621578	2 348743
END-1	3	51 42581	109 3869	-0 18055	0 314285
	4	75 703	194 0134	2 07446	4 391782
	1	7 62872	281 7145	-1 76368	27 0261
	2	58 27054	20 45018	1 740798	1 24545
MIDDLE	3	16 95765	25 71838	0 38133	44 58812
	4	-74 8508	280 6882	2 421485	23 21599
	1	57 8541	234 7701	1 92574	3 381044
	2	83 87508	136.8252	0 825592	2 095368
END-2	3	36 5082	68 58237	0 438936	0 77191
	4	0 389876	38 03678	-1 83232	3 845833
		Test No 3			
		Strain due to Vertical Forces		Strain due to Boundary Restraining Forces	
		Bending	Axial	Bending	Axial
Location	Position	Strain	Strain	Strain	Strain
	1	-72 018	179 2624	2 34747	27 78382
	2	40 7485	85 11404	-0 83880	2 88612
END-1	3	-24 0788	87 7203	0 081825	0 200136
	4	43 79819	31 89833	1 218413	0 742851
	1	74 8508	288 0288	-17 8038	27 44686
	2	15 79821	24 66475	0 477257	1 345041
MIDDLE	3	63 19286	17 67241	-1 30743	31 51415
	4	-14 4907	300 9578	0 482182	25 60272
	1	3 377549	52 01148	0 115838	0 772724
	2	30 8337	28 34088	-0 31291	0 414801
END-2	3	79 97185	127 3945	-0 98538	1 474824
	4	-54 0407	221 1205	10 86974	21 28812

NOTE The strains are in microinches/inches
REFER TO FIGURES 2 1 AND 2 3

Table K.2 (b) Strains in Bracing (Second Bridge)

Test No 6

Location	Position	Strain due to Vertical Forces: Bending Strain	Strain due to Vertical Forces: Axial Strain	Strain due to Boundary Restraining Forces: Bending Strain	Strain due to Boundary Restraining Forces: Axial Strain
	1	9 895535	5 767765	0 23295	0 647887
	2	39 3072	82 53131	0 584505	1 423042
END-1	3	4 86722	0 17	0 0134	0 163
	4	-16 1093	88 07471	0 32365	1 144717
	1	-26 7417	205.4987	4 59365	14 14294
	2	21 37195	4 248768	0 466293	0 192219
MIDDLE	3	25 77521	18 0509	-0 38514	20 87186
	4	51 0134	203 1855	1 225958	12 48372
	1	-39 8293	209 3226	0 97891	2 248012
	2	63 36407	127 7935	0 464422	1 452705
END-2	3	23 19789	79 78243	-0 20843	0 667063
	4	37 8036	131 9478	5.481638	9 177923

Test No 6

Location	Position	Strain due to Vertical Forces: Bending Strain	Strain due to Vertical Forces: Axial Strain	Strain due to Boundary Restraining Forces: Bending Strain	Strain due to Boundary Restraining Forces: Axial Strain
	1	74 2317	198 1206	1 612275	22 79759
	2	58 22696	137 931	-0 91458	3 25862
END-1	3	9 609673	24 56895	-0 02748	0 654457
	4	9.021328	112 1551	0 188217	1 958483
	1	53 8318	223 4482	-9 82105	15 96974
	2	28 24057	14 74137	0 839853	0 692568
MIDDLE	3	25 10282	7 872413	-0 38952	10 28131
	4	-31 8868	231 7241	0 787775	14 78471
	1	19 41546	11 2931	0 498549	0 125834
	2	-29 4173	80 0362	-0 2239	0 769307
END-2	3	15 88537	36 72413	-0 14679	0 318881
	4	-42 1648	109 4827	5 38077	7 90821

NOTE The strains are in microinches/inches

REFER TO FIGURES 2 1 AND 2 2

Table K.3 (a) Strains in Bracing (Third Bridge)

Test No 1

Location	Position	Strain due to Vertical Forces: Bending Strain	Strain due to Vertical Forces: Axial Strain	Strain due to Boundary Restraining Forces: Bending Strain	Strain due to Boundary Restraining Forces: Axial Strain
	1	40 8123	18 35488	1 25023	2 888781
	2	-23 2887	57 47126	0 452863	1 709769
END-1	3	38 58843	82 04017	-0 1388	0 228988
	4	-57 5272	145 5100	1 51139	3 199712
	1	-5 72004	218 7858	1 28496	19 62044
	2	44 4529	15 33784	1 288288	0 807399
MIDDLE	3	14 21838	18 28879	-0 27782	32 48583
	4	-58 1381	210 5244	1 764224	16 81450
	1	43 3805	178 0775	-1 40303	2 470617
	2	52 75704	102 6839	0 601502	1 526580
END-2	3	-27 4581	51 43677	0 318504	0 582391
	4	7 027482	29.20258	1 33497	2 656249

Test No 3

Location	Position	Strain due to Vertical Forces: Bending Strain	Strain due to Vertical Forces: Axial Strain	Strain due to Boundary Restraining Forces: Bending Strain	Strain due to Boundary Restraining Forces: Axial Strain
	1	-58 0711	139 5885	1 879892	22 24981
	2	31 72561	74 05377	0 67187	2 398341
END-1	3	18 7469	52 72509	0 073534	0 180272
	4	34 10079	24 83374	0 975725	0 504727
	1	38 2766	224 2494	14 2575	21 87989
	2	12 30003	18 20328	0 382185	1 237294
MIDDLE	3	49 20015	13 75823	-1 04701	25 23794
	4	-11 282	234 3171	0 388139	20 30507
	1	2 628663	40 49486	0 092604	0 618809
	2	24 0052	20 50534	-0 25058	0 332018
END-2	3	62.28364	99 18579	-0 78808	1 181083
	4	-42 0745	172 1581	8 704665	17 05428

NOTE The strains are in microinches/inches
REFER TO FIGURES 2 1 AND 2 2

Table K.3 (b) Strains in Bracing (Third Bridge)

Test No 5

Location	Position	Strain due to Vertical Forces: Bending Strain	Strain due to Vertical Forces: Axial Strain	Strain due to Boundary Restraining Forces: Bending Strain	Strain due to Boundary Restraining Forces: Axial Strain
	1	6 351415	3 720708	-0 12806	0 356987
	2	23 2589	40 21155	0 322074	0 784125
END 1	3	3 128827	0 21	-0 00738	0 33
	4	-10 3561	43 78231	-0 17633	0 630762
	1	17 191	132 1063	-2 5313	7 783048
	2	13 73911	2 731350	0 256836	0 105818
MIDDLE	3	16 38977	10 31843	-0 21222	11 38082
	4	-32 7843	130 6192	0 875326	5 878784
	1	25 4758	134 5645	-0 53895	1 237586
	2	40 73404	82 15298	0 255806	0 800470
END 2	3	14 8128	51 28870	-0 11374	0 387585
	4	24 3023	84 82358	3 028005	5 057222

Test No 7

Location	Position	Strain due to Vertical Forces: Bending Strain	Strain due to Vertical Forces: Axial Strain	Strain due to Boundary Restraining Forces: Bending Strain	Strain due to Boundary Restraining Forces: Axial Strain
	1	-50 3036	133 0818	1 12435	14 14381
	2	40 18872	83 38803	-0 55741	2 021874
END 1	3	8 520848	16 67179	-0 01704	0 033785
	4	8 121814	78 10524	0 116771	1 215065
	1	35 5885	151 6255	-5 88887	9 807737
	2	18 15331	30 66307	0 38687	0 428874
MIDDLE	3	17 09405	5 208280	-0 24188	8 388200
	4	21 5817	157 2413	0 484848	9 172554
	1	13 17477	7 683175	0 309303	0 078068
	2	-19 0817	40 77277	-0 1388	0 440059
END 2	3	10 77835	24 01884	-0 08108	0 197823
	4	-28 8118	74 29183	3 848273	4 906318

NOTE: The strains are in microinches/inches
REFER TO FIGURES 2 1 AND 2 2

Table K.4 (a) Strains in Bracing (Fourth Bridge)

Test No 1

Location	Position	Strain due to Vertical Forces: Bending Strain	Strain due to Vertical Forces: Axial Strain	Strain due to Boundary Restraining Forces: Bending Strain	Strain due to Boundary Restraining Forces: Axial Strain
	1	51 05546	33 07471	1 15568	2 483578
	2	29 2772	72 24938	0 4.8613	1 580439
END-1	3	48.48728	103 1362	-0 1264	0 211558
	4	-72 3.09	182 8269	1 39708	2 857717
	1	-7 1808	275 0451	-1 18778	18 20125
	2	55 68365	19 28160	1 172374	0 838772
MIDDLE	3	17 67454	24 24876	-0 25581	90 02873
	4	-70 5736	264 6592	1 830795	15 53525
	1	54 5481	221 3546	-1 28682	2 283764
	2	78 89457	129 1009	0 55501	1 411124
END-2	3	-34 5183	84 66337	0 29534	0 519857
	4	8 834548	36.71182	-1 23401	2 455356

Test No 3

Location	Position	Strain due to Vertical Forces: Bending Strain	Strain due to Vertical Forces: Axial Strain	Strain due to Boundary Restraining Forces: Bending Strain	Strain due to Boundary Restraining Forces: Axial Strain
	1	76 1333	189 5059	1 985288	23 48725
	2	43 07588	100 5500	-0 70854	3 533881
END-1	3	-25.4545	71 38003	0 077657	0 159257
	4	48 302	33 7.92.	1 030428	0 528070
	1	79 1279	304 4854	-15 0589	23 21226
	2	16 70085	25 87416	0 403623	1 388883
MIDDLE	3	88 80388	18 68226	1 10571	25 85198
	4	-15 3187	318 1553	0 407788	21 65258
	1	3 370551	54 98357	0 087795	0 553503
	2	-32 5858	27 84618	-0 28463	0 330833
END-2	3	64 54145	134 6742	-0 63335	1 247279
	4	57 1287	233 7580	9 192594	18 01043

NOTE The strains are in microinches inches
REFER TO FIGURES 2 1 AND 2 2

Table K.4 (b) Strains in Bracing (Fourth Bridge)

Test No 6

Location	Position	Strain due to Vertical Forces: Bending Strain	Strain due to Vertical Forces: Axial Strain	Strain due to Boundary Restraining Forces: Bending Strain	Strain due to Boundary Restraining Forces: Axial Strain
	1	5 837321	3 472858	0 04782	0 133275
	2	23 5843	37 53078	0 120241	0 282740
END 1	3	2 820332	0	-0 00275	0
	4	-8 5557	40 84462	0 06657	0 235484
	1	-18 045	123 2992	0 94502	2 908404
	2	12 82317	2 548260	0 085923	0 030542
MIDDLE	3	15 48512	9.83054	-0 07922	4 232501
	4	30 508	121 8113	0 252188	2 568078
	1	-23 7775	125.3835	0 20138	0 452035
	2	38 01844	78.8781	0 085338	0 288842
END 2	3	13 81881	47 86845	-0 04248	0 137224
	4	22 5821	79 16858	1 129768	1 888028

Test No 7

Location	Position	Strain due to Vertical Forces: Bending Strain	Strain due to Vertical Forces: Axial Strain	Strain due to Boundary Restraining Forces: Bending Strain	Strain due to Boundary Restraining Forces: Axial Strain
	1	-55 6595	173 7088	1 100878	13 84684
	2	52 45816	122 1574	-0 55548	1 979117
END 1	3	8 511424	21 78107	-0 01558	0 035074
	4	7 800317	98 33737	0 114313	1 189484
	1	47 7681	187 8112	-5 84331	9 898172
	2	25 01315	13 05884	0 388812	0 420828
MIDDLE	3	22 23392	5 795565	-0 23657	6 232175
	4	-38 3134	205 2413	0 484528	6 978448
	1	17 18555	10 00246	0 302798	0 078424
	2	-28 0553	53 21820	-0 13598	0 430795
END 2	3	14 08980	32 32708	-0 08815	0 193859
	4	-37 3459	88 87038	3 883184	4 803027

NOTE. The strains are in microinches inches
REFER TO FIGURES 2 1 AND 2 2

Table K.5 Strains in Bracing (Fifth Bridge)

Test No 1

Location	Position	Strain due to Vertical Forces Bending Strain	Strain due to Vertical Forces Axial Strain	Strain due to Boundary Restraing Forces Bending Strain	Strain due to Boundary Restraing Forces Axial Strain
	1	-87 7387	243 2848	2 366633	28 01072
END-1	2	55 30153	128 0845	0 84583	3 020578
	1	38 67053	105 8805	0 18581	0 778031
END-2	2	-41 8457	107 2454	-0 31548	0 417885

Test No 5

Location	Position	Strain due to Vertical Forces Bending Strain	Strain due to Vertical Forces Axial Strain	Strain due to Boundary Restraing Forces Bending Strain	Strain due to Boundary Restraing Forces Axial Strain
	1	-88.8365	182 1119	1 33838	14 51601
END-1	2	54 88848	128 5787	-0 58234	2 074478
	1	18 02854	10 48645	0 317443	0 080122
END-2	2	27 915	55 79432	-0 14238	0 451640

Test No 7

Location	Position	Strain due to Vertical Forces Bending Strain	Strain due to Vertical Forces Axial Strain	Strain due to Boundary Restraing Forces Bending Strain	Strain due to Boundary Restraing Forces Axial Strain
	1	5 371851	3 141930	-0 04335	0 120582
END-1	2	-21 3381	33 95842	0 108789	0 284860
	1	-21 513	113 6322	-0 18238	0 418033
END-2	2	34 38753	59 37361	0 085639	0 270381

NOTE The strains are in microinches inches
REFER TO FIGURES 5 1 AND 5 3

REFERENCES

1. Batchelor, B., Hewitt, B. E., Csagoly, P., and Holowka, M., "Investigation of the Ultimate Strength of Deck Slabs on Composite Steel/Concrete Bridges," Transportation Research Record, No 664, 1978, pp. 162-170

2. Standard Specifications for Highway Bridges, 13th Edition, American Association of State Highway and Transportation Officials, Washington, 1983.

3. Timoshenko, S., and Woinowsky-Krieger, S., Theory of Plates and Shells, 2nd Edition, McGraw-Hill Book Company, Inc., New York, 1959.

4. Guice L., and Rhomberg, E. J. "Membrane Action in Partially Restrained Slabs" Journal of the American Concrete Institute, July 1988, pp. 365-373

5. Ockleston, A. J., "Arching Action in Reinforced Concrete Slabs," The Structural Engineer, June 1958, pp. 197-201

6. Guyon, Y., Prestressed Concrete, John Wiley & Sons, New York, 1962.

7. Batchelor, B., Hewitt, B. E., Csagoly, P., and Holowka, M., "Load Carrying Capacity of Concrete Deck Slabs" Ontario Ministry of Transportation, SRR-85-03, Toronto, Canada, 1979.

8. Csagoly, P., Holowka, M., and Dorton, R. A. "The True Behavior of Thin Concrete Bridge Slabs," Transportation Research Record, No 664, 1978, pp. 171-179

9. Ontario Highway Bridge Design Code, Ontario Ministry of Transportation and Communications, 2nd Edition, Ontario, Canada, 1983.

10. Beal, D. B., "Strength of Concrete Bridge Deck," Research Report 89, New York State Department of Transportation, New York, July 1981.

11. Fang, I. K., Worley J. A., Burns N. H., and Klingner R. E., "Behavior of Ontario-Type Bridge Deck on Steel Girders," Research Report 350-1, Center for Transportation Research, University of Texas, Austin, TX, 1986.

12. Tsui, C. K., Burns N. H. and Klingner R. E., "Behavior of Ontario-Type Bridge Deck on Steel Girders," Research Report 350-3, Center for Transportation Research, University of Texas, Austin, TX, 1986.

13. Perdikaris, P. C., Beim, S.R., and Bousias, S. N., "Slab Continuity Effect on Ultimate and Fatigue Strength of Reinforced Concrete Bridge Deck Models," Journal of the American Concrete Institute, July 1989, pp. 483-491

14. Fenwick, R. C., and Dickson, A. R., "Slabs Subjected to Concentrated Loading", Journal of the American Concrete Institute, December 1989 pp. 672-678

15. Westergaard, H. M., "Computation of Stresses in Bridge Slabs Due to Wheel Loads," Public Roads, March. 1930, pp. 1-23

16. Bakht, B., Cheung, M. S., and Dorton, R., "A Comparison of Design Loads for Highway Bridges: Discussion," Canadian Journal of Civil Engineering, Vol. 9, No 1, 1982, pp. 138-140

17. Batchelor, B. and Tong, P.Y., "An Investigation of the Ultimate Shear Strength of Two-Way Continuous Bridge Slabs Subjected to Concentrated Loads," RR167, Research and Development Division, Ministry of Transportation and Communications, Ontario, 1970.

18. Hays, C. O., Hoit M. I., Selvappalam M., and Vinayagamourthy, M. "Develop Post-Processor for Program Brufem to Obtain Bridge Ratings of Nonpost-Tensioned Concrete Bridges", Structures and Materials Research Report No 89-1, Engineering and Industrial Experiment Station, University of Florida, Gainesville, FL, March 1989.

19. Snyder, R.E., Likins, G.E., and Moses, F., "Loading Spectrum Experienced by Bridge Structures in the United States," Report FHWA/RD-85/012, Bridge Weighing Systems, Inc., Warrensville, OH, Feb., 1985.

20. Batchelor, B., Hewitt, B.E., and Csagoly, P., "Investigation of the Fatigue Strength of Deck Slabs of Composite Steel/Concrete Bridges," Transportation Research Record, No. 664, 1978, pp. 153-161.

21. Keating, P. B., and Fisher, J. W., "Review of Fatigue Tests and Design Criteria on Welded Details," Fritz Engineering Laboratory Report 488-1(85), Lehigh University, Bethlehem, PA, Oct. 1985.

22. Hawkins, N. M., "The Shear Strength of Reinforced Concrete Members-Slabs," by the Joint ASCE-ACI Task Committee 426 on Shear and Diagonal Tension of the Committee on Masonry and Reinforced Concrete of the Structural Division, Journal of the Structural Division, ASCE, 100, August 1974(ST8), 1543-1591.

23. ACI-ASCE Committee 426. Suggested Revisions to Shear Provisions for Building Codes. Detroit, MI: American Concrete Institute, 1979, 82 pp.

24. Hewitt, B.E., and Batchelor, B., "Punching Shear Strength of Restrained Slabs," Proceedings, ASCE, ST9, September 1975, pp. 1827-1853.

25. Hoit, M. I., New Computer Programming Techniques for Structural Engineering, Ph.D. Dissertation, University of California at Berkley, November, 1983.

BIOGRAPHICAL SKETCH

The author was born on 24 October, 1959, in Cusco, Peru. After completing his bachelor's degree at the National Engineering University of Lima in the Civil Engineering Department in 1982, he worked in a research project to obtain the Professional registration. After that he worked as a design engineer and later he worked as a project engineer for a construction company. In August 1984 he entered the Graduate School at the University of Puerto Rico, Mayaguez Campus, where he was employed as a Graduate Research Assistant, and was awarded the degree of Master of Science in July 1986. In August 1986 he entered the Graduate School at the University of Florida at Gainesville to further his studies in structural engineering leading toward a degree of Doctor in Philosophy. From August 1986 until December 1986 he worked for the Civil Engineering Department of the University of Florida as a teaching assistant. Since that he has been working as a Graduate Research Assistant.

He is member of the College of Engineering in Peru, is also member of the A.S.C.E. and the Tau Beta Pi engineering honor society.

I certify that I have read this study and that in my opinion it conforms to acceptable standards of scholarly presentation and it is fully adequate, in scope and quality, as a dissertation for the degree of Doctor of Philosophy.

John M. Lybas, Chair
Associate Professor of Civil Engineering

I certify that I have read this study and that in my opinion it conforms to acceptable standards of scholarly presentation and it is fully adequate, in scope and quality, as a dissertation for the degree of Doctor of Philosophy.

Clifford O. Hays, Cochair
Professor of Civil Engineering

I certify that I have read this study and that in my opinion it conforms to acceptable standards of scholarly presentation and it is fully adequate, in scope and quality, as a dissertation for the degree of Doctor of Philosophy.

Fernando E. Fagundo
Associate Professor of Civil Engineering

I certify that I have read this study and that in my opinion it conforms to acceptable standards of scholarly presentation and it is fully adequate, in scope and quality, as a dissertation for the degree of Doctor of Philosophy.

Marc I. Hoit
Associate Professor of
Civil Engineering

I certify that I have read this study and that in my opinion it conforms to acceptable standards of scholarly presentation and it is fully adequate, in scope and quality, as a dissertation for the degree of Doctor of Philosophy.

James E. Keesling
Professor of Mathematics

This dissertation was submitted to the Graduate Faculty of the College of Engineering and to the Graduate School and was accepted as partial fulfillment of the requirements for the degree of Doctor of Philosophy.

August, 1990

for Winfred, M. Phillips
Dean, College of Engineering

Madelyn M. Lockhart
Dean, Graduate School